Development of Thermodynamic Model for Conventional SI Engine Simulation and Detailed Testing Analysis of a Lean Combustion in PFI SI Engine.

KANGUDE PRASAD ADINATH

A Dissertation Submitted to
Indian Institute of Technology Hyderabad
In Partial Fulfilment of the Requirements for
The Degree of Master of Technology

भारतीय प्रौद्योगिकी संस्थान हैदराबाद
Indian Institute of Technology Hyderabad

Department of Mechanical and Aerospace Engineering

June, 2016

Declaration

I declare that this written submission represents my ideas in my own words, and where others' ideas or words have been included, I have adequately cited and referenced the original sources. I also declare that I have adhered to all principles of academic honesty and integrity and have not misrepresented or fabricated or falsified any idea/data/fact/source in my submission. I understand that any violation of the above will be a cause for disciplinary action by the Institute and can also evoke penal action from the sources that have thus not been properly cited, or from whom proper permission has not been taken when needed.

(Signature)

(KANGUDE PRASAD ADINATH)

(ME14MTECH11009)

Approval Sheet

This thesis entitled "Development of Thermodynamic Model for conventional SI Engine Simulation and Detailed Testing Analysis of a Lean Combustion in PFI SI Engine" by Kangude Prasad Adinath is approved for the degree of Master of Technology from IIT Hyderabad.

Dr. Saptarshi Majumdar

Assistant Professor,

Department of Chemical Engineering,

Indian Institute of Technology, Hyderabad.

Examiner

Dr. Sarvanan Balusamy

Assistant Professor,

Department of Mechanical and Aerospace Engineering,

Indian Institute of Technology, Hyderabad.

Examiner

Dr. Pankaj S. Kolhe

Assistant Professor,

Department of Mechanical and Aerospace Engineering,

Indian Institute of Technology, Hyderabad.

Adviser

Acknowledgements

Abstract

The research presented in this thesis consists of two parts. The first one proposed to perform a detailed testing analysis of lean combustion in a PFI equipped SI engine and find out its operational envelope. The second one presented development of simplified thermodynamic model for conventional SI engine simulation, which can further be extended to lean burn operations.

The first part focuses on conducting an experimental investigation of parameters that facilitate lean burning and their implications on cyclic variability, exhaust emissions. The magnitudes of cyclic variability and exhaust emissions decide the operational range of lean burn. An air fuel ratio swing is carried under different loads and compression ratios from 14:1 to 22:1. The cyclic variability results have been presented in terms of normalised COV in IMEP. The results show an increment trend in COV with leaner mixtures for each load. The COV values reduce with the increase in loads. The CR findings indicate that increase in compression ratio substantially reduces cyclic variability. The NOx emissions increase significantly up to 5 times from AFR 14:1 to 22:1 for 3.36 bar load and CO emissions decrease with leaner mixtures drastically.

The second part focuses on developing in house MATLAB code for simulation of a conventional SI engine, which can be used as a teaching tool. A detailed thermodynamic quasi dimension model for each process and sub process that occurs in SI engine operation has been formulated and validated against experimental results from the literature. The model is developed on the basis of first law and second law of thermodynamics. The working fluid is considered as an ideal gas and combustion is modelled as a two zone model. The results show that the model gives quite a good match for in-cylinder pressure trace and mass fraction burned curve with that of the experiment. Also, results for performance parameters against speed show the shortcomings in the model for predicting the performance under variable speed conditions.

Based on the results of both parts, direction of further research is mentioned in the future scope.

Nomenclature

AFR	Air-Fuel ratio
A_{tm}	Thermo-mechanical availability (J)
A_R	Curtain flow area of inlet valve (m2)
A_f	Flame front area (m2)
CAD	Crank angle in degree
CR	Compression ratio
C	Carbon atom
C_D	Coefficient of discharge
CO	Carbon monoxide
CO2	Carbon dioxide
COV	Coefficient of variation (%)
Cp_u, Cp_b	Specific heat of unburned and burned mixtures at constant pressure (J/kg-K)
Cv_u, Cv_b	Specific heat of unburned and burned mixtures at constant volume (J/kg-K)
$\frac{dQ_{ch}}{d\theta}$	Net heat release rate (J/degree)
$\frac{dP}{d\theta}$	Rate of change of Pressure (Pa/degree)
$\frac{dV}{d\theta}$	Rate of change of volume (m3/degree)
ECU	Electronic control unit
EAR	Excess air ratio
H	Hydrogen atom
H_u, H_b	Enthalpy of unburned and burned mixtures (J)
h_u, h_b	Specific enthalpy of unburned and burned mixtures (J/kg)
HC	Unburned hydrocarbons
$H - H_0$	Enthalpy change of the system when it reaches a dead state condition (J)
IC	Internal combustion engine
IMEP	Indicated mean effective pressure (Pa)
K_u, K_b	Thermal conductivity of unburned and burned mixtures (W/m-K)
L_t	Turbulent eddy length Scale (m)
L_{max}	Maximum Valve lift (m)
MBT	Maximum brake torque (N-m)
$\dot{m}$	Instantaneous mass flow rate (kg/degree)
$\dot{m}_u, \dot{m}_b$	Instantaneous rate of mass change of unburned and burned mixture respectively (kg/degree)

m_u, m_b	Instantaneous mass of unburned and burned mixture (kg)
N	Speed of engine (rps)
nhrr	Net heat release rate
$nhrr_{max}$	Maximum net heat release rate
NOx	Oxides of nitrogen
NIMEP1	Indicated mean effective pressure normalized by inlet pressure
NIMEP3	Indicated mean effective pressure normalized by peak pressure
O	Oxygen atom
P,p	Instantaneous in-cylinder pressure
p_{max}	Peak pressure
p_1	Inlet pressure when the piston is at TDC
p_3	Peak pressure
PFI	Port fuel injection
P_0, T_0	Pressure and temperature of the system at the dead state condition
P_v	Static pressure at the downstream of inlet valve (Pa)
$\dot{P}_u, \dot{P}_b$	Rate of pressure change of unburned and burned mixtures (Pa/degree)
P_u, P_b	Pressure of unburned and burned mixtures (Pa)
P_{EOE}, T_{EOE}	Pressure and Temperature of mixture at the end of expansion respectively
$\dot{Q}_{wu}, \dot{Q}_{wb}$	Rate of heat transfer from unburned and burned mixtures to chamber wall (J/degree)
RON	Research octane number
R	Gas constant (J/kg-K)
R_c	Radius of cylinder (m)
SP_m	Stagnation pressure at the upstream of inlet valve in the manifold (Pa)
SI	Spark ignition engine
SFC	Specific fuel consumption (kg/kW-hr)
$S - S_0$	Entropy change of the system when it reaches dead state condition (J/K)
S_u, S_b	Entropy of unburned and burned mixtures (J)
s_u, s_b	Specific entropy of unburned and burned mixtures (J/kg)
S_l	Laminar Flame Speed (m/s)
S_{l0}	Laminar Flame Speed at standard condition P_0, T_0 (m/s)
$\dot{T}_u, \dot{T}_b$	Rate of temperature change of unburned and burned mixtures (K/degree)
T_u, T_b	Temperature of unburned and burned mixtures (K)
T_w	Temperature of cylinder wall (K)

U_t	Turbulent eddy velocity Scale (m/s)
U_v	Velocity of charge at the inlet valve (m/s)
$V - V_0$	Volume change of the system when it reaches dead state condition (m^3)
V_d	Swept volume (m^3)
V	Instantaneous in-cylinder volume (m^3)
V_u, V_b	Volume of unburned and burned mixtures (m^3)
WOT	Wide open throttle
W_c	Work done per cycle (J/cycle)
x_b	Mass fraction burned
Φ	Equivalence ratio
γ	Ratio of specific heats
λ	Excess air ratio
ΔA	Change of availability of the system (J)
θ_{pmax}	Crank angle at which peak pressure reaches (degree).
$\theta_{nhrrmax}$	Crank angle at which maximum net heat release rate reaches (degree).
ρ_u, ρ_b	Density of unburned and burned mixtures (kg/m^3)
τ	Turbulent eddy time Scale (s)
θ_{SA}	Spark timing crank angle (degree)
$\Delta\theta_d$	Flame development angle (degree)
$\Delta\theta_b$	Rapid burn angle (degree)

Contents

List of Figures

List of Tables

1 Introduction:

1.1 Background of Lean Combustion

The internal combustion (IC) engine has been a primary power source for most of the transportation systems and small power generating stations, around the world for many decades. As the world has been growing very rapidly, the use of IC engines has tremendously increased in the last several decades. The growth of the IC engine has brought many difficulties. The IC engines operate on naturally occurring fossil fuels, which are non-renewable in nature. In the 1960's the automobile began to be associated with several problems such as air pollution, smog and the destruction of the ozone layer. Currently, global warming is attributed to emissions of gases like methane and carbon dioxide that increase the greenhouse effect. Oil crisis has led to shortages of fuel and increased prices. With the current use of these fossil fuels, it is estimated that fossil fuel reservoirs will be depleted completely in the next 50 to 70 years. All of these factors have had an impact upon engine development with the governments tightening the emission regulations. Today's legislation has been pushing current engine research towards two key parameters; efficiency improvements (efficient use of fuel chemical energy) and emissions reduction.

Lean burn combustion is one of the promising technologies that can improve the performance and emission of an internal combustion engine. Lean burn refers to a burning of fuel with an excess of air in an IC engine. The AFR needed to stoichiometrically combust gasoline is 14.6:1. The burning of a mixture with greater AFR than 14.6:1 is considered as lean burning. Lean burning with AFR within an accepted limit may improve thermal efficiency and reduce exhaust emission. However, it is often limited by the onset of unacceptable cyclic variation in the overall combustion rate. As the AFR of a homogeneous mixture is moved lean of stoichiometric, the associated change in mixture properties favours improved thermal efficiency and reduced exhaust emission. During a part load operation, lean mixture improves overall efficiency by reducing throttling losses. Pollutant emissions are reduced because flame temperatures are typically low, reducing the thermal nitric oxide formation. In addition, for hydrocarbon combustion, when leaning is accomplished with excess air, complete burnout of fuel generally results, reducing hydrocarbon and carbon monoxide emissions. However, a corresponding decrease in heat release rates causes a large cycle to cycle variation in power and ultimately, unaccepted partial burn and an occasional misfire overwhelm the advantage

in lean mixture properties. The effect of lean mixture on the thermodynamic cycle processes has been explored quantitatively in this thesis.

A lot of research has been taking place in the field of Lean combustion, but most of it focuses on an evaluation of performance and emission characteristic of lean burn SI engine and evaluation of different techniques which tend to extend the operational range of lean burn. Wang et al [1] have studied an effect of hydrogen blending on the performance of SI engine at WOT. Ceviz & Yüksel [2] have compared lean burn LPG and Gasoline engines in terms of cyclic variability. Ismail and Mehta [3] evaluated the effects of fuels and combustion-related processes on an exergetic efficiency of combustion by using SI engine simulation. However, limited research has been done on how lean combustion affects an individual process in the actual operating cycle of an SI engine. Improvement in the performance of a lean burn engine is not sufficiently justified by quantifying the different losses occurred in the lean operating cycle due to different thermodynamic effects. The cyclic variability in the combustion process is also not presented in a way so as to compare the stability of two different sized engines or same engine with different atmospheric conditions.

1.2   Background of Numerical Simulation

A mathematical model is a description of a system using mathematical expressions and the process of developing a mathematical model is termed mathematical modelling. A model may help to explain a system and to study the effects of different parameters, and to make predictions about the behaviour.

The evaluation of performance of IC engines could be done in more detailed manner by applying second law of thermodynamics to the averaged operating thermodynamic cycle of IC engine. But, it is cumbersome and costly affair to conduct experiments at every operating condition to do the very analysis. Numerical simulation is one of the methods by which thermodynamic cycle can be simulated easily and with considerable accuracy for different operating conditions. So it is a very productive method to predict the performance of the IC engine and second law analysis can be easily applied to this simulated cycle to understand the reasons behind the behaviour of the engine at that condition. The outcomes of this analysis can be utilized to optimize the performance of the engine. Engine designers always need this numerical simulation tool to design better and optimized engines. These models also enrich our understanding of the processes occurring in the operation of an IC engine.

1.3   Objectives of research

This research thesis has two main objectives.

1. To investigate the parameters that facilitates lean burning in an SI engine and their implications on the cyclic variability and availability destruction.

2. To develop a MATLAB code which can predict the performance of SI engine under different operating conditions as well as investigate the availability destruction during each process of thermodynamic cycles. The code is available in appendix section.

The focus of the first part of the study is to find out the operational envelope of an existing facility of an SI gasoline engine equipped with PFI injection running under lean burn conditions. The effect of compression ratio on the lean combustion is also investigated. It is proposed to analyse engine combustion stability through cyclic variations in the combustion related parameters under lean operating conditions at part loads. Availability analysis is performed over each process and sub process of operating cycle to quantify availability transfer and availability destruction.

The second part of the study will focus on developing a mathematical model to simulate a thermodynamic operating cycle of four stroke SI engine. A detailed thermodynamic analysis is performed by using first and second law of thermodynamics to evaluate the performance of SI simulated cycle under given operating conditions.

This study will help in understanding the basic knowledge of lean combustion and associated cyclic variations. Overall, it will assist in improving the performance of lean burn SI engine by knowing the operating parameters that affect the cyclic variations and availability balance. The Numerical simulation model will assist in comprehension of different processes that affect the performance of IC engines.

1.4   Motivation:

Today's world, gasoline and diesel engines are most commonly utilized among other IC engines, despite alternative fuel engine technology have been showing promising potential. Diesel engine usually operates on the overall lean equivalence ratio over the entire operating range. So it offers greater thermal efficiency, but produces the greater amount of exhaust emissions like particulate matter and smoke. Exhaust emissions can be lowered, but requires sophisticated and costly equipment for treating exhaust gases. As opposite to this, gasoline

engine operates on the equivalence ratio ranging from 0.8-1.2. Because of the narrow operating range, it gives low efficiency at part load condition. Exhaust emissions can be lowered to a very low value by using widely used technology, 3-way catalytic converters.

Recent technological developments are focussed on improving overall engine efficiency and reducing exhaust emissions within accepted standards. Gasoline engine operated on lean AFR mixture may give combined benefits of a diesel engine (higher efficiency) and a stoichiometric gasoline engine (lower exhaust emissions).

As discussed above in couple of paragraphs, to keep up with the recent technological development in IC engines, students should know the basic knowledge of IC engine in detail. Numerical simulation is a very easy and cheap tool in this context to groom the students. Though commercial software is available, they are not able to provide the information about what is happening actually in background.

In-cylinder pressure measurement device used does not measure pressures precisely and accurately during intake and exhaust processes. The effect of this error in pressure measurement on the each test result is considered identical for each test, since the study is being carried out relatively. The engine is highly susceptible to unstable operation at 2kg load i.e. approximately zero throttle opening condition. So experiments are conducted on loads varying from 4kg to 8 kg only.

This chapter introduces lean combustion and simulation model in SI engine briefly. It also explains the necessity and aim of this thesis. The next chapter will be the review of research done in the field of lean combustion and Numerical simulation of SI engine.

2 Literature Review

2.1 History

Lean combustion was considered only with regards to explosion hazards until the late 1950s, when lean flames were introduced as useful diagnostic tools for identifying detailed reaction behaviour. However, it was not until the late 1960s that lean combustion began to be discussed as a practical technology, particularly for trying to improve fuel economy and reduce emissions from spark-ignited reciprocating internal combustion engines. The emission requirements of CO, HC and NOx kept lean combustion a viable and important technology for IC engines for almost two decades [9].

The extreme of lean combustion is represented by an in-flammability limit. Firstly, Davy reported lean limits of the in-flammability in his efforts to prevent explosions of methane gas in coal mines. In modern terminology, this represents an equivalence ratio range. Further, Parker added that the limit of in-flammability depends on the vessel used for the test, among other experimental variations. It also depends on the oxidizer and diluents composition. Mason and wheeler found that lean in-flammability limit depends on the chemical and physical properties of the reactant mixture, the temperature of the mixture, details of the combustion vessel and ignition method. However, in IC engines, the extreme of lean combustion is represented by the stable lean operating limit. It is the limit of lean AFR beyond which COV in IMEP increases above 2% for low loads & 10% for high loads and drivability of the engine becomes difficult [9].

The main limitation to lean combustion is increasing cyclic variations at high AFR, which makes combustion unstable and causes an increase in hydrocarbon emission. Minimization of a cycle to cycle variation is a key factor in effective operating near to or extending the stable lean limit. Many different methods for this have been suggested by the researchers. Ceviz & Yuksel [2] have studied a cyclic variation of LPG and Gasoline lean burn SI engine. Cylinder pressure, IMEP, MFB and combustion duration have been presented in relation to cyclic variation. Variations in the CO, CO2 and HC emissions have also been discussed. The findings showed that LPG reduces the cyclic variability and exhaust emission at the same operating condition compared to gasoline. The same study has been done by many other people with different fuels possessing better combustion characteristics than that of pure gasoline. Badr et al. [7] carried out a parametric study on the lean operating limits of an SI

engine using propane and LPG as fuels, and effects of compression ratio, spark timing, intake pressure and temperature on engine operational limits were examined. The results showed that MBT timings need to be advanced for a lean mixture to provide more time for completion of the reactions. The engine speed and intake temperature increase lean misfire limit. Ayala et al. [8] investigated the effect of different operating variables on the engine efficiency under lean condition. The finding shows that increase in engine efficiency and COV in IMEP as AFR increases. The increase in COV is small at the beginning, and after a certain AFR value is reached, it rises sharply. Engine efficiency starts decreasing after the same AFR. Burn durations are evaluated based on the experimental results over a wide range of operating conditions. It showed that 2% COV in IMEP, which is often used as the stability limit, is corresponding to about 40 degrees of 0-10% burn duration. By analysing burn duration and IMEP of lean combustion with fixed average load, the authors found that the distribution of 0-10% burn duration keep normal distribution even though the combustion becomes more unstable. However the average value of 0-10% changes significantly as lean level increases. The distribution of 10-90% burn duration is close to normal distribution when the leanness of AFR is low. When lean level increases, the distribution becomes asymmetric and small amount of cycles with extremely small IMEP values appear. These small IMEP cycles are the results of partial burn or misfire which increases cyclic variations. The findings also show that the cycle to cycle variability of combustion has close relation to the early flame kernel growth. This can be justified since the average values of 0-10% burn duration distributions change significantly under different lean conditions. However, gasoline has been widely used fuel in SI engine, the researchers focussed on improving the characteristics of gasoline by blending of fuels.

Wang et al. [1] studied lean burn performance of hydrogen blended gasoline engine at the WOT condition. The engine was operated at 1400rpm and two hydrogen blending levels of 0% and 3%. The combustion and performance parameters have been presented. The results showed that hydrogen addition enhances combustion and improves thermal efficiency at lean conditions. It reduces cyclic variation and emission such as HC and CO. However NOx emissions are increased due to the raised cylinder temperature. The performance of such blended fuel lean burn engine can further be improved by optimizing the combustion parameters. Goldwitz [4] studied combustion optimization in a hydrogen enhanced lean burn SI engine. Combustion was optimized by varying ignition systems, charge motion in the inlet ports and mixture preparation. The results indicated that optimization of the combustion system in conjunction with hydrogen enhancement can extend the lean limit of operation by

roughly 25% compared against the baseline configuration. Nearly half of this improvement may be attributed to improvements in the combustion system. The inductive ignition system in conjunction with a high tumble motion inlet configuration leads to the highest levels of combustion performance. Furthermore, hydrogen enhancement affects a nearly constant absolute improvement in the lean misfire limit regardless of baseline combustion behaviour. Mahato [5] studied lean burn and stratified combustion in small utility engine. In this, the effect of spark plug variation, load control and charge stratification on cyclic variability and exhaust emission have been evaluated. The findings showed that spark discharge energy had a major influence on engine performance. The initial stages of flame kernel development are largely influenced by sparking characteristics. Low load operations, increase cyclic variability suggesting that initiating a stable flame gets harder with decreasing charge density. Charge stratification does not affect the 0-10% burn duration noticeably, a significant reduction in the 10-90% burn duration was observed, indicating a faster burn cycle. An engine operation optimization study showed that exhaust emissions are reduced below regulatory limits without the use of catalytic converters and overall fuel economy increases by about 6% over baseline configuration. Charge stratification improves the performance of lean burn SI engine by extending its lean operational range by repetitively initiating combustion of slightly rich mixture pockets produced in the vicinity of the spark plug.

Peres & T.J [6] evaluated port fuel strategies for a lean burn gasoline engine at low load and speed, to extend the limit of lean combustion through the introduction of charge stratification. Novel port fuel injection strategies such as dual split injection, multiple injections, and phased injection were developed to achieve this goal. Each strategy is analysed through parameters such as combustion duration, combustion stability, and unburned hydrocarbon emission, to propose the optimum strategy suitable for extension of the lean operation. Combustion stability was improved for lean AFR extending up to 22:1 with 1800rpm and 1.8 GIMEP by using phased and multiple injection strategies.

Availability balance analysis of actual lean burn SI engine has not been done extensively and there has been more interest in the availability analysis of the simulated thermodynamic cycle of SI engine. Rakopoulos & Giakoumis [11] reviewed literature concerning the application of the second law of thermodynamics to IC engines. The identification and quantification of the irreversibility of various processes and subsystems have been discussed. Some interesting cases of low heat rejection engines, use of alternative fuels and transient operation have also been reviewed along with various parametric studies. Ismail & Mehta [3] evaluated the effects

of fuel and combustion related processes on exergetic efficiency. A method of estimating the availability destruction and exergetic efficiency of combustion has been discussed for four classes of fuels like hydrogen, hydrocarbons, alcohols and biodiesel surrogates. The results showed that availability destruction is greater for heavier hydrocarbon and oxygenated fuels with higher oxygen fraction. The unsaturated hydrocarbon fuels give poor exergetic efficiency as a significant fraction of the fuel availability is lost in the products. Leaner mixtures provide increased exergetic efficiency. It is also found that preheating the reactants tends to mitigate availability destruction. Rezapour [12] investigated availability analysis of a bi-fuel SI engine model for improvement in its performance. The engine model is developed in a two zone model, to compute thermodynamic properties and equilibrium product composition. The Simultaneous model based on availability analysis is also developed to investigate the engine performance. The flow of different availabilities in the engine operating cycle has been presented for gasoline and CNG mode. The parametric studies have been carried out to evaluate the effects of equivalence ratio, spark timing and engine speed on the availability balance. The results showed that lean mixtures improve exergetic efficiency. Exegetic efficiency does not vary significantly with engine speed. The optimum spark advance gives maximum exergetic efficiency.

A lot of Engine simulation models have been attempted and developed successfully by many researchers for performance and emissions predictions till date which vary from simplistic to more sophisticated models. Benson et al. [15] developed a full-fledged simulation model of a four stroke cycle, single cylinder, SI engine in 1974. The model was capable of handling gas dynamics in intake and exhaust manifold along with chemical reactions in the exhaust pipe. Two zone combustion model and chemical equilibrium composition of products were taken into consideration. The model could predict the NO compositions in good agreement with the experimental results for different equivalence ratios. Benson & Baruah [16] further extends this approach to multi-cylinder SI engine. The authors concluded that the simulation programs developed from single cylinder combustion models together with gas exchange models with allowance for variation of composition and specific heats along path lines may be used in multi-cylinder engine calculations. In late 70's computers were not so powerful to handle these complicated models, it became time consuming and costly affair to use these models. So researchers focussed to develop more simplistic models, which are easy to understand and moderate or less in accuracy for academia. In opposite, the models for commercial use have been evolving in more complex ways to match up with the actual engine behaviour. In more recent, researchers have applied this modelling tool for different fuels combustion cycle to predict the potential of these fuels as an alternative fuels to conventional one. The effect of

variable valve timing, variable valve lift, valve deactivation, supercharging, EGR etc. have been studied by using this tool. Bayraktar [18] developed a simplistic, two zone mathematical model in 2003 by using combinations of analytical and empirical equations to predict the performance of SI engine. The model was able to simulate the thermodynamic cycles for different combustion geometries with reasonable agreement with that of experiments.

The indispensable role of these mathematical modelling is to analyse each and every sub process and process through the perspective of exergy law of thermodynamics. Rakopoulos & Giakoumis [11] reviewed second law analyses applied to IC engine simulation. Different availability transfer and destruction terms have been presented for each thermodynamic process in the SI and CI engine. Karimi & Kamboj [22] studied effect of fuel and compression ratio on energetic and exergetic efficiency of SI engine simulation. Detailed analysis of availability destruction during each process is being performed. The results show that maximum availability destruction occurs during combustion and it decreases with increase in compression ratio. The shortcoming of the formulation is that heat addition process is considered as a constant volume process and heat transfer effects are not included during compression and expansion process.

2.2 Premixed Lean Combustion

2.2.1 What is lean Combustion
A characteristic feature of the spark-ignition engine is that combustion occurs as a premixed flame, i.e., a flame front moves through a mixture of fuel and air which has been premixed to be at, or very near, stoichiometric conditions. The premixed air-fuel charge for a conventional spark-ignited engine is homogeneous in composition, providing a uniform equivalence ratio everywhere in the cylinder. This air fuel ratio must be kept within the combustible limits of the mixture, somewhere between the rich limit and the lean limit of the particular fuel-air mixture being used. The lean limit is of practical importance, however, since lean operation can result in higher efficiency and can also result in reduced emissions. The lean limit is where misfire becomes noticeable, and is usually described in terms of the limiting equivalence ratio, Φ, which will support complete combustion of the mixture. In most engines, a value of $\Phi=0.7$ is usually the leanest practical mixture strength. The requirement for a near constant air-fuel ratio at all operating conditions result in one of the main weaknesses of the spark-ignition engine. For part-load operation, as the supply of fuel is reduced, the supply of air must also be reduced to maintain the correct air-fuel ratio. In order to achieve this, the air supply must be throttled using the throttle valve. This throttling of the mixture results in additional

pumping losses (work required to pump the mixture past a partially closed throttle). This throttling operation results in poor part-load efficiency of the spark-ignition engine compared to the un-throttled diesel engine. The homogeneous fuel-air mixture always present in the cylinder results in another characteristic of the spark-ignition engine - knock. Knock occurs when unburned mixture self-ignites due to the increasing cylinder pressure as a result of combustion of the bulk of the mixture. Persistent knock causes very rough engine operation, and can cause engine failure if it is not controlled. This problem is exacerbated by high compression ratios and fuels, which readily self-ignite at the temperature achieved following compression (low octane fuels). Knock is the principal reason why spark ignition engines are usually limited to a compression ratio of less than approximately 10:1 with currently available fuels. This relatively low compression ratio result in lower thermal efficiency compared to diesel engines operating at approximately twice the compression ratio [9].
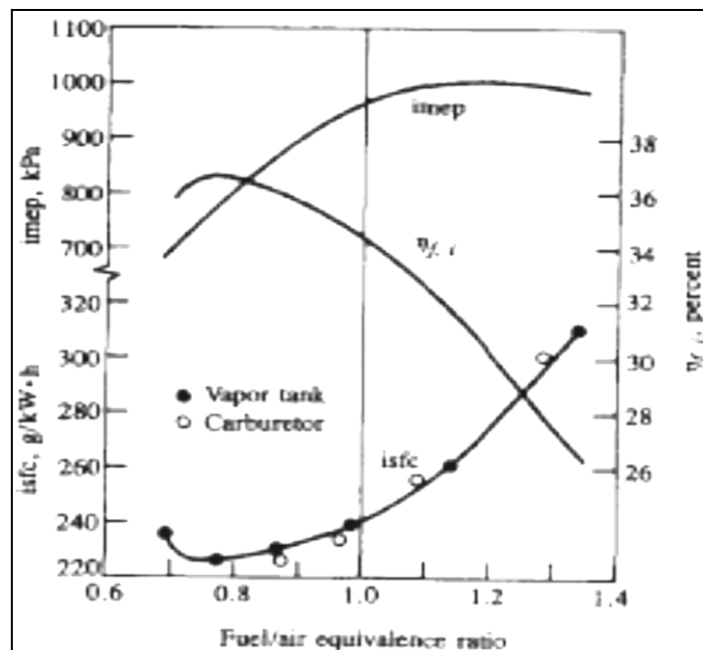
Figure 1: Effect of the equivalence ratio variations on IMEP, SFC and fuel conversion efficiency of a 6 cylinder spark ignition engine at WOT and 1200 rpm [10].

The theoretical analysis indicates that for high efficiency, the ratio of specific heats of the working fluid should be as high as possible. In practice, it turns out that γ for air (1.4) is greater than γ for the air-fuel mixture for typical hydrocarbon fuels. This means that the value of γ will be higher for mixtures with more air (i.e., lean mixtures) than for rich mixtures. It indicates that thermal efficiency is higher for lean mixtures (mixtures with excess air) than for rich mixtures. But in practice length of the burning time, or combustion duration, also has

an effect on thermal efficiency. Since burning rates are generally highest close to the stoichiometric air-fuel ratio, operating an SI engine lean, with an equivalence ratio of less than one, results in increased combustion duration which then reduces power output and thermal efficiency, thereby tending to counteract the increased efficiency of lean operation due to an increased ratio of specific heats [10].

The emission levels of a spark-ignition engine are particularly sensitive to air-fuel ratio. At rich air-fuel ratios, with Φ greater than 1.0, unburned hydrocarbon levels (HC) are high since there is not enough air to completely burn all the fuel. Similarly, CO levels are high, because there is not enough oxygen present to oxidize the CO to CO_2. For lean mixtures, with Φ less than 1.0, there is always excess air available, so that CO almost completely disappears, while HC emissions reach a minimum near $\Phi = 0.9$. For Φ less than about 0.9, some increased misfiring occurs because of proximity to the lean misfire limit, and HC emissions begin to rise again. The main factor in production of NO is combustion temperature: the higher the temperature, the greater the tendency to oxidize nitrogen compounds into NO. Since the combustion temperature is at a maximum near stoichiometric conditions where $\Phi = 1.0$, and falls off for both rich and lean mixtures, the NO curve takes the bell shape [9].

Lean operation can therefore be used both to increase thermal efficiency, and reduce exhaust emissions. However, there is a lean limit of operation, beyond which it is impossible to maintain reliable ignition and combustion, resulting in an increased cyclic variation in combustion, pressure and misfire.

In order to achieve stable combustion with improved thermal efficiency and reduced emissions even at extremely high lean limits, We might have following techniques which have been developed over a number of years in order to extend the lean limit of operation of a spark ignited, homogeneous-charge engine. These methods are meant to represent the kinds of approaches that can be used to create practical lean-burn spark-ignited engines [9].

> Extending the lean limit through increased turbulence Generation

It is aimed at increasing turbulence generation in the combustion mixture just before ignition and during the combustion process, involves a new combustion chamber designed specifically for lean-burn engines.

> Extending the lean limit through partial stratification

The concept is to produce a small pocket of the relatively rich mixture near the spark plug so that it would ignite more readily than the main, very lean, combustion charge.

➢ Extending the lean limits through fuel blending

The fuels having superior combustion characteristics such as hydrogen, ethanol, LPG etc. can be blended with pure gasoline.

2.2.2 Cyclic variability in lean combustion

It has been observed from the in cylinder pressure data that there exists a substantial variation in the combustion process on a cycle-by-cycle basis even under steady operation of SI engine. Cyclic variations in the lean combustion process are important to study for two reasons. First, since the optimum spark timing is set for the "average" cycle, slower than average cycles have retarded timing, so losses in power and efficiency result. Second, it is the extremes of the cyclic variations that limit engine operations. The slowest burning cycles, which are retarded to optimum timing, are most likely to burn incompletely. Thus, these cycles set the practical lean operating limit of the engine. Beyond this limit, engine efficiency decreases and emissions like HC and CO increase drastically [10].

The cyclic variations in the combustion process are usually caused by variations in mixture motion within the cylinder at the time of the spark, variations in the amounts of air and fuel fed to the cylinder each cycle and variations in the mixing of fresh mixture and residual gases within the cylinder each cycle, especially in the vicinity of the spark plug. Along with that, the cyclic variations in the lean mixture are mainly affected by [10]:

1. Mixture composition

As the mixture is leaned out, the chemical energy density of the mixture and flame temperature decreases. The flame front speed decreases and it becomes thicker. Thus more time is available for heat losses from the inflammation zone; less energy is available to offset these heat losses and the rate of energy transfer into the zone decreases. It makes the formation of stable flame kernel difficult in lean mixtures. The initial stages of flame kernel growth and development vary substantially, since small laminar speed. This causes cyclic variations in the subsequent combustion stages.

2. In-cylinder mixture motion

The in-cylinder mixture motion of an IC engine is highly turbulent. Turbulence is beneficial in that it accelerates combustion by increasing the flame front area and enhancing heat and mass transport between the burned and unburned mixture. But turbulence can cause random variations in the local equivalence ratio, degree of mixture dilution and in the mean velocity cycle by cycle, both in the vicinity of the spark plug and throughout the combustion chamber. Velocity variations contribute in a major way to variations in the initial motion of the flame centre as it grows from the kernel established by the spark, and in the initial growth rate of the flames; they can also affect the burning rate once the flame has developed to fill a substantial fraction of the combustion chamber. Variations in the turbulent velocity fluctuations near the spark plug will result in variations in the rate at which the small initially laminar like flame kernel develops into a turbulent flame.

3. Spark and spark plug effects

As mentioned in the mixture composition, flame kernel growth can be increased by increasing the rate and amount of energy deposited by the ignition system. About 0.2 mJ of energy is required to ignite a quiescent stoichiometric fuel air mixture at normal engine condition by means of a spark. For substantially leaner mixture, and where the mixture flows past the electrodes, an order of magnitude greater energy (~3mJ) may be required. The spark with less energy discharge may result in a partial burn or misfire; giving rise to cyclic variations in the overall combustion process. So to reduce the cyclic variations, a proper ignition system which can provide required ignition energy system has to be chosen for lean operation.

The cyclic variability can be measured in different ways. It can be defined in terms of variations in the cylinder pressure between cycles, or in terms of variation in the details of the burning process. One important measure of cyclic variability, derived from the pressure data, is the coefficient of variation in indicated mean effective pressure [10]. It is usually expressed in percent:

$$COV_{imep} = \frac{\sigma_{imep}}{imep} * 100$$

It defines the cyclic variability in indicated work per cycle, and it has been found that vehicle driveability problems usually result when COV_{imep} exceeds about 10 percent.

2.2.3 Availability Analysis

The first law based methods for evaluating IC engine performance do not explicitly identify those processes within the engine systems that cause unrecoverable degradation of the thermodynamic state of the working fluid. However, second law based analysis methods do provide the capability to identify and quantify this unrecoverable state degradation. Thus cause and effect relationships which relate these losses to individual engine processes can be determined. The first law analysis approaches are based on the fact that energy is conserved in every device and process. Thus, they take account of the conversion of energy from one form to another: e.g., chemical, thermal, mechanical. Although energy is conserved, second law analysis indicates that various forms of energy have differing levels of ability to do the useful mechanical work. This ability to perform useful mechanical work is defined as availability [10].

The availability of a system at a given state is defined as the amount of useful work that could be obtained from the combination of the system and its surrounding atmosphere, as the system goes through reversible processes to reach thermal, mechanical and chemical equilibrium with the atmosphere. It is a property of the system and its surrounding atmosphere. Usually, the terms associated with thermo-mechanical and chemical equilibration are differentiated and calculated separately. For an open system experiencing heat and work interactions with the environment, the thermo-mechanical availability is given by,

$$A_{tm} = (H - H_0) + P_0(V - V_0) - T_0(S - S_0)$$

Availability is not a conserved property; availability is destroyed by irreversibility in any process the system undergoes. The change in availability of any system undergoing any process where work, heat, and mass transfer across the system boundary occur can be written as,

$$\Delta A = A_{in} - A_{out} - A_{destroyed}$$

When availability destruction occurs, the potential for the system to do useful mechanical work is permanently decreased. Thus to make a proper evaluation of the processes occurring within an engine system, both energy and availability must be considered concurrently [10].

2.2.3.1 Effect of Equivalence ratio
The fuel-air cycle with its more accurate models for working fluid properties can be used to examine the effect of variations in the equivalence ratio on the availability conversion efficiency. During combustion, entropy increase is the result of irreversibilities in the

combustion process and mixing of complete combustion products with excess air. The significance of these combustion related losses- the destruction of availability that occurs in this process is shown in fig. 2. The loss of availability increases as the equivalence ratio decreases. The combustion loss is a stronger function of the rise in temperature and pressure which occurs than of the change in the specific heat ratio that occurs [10].
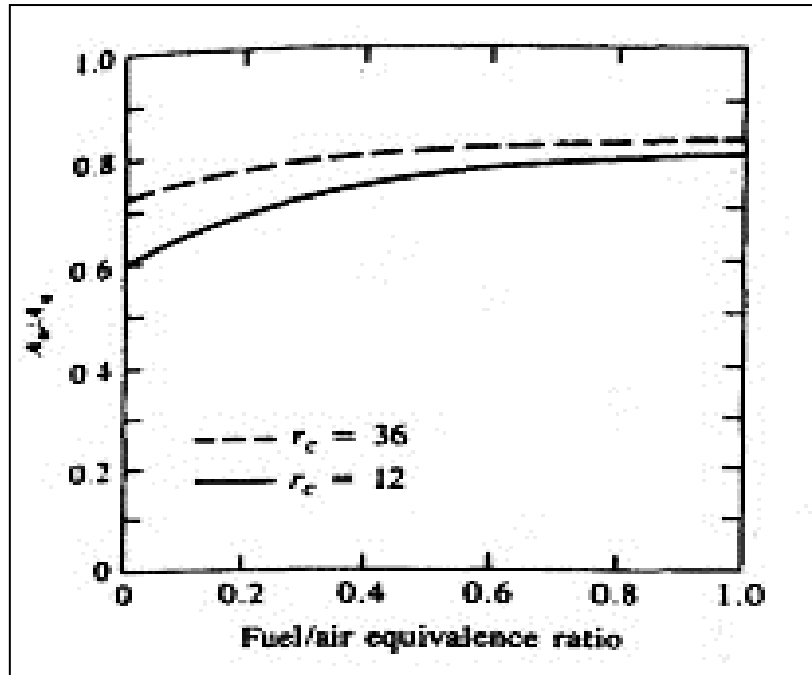
Figure 2: Ratio of availability of burned gases after CV combustion to availability of unburned charge before combustion as a function of equivalence ratio [10].

What is the reason behind increasing engine efficiency with decreasing equivalence ratio then? The reason is that the expansion stroke work transfer, as a fraction of the fuel availability, increases as the equivalence ratio decreases; hence, availability lost in the exhaust process, again expressed as a fraction of the fuel availability, decreases. The increases in the expansion work as the equivalence ratio decreases more than offsets the increase in the availability lost during combustion. The availability accounting per mass of fuel for each process for different equivalence ratios is shown in the following Figure 3.
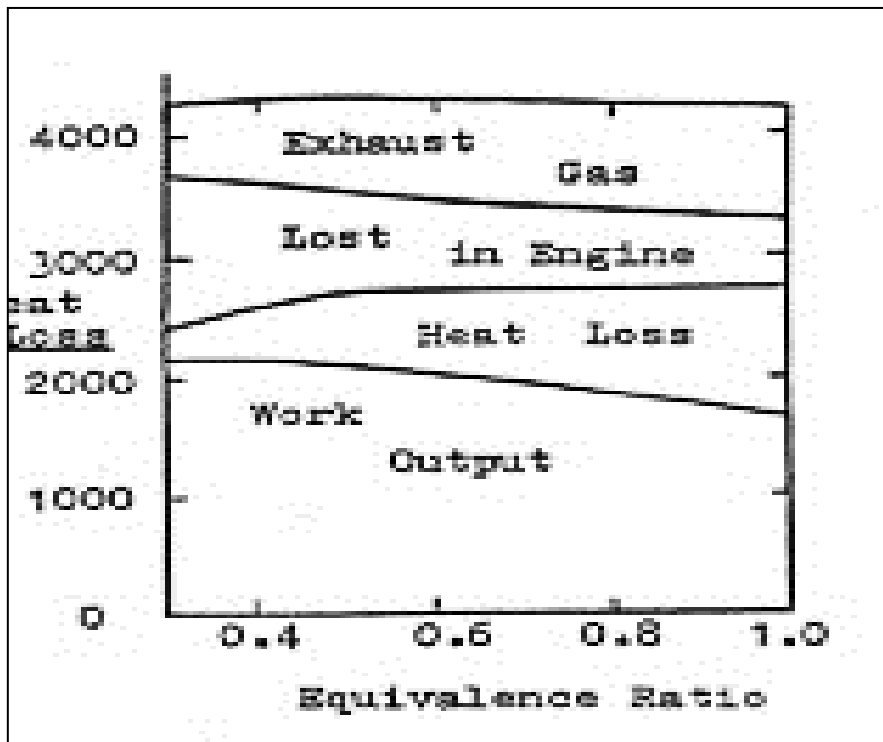
Figure 3: Availability accounting per mass of fuel for different processes as a function of equivalence ratio for dissociated methanol [10].

2.2.4 Exhaust Emissions

One of the most important variables in determining SI engine emissions is the equivalence ratio. The SI engine has normally been operated close to stoichiometric, or slightly fuel rich, to ensure smooth and reliable operation. Figure (4) shows qualitatively how NO, CO, and HC exhaust emissions vary with equivalence ratio. It shows that leaner mixtures give lower emissions until the combustion quality becomes poor, when HC emissions rise sharply and engine operation becomes erratic. The shapes of these curves indicate the complexities of emission control.
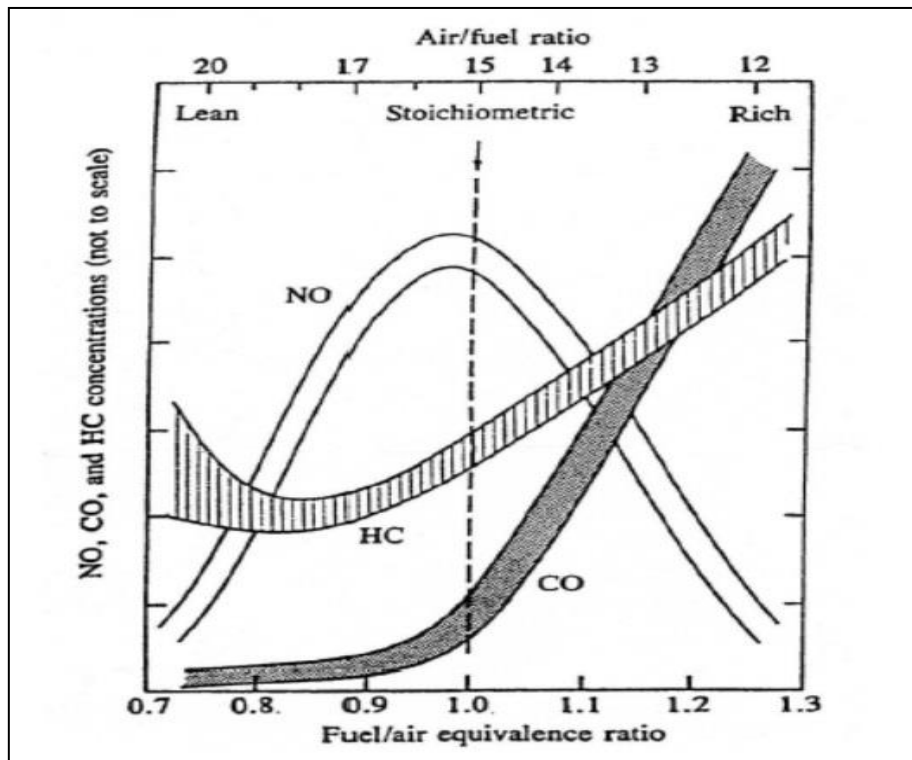
Figure 4: Variation of HC, CO, and NO concentrations in the exhaust of a conventional SI engine with equivalence ratio [10].
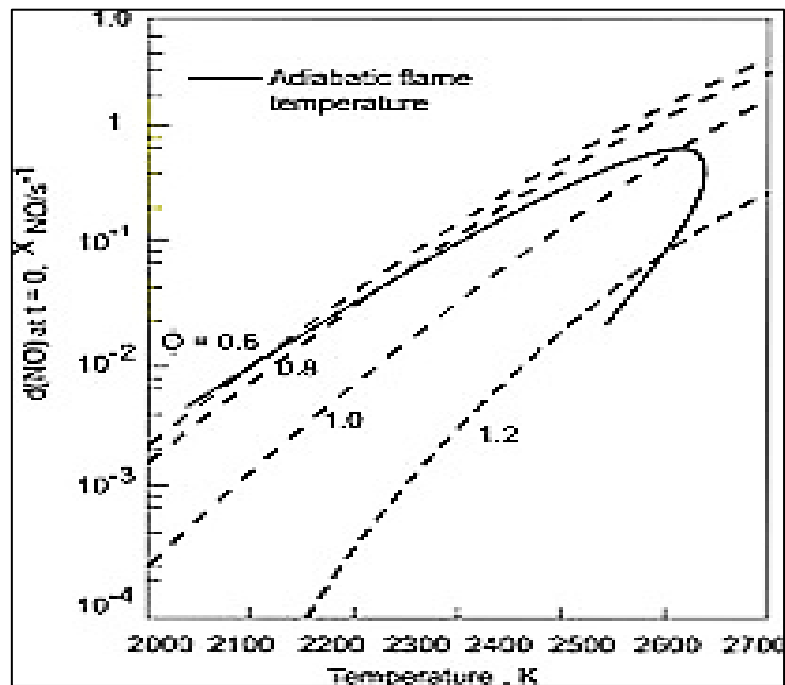
Figure 5: Initial NO formation rate as a function of temperature for different equivalence ratios and 15.20 bar pressure [10].

The nitric oxide and nitrogen oxide are usually grouped together as NOx emissions. The principal source of NO emissions in SI engine is the oxidation of atmospheric nitrogen. NO forms in both the flame front and the post flame gases. The NO formation in the post flame gases almost always dominates any flame front produced NO. The kinetics of NO formation shows its strong dependence on temperature. High temperature and high oxygen concentrations result in high NO formation rates. Figure (5) shows the NO formation rate as a function of gas temperature and equivalence ratio in post flame gases [10].

For lean mixtures, CO concentrations in the exhaust vary little with equivalence ratio and are of order of 10^{-3} mole fraction.

This chapter gives an overview of research that has been done in the field of lean combustion and numerical simulation in SI engine. It summarizes what is lean combustion, how it enhances the performance of SI engine, what are the limitations to it and methods to achieve stable lean operation. It also gives brief information about cyclic variability, availability analysis, and exhaust emissions in a SI engine.

3 Experimentation

3.1 Experimental Setup

A two cylinder optical access research engine shown in Figure (6) is used for this study. Out of two cylinders, one is working cylinder in which combustion occurs continuously, called thermodynamic cylinder and other cylinder is optically accessed in which combustion occurs whenever it is required. This study does not consist of any optical diagnosis of the combustion process, so the optical accessed cylinder is cut off throughout the experimentation. The combustion chamber geometry is a toroidal bowl in a piston top, ensuring fast burning and compact combustion chamber. The engine is equipped with two overhead camshafts driving 4 inlet valves (2 for each cylinder) and 4 exhaust valves.
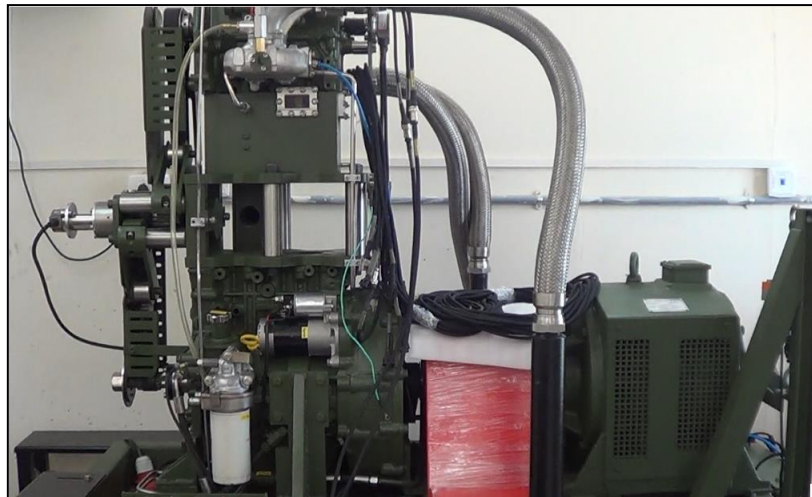
Figure 6: Optical access research engine

An electronically controlled throttle body is used to control flow of air to the engine. It is mounted on the inlet manifold upstream to the positions of PFI injectors. The air flow rate is measured by an air box instrument, wherein, air from a large volume box passes through the orifice plate and the pressure drop across the orifice is measured. This pressure drop signal is fed to the ECU to calculate the accurate air flow rate.

A fuel flow rate is measured by an automatic volumetric fuel flow meter. It consists of two sensors, one at the bottom and another at the top of a 100 ml measuring burette. The fuel is made to pass through this burette and time required for emptying the burette is recorded and fed to the ECU. The ECU then calculates the mass flow of fuel based on density of fuel fed

to it manually. The fuel properties are mentioned in the Table 2.The specifications and valve timings of the engine are given in the Table 1.

No of running cylinders	1 out of 2
Stroke (mm)	100
Bore (mm)	94
Connecting rod length (mm)	235
Compression ratio	10:1
Speed range (rpm)	1000-1200
Inlet open (degree)	5 ATDC
Inlet close (degree)	21 ABDC
Exhaust open (degree)	25 BBDC
Exhaust close (degree)	9 BTDC
Injection system	PFI
Injection pressure (bar)	3
Injection timing (degree)	-90 before start of intake stroke
Spark plug	TVS
Ignition system	Ignition coil system

Table 1: Specifications of research engine

Fuel property	**Value**
Name	Gasoline
Octane rating	~91 RON
Density (kg/m^3)	740
Calorific value (kJ/kg)	44000

Table 2: Properties of a fuel

The in-cylinder pressure is measured using a piezoelectric pressure transducer. It is fitted to the cylinder head, receiving gas pressure through a passage drilled in the head, up to the centre of the cylinder head, opened to the combustion chamber. An eddy current dynamometer is directly coupled to the engine's crankshaft to apply and measure the load on the engine. Its load range varies from 0kg to 10 kg.

The engine is equipped with PFI injection system. It consists of PFI driver module and PFI kit, which control spark timing, injection pressure, injection timing and duration. The schematic diagram of PFI system is shown in Figure (7).
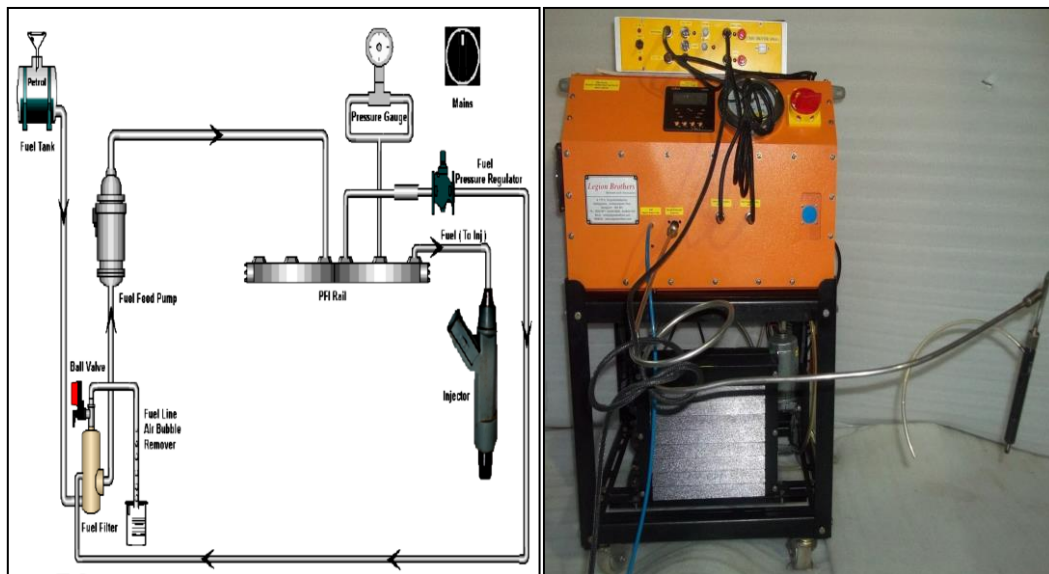
<div align="center">(a)   (b)</div>

Figure 7: PFI system. (a) Schematics of fuel flow in PFI; (b) PFI kit

The acquisition software is legion brother's software. This system allows real-time, on screen display of recorded parameters such as in-cylinder pressure, exhaust gas temperature, temperatures of cooling water to the engine and the calorimeter. It also displays calculated parameters such as air-fuel ratio, volumetric and brake thermal efficiency. For every test point, pressure data is recorded for 400 consecutive cycles and averaged. The parameters like IMEP, peak pressure etc. are calculated for each cycle and then averaged.

3.2 Experimental Procedure

3.2.1 Test methodology

It is advisable to read the operating and safety manual of research engine, provided by the engine supplier before embarking any work on an engine first time. It is necessary to attend certain daily check points for better and uninterrupted operation, before cranking the engine.

Before each test, it is required to warm up the engine for approximately 10 minutes to ensure a steady state operation. The spark plug is regularly cleaned for better performance during lean mixtures.

3.2.2 Test procedure

The focus of this study is to evaluate the performance of lean operation of PFI equipped gasoline engine (CR=10) at different loads and constant speed. The load varies from 4kg to 8kg in the increment of 2kg and the speed is kept at 1100(±50) rpm. Firstly, ignition timing swing is performed to determine the MBT timings for each load with air fuel mixture being stoichiometric. Then, at each load, air fuel ratio swing is conducted from 14:1 to 22:1 with ignition timing fixed to their respective stoichiometric MBT. The Performance, cyclic variability and availability parameters are calculated for each air fuel ratio and load conditions.The same tests are repeated on the engine with compression ratio increased to 12.

The cyclic variability is measured in terms of COV in indicated mean effective pressure normalised by inlet pressure and peak pressure. The IMEP is calculated for each cycle as below,

$$IMEP = \frac{W_c}{V_d} \ \& \ W_c = \oint P \, dV$$

The COV in NIMEP1 and COV in NIMEP3 are calculated as per the formula defined in the cyclic variability section. To measure the cyclic variability in the combustion process, the net heat release rate is given by,

$$\frac{dQ_{ch}}{d\theta} = \frac{\gamma}{\gamma-1} * P * \frac{dV}{d\theta} + \frac{1}{\gamma-1} * V * \frac{dP}{d\theta} \tag{1}$$

The combustion duration is measured in crank angle. It is defined as the count of crank angles between spark discharges and ceasing of net heat release rate event.

The basic approach is used to evaluate average rate of availabilities change during different processes of SI engine. It is as follows [23],

$$A_{in} = (1.033 * m_f * LHV)/3600; \tag{2}$$

$$A_{CW} = (m_w/3600) * \{(c_{pw} * (T_{wo} - T_{wi}) + (T_0 * (c_{pw} * \ln\left(\frac{T_{wi}}{T_{wo}}\right)))\}; \tag{3}$$

$$A_{ex} = Q_{ex} + [(m_{ex}/3600) * T_0 * \{\left(c_{pex} * ln\left(\frac{T_0}{T_{exo}}\right)\right) - (R_{ex} * \ln(\frac{P_0}{P_{exo}})\}]; \tag{4}$$

$$A_{destroyed} = A_{in} - (A_{shaft} + A_{cw} + A_{ex}); \tag{5}$$

$$A_{efficiency} = \left\{1 - \frac{A_{destroyed}}{A_{in}}\right\} * 100. \tag{6}$$

4 Mathematical Model

This model is formulated on a thermodynamic based analysis. It includes modelling of intake, compression, combustion and expansion processes of single cylinder isooctane fuelled SI engine. The model is based on certain assumptions which make the calculations easy. Since there are some processes which cannot be described by the analytical equations, both analytical and empirical equations have been used in this model to achieve the goal.

4.1 Model Assumptions:

1) A working fluid (mixture of air, fuel vapour and residual burned gas) is assumed as an ideal gas and observes variable specific heat values with temperature.

2) A mixture of air and fuel vapour is considered to form homogeneous mixture with residual burned gases. So thermodynamic state is not a spatial function, but a time dependant function.

3) Combustion is modelled as two zone model separated by a thin reaction flame front. Both unburned and burned zones are assumed as homogeneous mixtures separately.

4) The unburned mixture is considered as frozen mixture and burned mixture is also considered as a frozen mixture with the frozen composition being composition without dissociation.

4.2 Chemical reaction

The fuel used in this modelling is isooctane and oxidizer being ambient air. The basic chemical reaction of this fuel to simulate the burning process is given as,

$$C_xH_y + \frac{(x + {}^y/_4)}{\phi} * (O_2 + 3.76 * N_2) \rightarrow$$

$$\rightarrow xCO_2 + \frac{y}{2}H_2O + \left(\frac{(x + {}^y/_4)}{\phi} - x - \frac{y}{4}\right)O_2 + 3.76 * \frac{(x + {}^y/_4)}{\phi}N_2$$
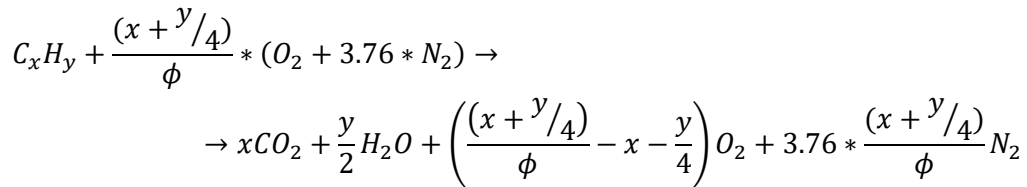
Where, x=8, y=18 and $\phi \leq 1$

Standard molecular weights of C, H, O and N have been taken to calculate molecular weights of the species in the reaction. Thermodynamic properties of each species are calculated from polynomial curve fitting to thermodynamic data provided by Heywood [10] appendix for each species.

4.3 Intake Process

In a conventional SI engine the fuel and air are mixed together in the intake system, inducted through the intake valve into the cylinder. The charge is usually cooler than the intake manifold and so it gets heated as it flows through the manifold.

To model intake process, it is necessary to model flow through the intake system. The intake system consists of air filter, finite length pipe, throttle body, intake manifold &port, and intake valve. It becomes very difficult and complex to model flow through each component, as it is viscous, unsteady, multidimensional, oscillating, and compressible flow. So in this study, length of the intake system is virtually neglected and flow through intake valve is only modelled using quasi-steady model to calculate thermodynamic state in the cylinder during the intake process.

The mass flow rate through a poppet valve is usually described by the equation for compressible flow through a flow restriction. This equation is derived from one dimensional isentropic flow analysis, and real gas flow effects are included by means of calibrated discharge coefficients C_D.[10].

$$\dot{m} = \left(\frac{(C_D * A_R * SP_m)}{\sqrt{(R * ST_m)}}\right) * \left(\frac{P_v}{SP_m}\right)^{\frac{1}{\gamma}} * \sqrt{\frac{2\gamma}{\gamma - 1} * \left[1 - \left(\frac{P_v}{SP_m}\right)^{\frac{\gamma-1}{\gamma}}\right]} \qquad (7)$$

When the flow is chocked, i.e. $P_v/SP_m \leq [2/\gamma + 1]^{\gamma/\gamma - 1}$, the appropriate equation is

$$\dot{m} = \left(\frac{(C_D * A_R * SP_m)}{\sqrt{(R * ST_m)}}\right) * \gamma^{0.5} * \left(\frac{2}{\gamma + 1}\right)^{\gamma+1/2(\gamma-1)} \qquad (8)$$

Where $A_R = \pi * D_v * L_v$ is a curtain area of the intake poppet valve and P_v is supposed to be approximately equal to in-cylinder pressure.

In-cylinder pressure is then computed by following equation

$$\dot{P} = \left((\gamma - 1) * \dot{m} * Cp_u * T\right) - \left(\gamma * P * \frac{\dot{V}}{V}\right) \qquad (9)$$

The equations (7-9) are integrated over crank angle to compute the mass of charge inducted and in-cylinder pressure per crank angle simultaneously. Then, charge temperature is calculated by using ideal gas law.

4.4   Compression process

This process begins at intake valve closure. The inducted charge is positively compressed by the upward motion of a piston in the cylinder, to increase its pressure and temperature. This process ends at the time of spark discharge. Thermodynamic state at the IVC is known from the previous process calculations. The equations (10&11) describing states of the cylinder content are formulated by applying the first law of thermodynamics to closed cylinder volume [10].

$$\dot{T}_u = \left(\frac{B}{A}\right)_u * \left(-\left(\frac{\dot{V}}{V}\right)_u - \left(\frac{\dot{Q}_w}{(B*m)}\right)_u\right) \tag{10}$$

$$\dot{P}_u = \left(\frac{\rho}{\partial\rho/\partial P}\right)_u * \left[-\left(\frac{\dot{V}}{V}\right)_u - \left(\frac{\partial\rho/\partial T}{\rho}\right)_u * \dot{T}_u\right] \tag{11}$$

$$A = \left(1/\rho * \left(\frac{\partial\rho/\partial T}{\partial\rho/\partial P}\right)\right) + Cp_r; \ \& \ B = 1/\frac{\partial\rho}{\partial P};$$

$$\frac{\partial\rho}{\partial P} = \frac{1}{R*T_u} * \left(\frac{Cv_r}{Cp_r}\right); \ \& \ \frac{\partial\rho}{\partial T} = \frac{\rho*Cv_r}{R_u*T_u};$$

Availability rate (J/degree) is given by equation (12),

$$\dot{A}_u = \left(1 - \left(\frac{T_0}{T_u}\right)\right) * \dot{Q}_w - \left[(P_u - P_0) * \dot{V}\right] - \left[T_0 * \left(\dot{S}_u + \frac{\dot{Q}_w}{T_0}\right)\right] \tag{12}$$

The above first order ordinary differential equations (10&11) for $\dot{T}$ and $\dot{P}$ are solved by FDM method, to get T and P values for each crank angle. An ideal gas law provides density of the cylinder content. The equation (12) is integrated over total compression angle to calculate availability change and last term in the equation (12) gives availability destruction.

4.5   Combustion process

Under normal operating conditions, combustion is initiated towards the end of the compression stroke at the spark plug by an electric discharge. Following spark discharge, there is a period during which the energy release from the developing flame kernel is too small for pressure rise due to combustion to be discerned. This period is called ignition delay period

during which flow conditions are laminar like (Near wall effect) and so flame kernel developed by spark discharge grows and propagates, through unburned mixture, approximately smooth and spherical with laminar burning speed. Once it reaches out to bulk unburned mixture away from the walls and interacts with turbulent flow field, the flame front becomes highly wrinkled, distorted in shape and propagates with turbulent burning speed. This period is called rapid burning period during which pressure and temperature rises substantially. The pressure reaches a maximum after TDC but before the cylinder charge is fully burned, and then decreases as the cylinder volume continues to increase during the remainder of the expansion stroke. The flame front continues to propagate until it reaches the farthest combustion chamber wall and then extinguishes. But the experiments have proved that even though flame front extinguishes, there exists localised pockets of unburned gases within the enflamed volume. These pockets will eventually be burned depending upon the availability of oxygen and burn gas dilution. This period is called flame termination. Thus, during combustion in actual SI engine, there exists two volumes, unburned and burned, separated by thin propagating flame front [10].

In this study, the combustion is also modelled as a two zone model wherein, cylinder volume is considered to be divided into two zones, unburned mixture and burned mixture, which are separated by thin wrinkled turbulent propagating flame front. The flame front propagates through the unburned mixture and it is assumed to be spherical at all times. The combustion is also assumed to occur in three steps, ignition delay and rapid burning and flame termination process. Ignition delay period is taken as period required for 0%-5% mass to burn, rapid burn period is that period in which 5%-95% mass gets burned, and remainder is flame termination, which is modelled separately by empirical formulae.

4.5.1 Wiebe function

A functional form of mass fraction burned with crank angle is essential for estimation of burned and unburned volumes during flame propagation at each crank angle. There are a couple of methods by which mass fraction burned is estimated from experimentally calculated cylinder pressure. One of these methods is that developed by Rassweiler and withrow [18]. But for modelling purpose, the mass fraction burned is often computed by using Wiebe function as cylinder pressure is unknown quantity. It is an empirical equation used to represent the mass fraction burned versus crank angle in SI engine.

$$x_b = 1 - \exp\left[-a * \left(\frac{\theta - \theta_0}{\Delta\theta}\right)^{m+1}\right]$$

(13)

Where, $a = 5 \ \& \ m = 3$. $a \ \& \ m$ are adjustable parameters to match the shape of mass fraction burned curve with that of experimental one. $\Delta\theta$ is combustion duration. It is usually taken as sum of flame development duration (ignition delay) and rapid burn duration. The flame termination duration is not included in it because it is very difficult to quantify. During this stage, energy release rates are comparable to other energy transfer processes that are occurring. Originally, Hires S D et al developed the empirical equations for the prediction of ignition delay and rapid burn durations for homogeneous charge in SI engine. These equations were developed by effectively integrating mass burn rate equation over the relevant portion of the total combustion process. But it contains some constants which are actually determined by matching these equations with the engine data [10]. So for prediction simulation purposes, these equations are inadequate. Mixture burning rate is substantially influenced by speed. And so, in this study, speed dependant empirical formula is used to predict the overall combustion duration [19].

$$\Delta\theta = -1.6189 \left(\frac{N}{1000}\right)^2 + 19.886 \left(\frac{N}{1000}\right) + 39.951 \tag{14}$$

4.5.2 State Equations

The state equations for unburned and burned mixtures are formulated by assuming each zone as a separate control volume bounded by flame front & cylinder walls, with volumes $V_u \ \& \ V_b$ respectively, where $V_u + V_b = V$.
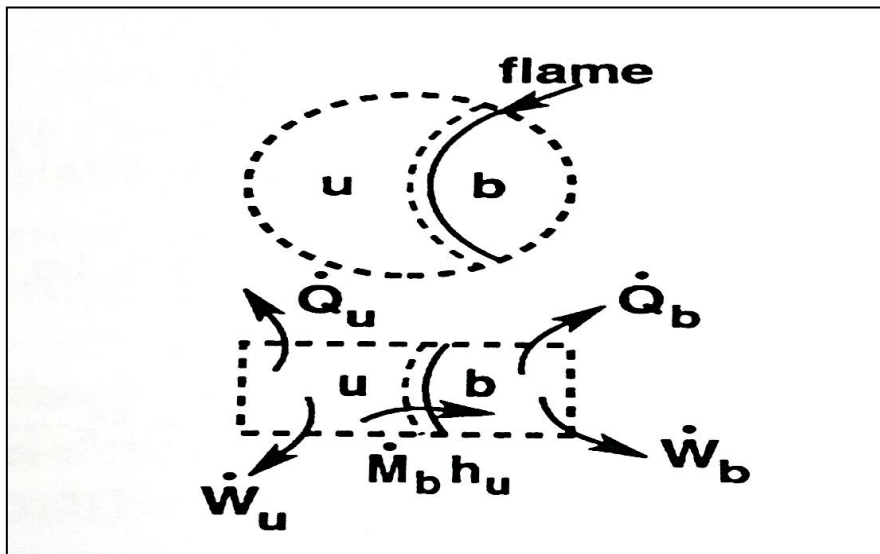

Figure 8: Cartoon of the energy balance in the burned and unburned zones.

$$\dot{T}_i = \left(\frac{B}{A}\right)_i * \left[\left(\frac{\dot{m}}{m}\right)_i * \left(1 - \frac{h_i}{B_i}\right) - \left(\frac{\dot{V}}{V}\right)_i + \left(\frac{1}{(B * m_i)} * (-\dot{Q}_{wi} + \dot{m}_i h_u)\right)\right] \tag{15}$$

$$\dot{P}_i = \left(\frac{\rho}{\partial\rho/\partial P}\right)_i * \left[-\left(\frac{\dot{V}}{V}\right)_i - \left(\frac{\partial\rho/\partial T}{\rho}\right)_i * \dot{T}_i + \left(\frac{\dot{m}}{m}\right)_i\right] \tag{16}$$

$$A = \left(\left(\frac{1}{\rho} - \frac{\partial h}{\partial P}\right) * \left(\frac{\partial\rho/\partial T}{\partial\rho/\partial P}\right)\right) + Cp_r; \quad \& \quad B = \frac{1 - \left(\rho * \frac{\partial h}{\partial P}\right)}{\frac{\partial\rho}{\partial P}};$$

$$\frac{\partial\rho}{\partial P} = \frac{\rho^n - \rho^{n-1}}{P^n - P^{n-1}}; \quad \& \quad \frac{\partial\rho}{\partial T} = \frac{\rho^n - \rho^{n-1}}{T^n - T^{n-1}};$$

$$V_u = (1 - x_b) * V; \quad \& V_b = x_b * V;$$

$$P = P_u + P_b; \tag{17}$$

$$T = \frac{P * V}{m * R} \tag{18}$$

Equations (19&20) represent availability rate for unburned and burned gases,

$$\dot{A}_u = \left(1 - \left(\frac{T_0}{T_u}\right)\right) * \dot{Q}_{wu} - \left[(P_u - P_0) * \dot{V}_u\right] - \left(\dot{m}_b * (h_u - T_0 s_u)\right) - T_0\left[\dot{S}_u + \frac{\dot{Q}_{wu}}{T_0} - \dot{m}_b s_u\right] \tag{19}$$

$$\dot{A}_b = \left(1 - \left(\frac{T_0}{T_b}\right)\right) * \dot{Q}_{wb} - \left[(P_b - P_0) * \dot{V}_b\right] + \left[\dot{m}_b * \left((h_b - T_0 s_b) - (h_u - T_0 s_u)\right)\right]$$
$$- T_0\left[\dot{S}_b + \frac{\dot{Q}_{wb}}{T_0} - \dot{m}_b(s_b - s_u)\right] \tag{20}$$

Dissociation effects are neglected and so $\frac{\partial h}{\partial P} = 0$. Above, for unburned mixture $i = u$ and for burned mixture $i = b$.

4.5.3 Mass burn rate model

The combustion process in SI engine takes place in a turbulent flow field. This flow field is produced by the high shear flows set up during the intake process and modified during compression. It was proved through experiments that turbulent flow field substantially affects rate of flame propagation. Understanding the structure of this flame and the speed at which it propagates, and how that structure and speed depend on charge motion, charge composition and, chamber geometry, are critical to engine simulation and its optimization [10]. So for realistic combustion, it is necessary to consider turbulent flame propagation through the unburned mixture with turbulent burning speed during rapid burn process. For this purpose, method that was postulated by Blizard & Keck [17] and extended by Keck and co-workers is used [18]. Turbulent eddy entrainment model is used to predict the mass burn rate during combustion. According to this model, turbulent eddies, in front of the propagating flame front,

having characteristics length L_t are entrained into the flame brush with the entrainment velocity U_t and burn in a characteristic time τ. The mass burn rate formulation is given by,

$$\dot{m}_e = \rho_u * A_f * (S_l + U_t) \tag{21}$$

$$\dot{m}_b = \rho_u * A_f * S_l + \frac{(m_e - m_b)}{\tau} \tag{22}$$

Where, S_l is a laminar burning speed and is defined as the velocity, relative to and normal to the flame front, with which unburned gas moves into the flame front and transformed to products under laminar flow conditions [10]. For isooctane and gasoline, it is given by empirical power law equation (23) as follows,

$$S_l = S_{l0} * \left(\frac{T_u}{T_0}\right)^\alpha * \left(\frac{P}{P_0}\right)^\beta \tag{23}$$

Where, S_{l0}, α, β are constants for a given fuel, equivalence ratio, and burned gas diluent fraction. For isooctane, these constants can be represented by [10],

$$\alpha = 2.18 - 0.8 * (\emptyset - 1) \ \& \ \beta = -0.16 + 0.22 * (\emptyset - 1)$$

$$S_{l0} = 0.263 - 0.847 * (\emptyset - 1.13)^2$$

U_t is determined empirically depending on the mean inlet gas speed and the ratio of unburned gas density to inlet gas density. L_t is calculated empirically depending on the maximum intake valve lift and density ratio as follows [18],

$$U_t = 0.08 * U_v * \sqrt{\frac{\rho_u}{\rho_v}} \tag{24}$$

$$L_t = 0.8 * L_{max} * \left(\frac{\rho_v}{\rho_u}\right)^{3/4} \tag{25}$$

$$\tau = \frac{L_t}{U_t}$$

4.5.4 Geometrical model [14]

It is used to estimate relationship of flame front volume, flame front surface and the wall surface area enveloped by the enflamed gases with the flame front radius. Earlier 1970, even for simplest geometry applicable to an internal combustion engine, direct analytical

relationships did not exist, and so pre-computed numerical data, either tabulated or reduced to empirical fitted equations had to use. Originally, Annand [14] described an analytical method for calculations of these parameters for a flat disc combustion chamber with flame origin at any chosen point on one of the flat surfaces. This method can be adaptable to any chamber form. The flame front radius is estimated empirically as follows,

$$r_f = \frac{\left[\theta - \theta_{SA} - \Delta\theta_d * \left(1 - \exp\left(\frac{-(\theta - \theta_{SA})}{\Delta\theta_d}\right)\right)\right]}{\Delta\theta_b} * R_c \tag{26}$$

The figure (9) shows the schematics of spherical flame flame propagation from a spark plug location toward cylinder walls in an SI engine. The bottom part is a cut view at section z-z from the top of the cylinder. For each crank angle, different geometrical constraints are applied as follows,
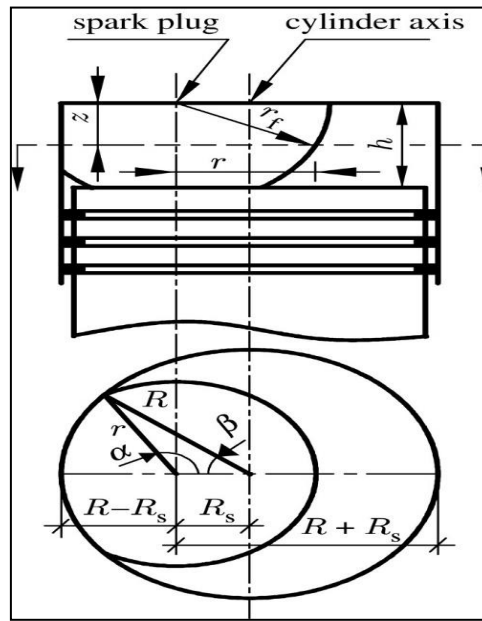
Figure 9: Schematic of flame front propagation geometry in typical SI engine

Condition 1: Check r_f is greater or smaller than h .

Condition 2: Check r_f is greater or smaller than $R - R_s$.

Condition 3: If r_f is greater than $R - R_s$ then, check following 3 different conditions.

$$r \leq R - R_s, r \geq R + R_s, \& r > R - R_s \&\& r < R + R_s$$

With these conditions flame front and heat transfer areas are caluculated for each crank angle.

4.6 Expansion process

It begins after complete burning of unburned mixture into burned gases. The equations describing states of the cylinder content are formulated same as compression process.

$$\dot{T}_b = \left(\frac{B}{A}\right)_b * \left(-\left(\frac{\dot{V}}{V}\right)_b - \left(\frac{\dot{Q}_w}{(B*m)}\right)_b\right) \tag{27}$$

$$\dot{P}_b = \left(\frac{\rho}{\partial\rho/\partial P}\right)_b * \left[-\left(\frac{\dot{V}}{V}\right)_b - \left(\frac{\partial\rho/\partial T}{\rho}\right)_b * \dot{T}_b\right] \tag{28}$$

$$A = \left(1/\rho * \left(\frac{\partial\rho}{\partial T}\middle/\frac{\partial\rho}{\partial P}\right)\right) + Cp_p; \ \& \ B = 1\middle/\frac{\partial\rho}{\partial P};$$

$$\frac{\partial\rho}{\partial P} = \frac{1}{R_p*T_b} * \left(\frac{Cv_p}{Cp_p}\right); \ \& \ \frac{\partial\rho}{\partial T} = \frac{\rho*Cv_p}{R_p*T_b};$$

The equation (29) represents availability rate during expansion,

$$\dot{A}_b = \left(1 - \left(\frac{T_0}{T_b}\right)\right) * \dot{Q}_w - [(P_b - P_0) * \dot{V}] - \left[T_0 * \left(\dot{S}_b + \frac{\dot{Q}_w}{T_0}\right)\right] \tag{29}$$

The equations (27&28) are solved simultaneously by FDM method to compute T & P inside the cylinder during expansion process.

4.7 Exhaust process

It can be modelled exactly same as that of intake process except cylinder pressure is considered as upstream stagnation pressure and exhaust manifold pressure is a downstream static pressure to compute the mass flow rate through exhaust poppet valve. But, here it is modelled by using simple method developed by Durgun. The exhaust pressure is a function of ambient pressure and exhaust temperature is a function of burned gas temperature at the end of expansion and ratio of burned gas pressure at the end of expansion to the exhaust pressure [18].

$$P_{ex} = \frac{1.05}{1.25} P_0 \ \&$$

$$T_{ex} = \frac{T_{EOE}}{\left(\frac{P_{EOE}}{P_{ex}}\right)^{1/3}} \tag{30}$$

4.8 Heat transfer through wall

Prediction of precise and accurate heat flux transfer from cylinder content to chamber walls during operation is indispensable in engine modelling because heat transfer affects engine performance, efficiency, and emissions. For a given mass of fuel within the cylinder, higher heat transfer to the combustion chamber walls will lower the average combustion gas temperature and pressure, and reduces work per cycle transferred to the piston. Thus specific power and efficiency are affected by the magnitude of engine heat transfer [10]. In actual engine, heat transfer takes place during each operating process and sub-process. An ability to predict the magnitude of the heat transfer between the working fluid, the walls of the intake system, combustion chamber, and exhaust system, and to the coolants is of obvious importance to the engine designer.

The heat transfer can occur by three modes in IC engine, conduction, convection, and radiation. A number of correlations have been proposed on the basis of dimensional analysis with assumption that the Nusselt, Reynolds, and Prandtl number relationship follows that found for turbulent flow in pipes or over flat plate. These correlations are categorised to predict time averaged heat flux to chamber walls, the instantaneous spatially averaged heat flux to walls(which is required for engine performance analysis), and the instantaneous local heat fluxes (which are not uniform over the combustion chamber and may be required for thermal stress calculations) [10]. In this study, instantaneous spatially averaged heat flux approach is used and it is assumed as a quasi-steady approach wherein, heat flux transfer is assumed uniform over the combustion chamber at any instant of time. The empirical correlation developed by Annand [13] is employed here to estimate instantaneous heat flux as follows,

$$\dot{Q}_{wi} = A_{wi} * \left[a \frac{K_i}{D} Re_i{}^b (T_i - T_w) + c(T_i{}^4 - T_w{}^4) \right]$$

(31)

Where, a, b, c are constants and taken as $a = 0.35 - 0.8$, $b = 0.7$, and $c = 4.3 * 10^{-9} \; {}^W\!/_{(m^2 \, * \, k^4)}$ (for combustion and expansion). Typical values of Re for gasoline are of the order of $10^4 - 10^5$. i represents unburned or burned gases.

4.9 FDM method

Finite difference methods are numerical methods for solving differential equations by approximating them with difference equations, in which finite differences approximate the derivatives. FDMs are thus discretization methods. As it contains approximations, the solution does not match with the analytical solution. The difference between these two solutions is called error. The two sources of error are present in FDMs. Round off error- the loss of precision due to computer rounding of decimal quantities, and truncation or discretization error- the difference between the exact solution of the original DE and the exact quantity assuming perfect arithmetic.

There are three different sub-methods in which FDM can be applied to the differential equations.

1. Explicit method   2. Implicit method   3. Crank-Nicolson method

These methods are numbered in increasing order of accuracy and complexity in implementations. In this study, explicit method is employed to solve the quasi-dimensional ordinary differential equations. The method is first order accurate, which means local error (error per step) is directly proportional to the square of the step size, and the global error (error at a given time) is proportional to the step size. The method is explained as follows,

Consider an ordinary differential equation,

$$y'(\theta) = f(\theta) + c \tag{32}$$

The derivative term is approximated as,

$$y'(\theta) = \lim_{\Delta\theta \to 0} \frac{y(\theta + \Delta\theta) - y(\theta)}{\Delta\theta} \tag{33}$$

Then, equating R.H.S of equations (32&33),

$$\lim_{\Delta\theta \to 0} \frac{y(\theta + \Delta\theta) - y(\theta)}{\Delta\theta} = f(\theta) + c \tag{34}$$

Lastly, finite difference equation is,

$$y(\theta + \Delta\theta) = \{\Delta\theta * (f(\theta) + c)\} + y(\theta) \tag{35}$$

The RHS term $y(\theta)$ is known as an initial or previous step value and then solution can be calculated at each step of size $\Delta\theta$.

5 Simulation Procedure

The simulation is an imitation of the operation of a real world processes or system over time. Here, it is a graphical representation of the solutions of the governing differential equations, which describe the behaviour of a physical system. Here, SI engine's operation is simulated as follows.

1. A geometrical specifications of the SI engine are defined. The specifications include bore, stroke, connecting rod length, compression ratio, valve diameter, valve lift, valve timings, ambient pressure and temperature, fuel, residual mass fraction, and spark plug location etc.

2. A chemical reaction between fuel and air for lean mixtures, without dissociation, is described to estimate the reactants and products composition. It is necessary to determine thermodynamic properties of reactants and products at each crank angle.

3. For each process, instantaneous cylinder volume and surface area for heat loss are computed by using standard equations based on the kinematics of slider crank mechanism. But during combustion, surface areas for burned and unburned volumes are estimated by geometrical model.

4. The equation (31) is used to predict heat flux loss to chamber wall during compression, combustion and expansion process.

5. Engine process modelling starts with intake process modelling. Here, the input variables required to solve equations (7-9) are determined from step 1. The equations (7-9) are solved numerically by using FDM method, to get the mass inducted and state of the cylinder content at each crank angle.

6. The cylinder state of the last crank angle is fed to the compression process as an initial state. The equations (10&11) are solved by the FDM method to get the pressure and temperature values. Density is calculated by using an ideal gas equation. This process ends at spark timing.

7. In combustion process, firstly, combustion duration is calculated by the empirical equation (14). Then, Wiebe function (13) is defined to calculate burned and unburned volume fractions for all crank angles, and ignition delay and rapid burn periods. Initially, at the spark timing, mass burned fraction is calculated by using Wiebe function. The initial temperature of burned gases is taken as adiabatic temperature. Ignition delay is modelled as a laminar flame kernel propagation by considering turbulent eddy velocity zero and rapid burn is modelled as turbulent flame

propagation by including turbulent eddy model into mass burn rate model. The Geometrical model described in sub section 7.5.4 gives the flame front area, area exposed to burned and unburned gases for heat transfer at each crank angle. These areas and turbulent scales (24&25) are required to determine mass burned rate. Then, equations of state are solved separately for burned and unburned zones, to determine pressure, temperature, and density in each zone. The mass burn fraction for next crank angle is computed on actual mass burned value calculated from the mass burn rate equations (21&22). The combustion is considered to be finished when mass fraction burned reaches 95%. The equations (17&18) give total cylinder pressure and temperature, respectively for every crank angle.

8. During expansion, cylinder content is assumed to be completely burned gases. Last state of the combustion is taken as an initial state for expansion. The equations (27&28) are solved in similar manner as that of compression process.

9. At last, exhaust process is modelled by using simple power law equations (30).

10. The state at the end of exhaust process is fed back to start of intake process and thus cycle is repeated.

6 Results and Discussions

This chapter analyses the basic performance, stability and associated irreversibility of the lean burn operation in the PFI equipped gasoline engine and validation of the SI simulation is performed.

The MBT timings for different loads are presented in the Table 3. MBT timing depends on the inlet pressure which changes with load on the engine.

Load (kg & bar)	MBT timing (BTDC in CAD)
5 & 2.13	23
6 & 2.50	20
8 & 3.36	18

Table 3: MBT timings for different load conditions.

6.1 Cyclic variability Results

The cyclic variations in $\frac{IMEP}{P_1}$, $\frac{IMEP}{P_3}$ have been measured for each test, i.e. for each load and air fuel ratio condition. The variations of these parameters are shown in Figure (10-12) to evaluate the engine stability and drivability. The brake thermal efficiency is also plotted to see the effect of cyclic variability on the engine performance.
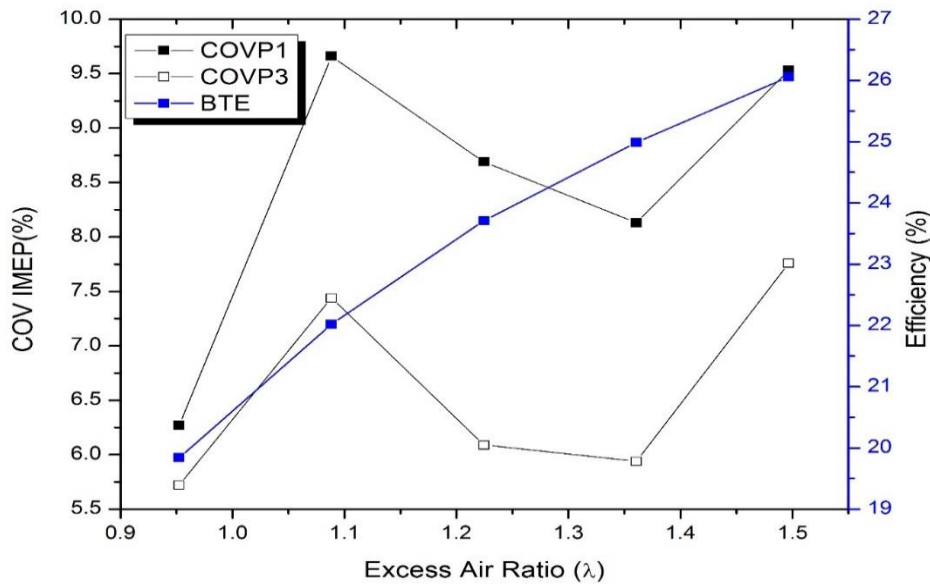

Figure 10: Variation of cyclic variability parameters and brake thermal efficiency with EAR at 2.13 bar.
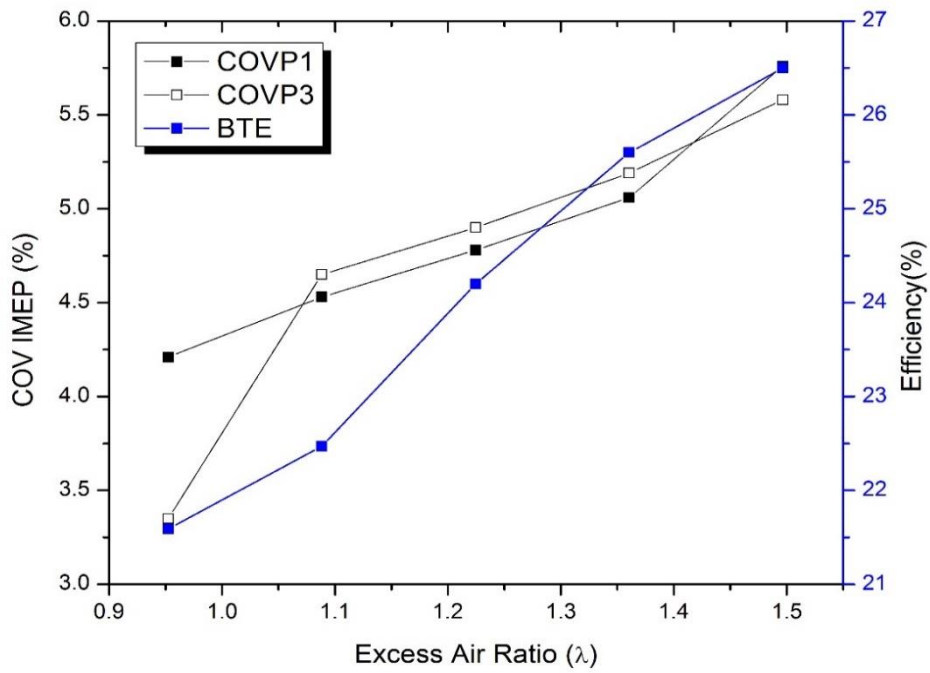
Figure 11: Variation of cyclic variability parameters and brake thermal efficiency with EAR at 2.50 bar.
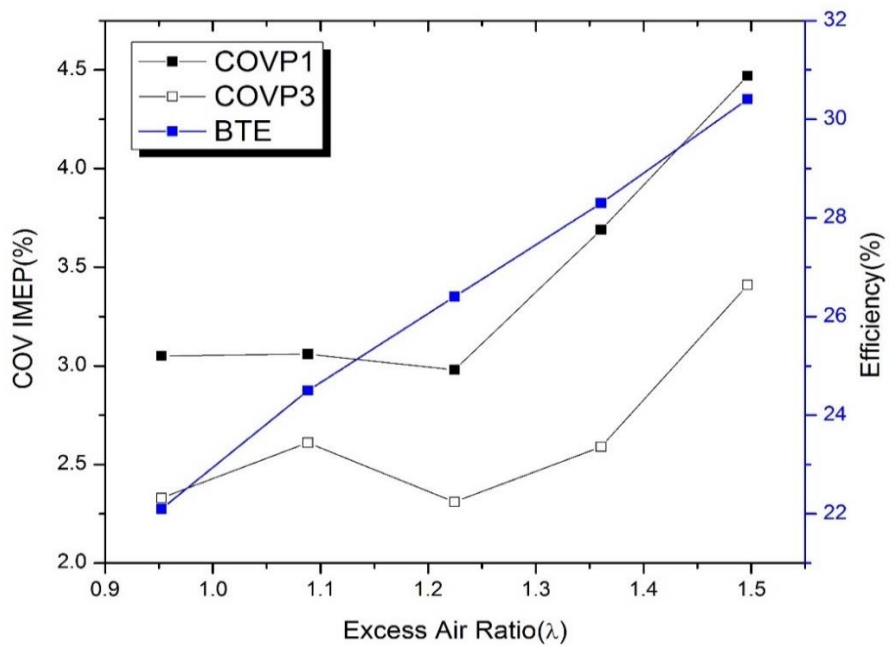

Figure 12: Variation of cyclic variability parameters and brake thermal efficiency with EAR at 3.36 bar.

The Figures (10-12) indicate that cyclic variations in the engine operation are more predominant at low load conditions. For each load condition, the engine is running close to stable operation under lean condition, up to air-fuel ratio 22 has reached. The COVP1 curves show that there are more cycle to cycle variations in overall engine operation compared to that in the combustion process. The COVNIMEP1 and COVNIMEP3 curves are almost parallel to each other indicating that IMEP and peak pressure vary cycle to cycle approximately by the same amount.

At low brake load engine operations, the engine is running under highly throttled condition. It reduces intake pressure and thereby, intake mass of charge. It also increases the mass fraction of burned residual gases. This causes a decrease in volumetric efficiency and charge energy density. It lowers flame temperature and makes stable flame kernel formation difficult which lead to more cyclic variations in the combustion process.

As far as the engine runs stable, brake thermal efficiency increases with air-fuel ratio. This is the result of improvement in the thermo-physical properties of air-fuel mixture, reduction in pumping work and dissociation under lean operation.

To gain more insight into the cyclic variability of combustion process, cycle to cycle variation in peak pressure, maximum net heat release rate have been presented in Figures (13&14). Each of these variables get affected by cyclic variations and vice a versa. The COV in these parameters and their mean values are presented in the Tables (4-6).

C.R= 10	Peak pressure (bar)		Spark timing pressure (bar)		Max. Rate of pressure rise (bar/degree)		Max. Rate of net heat release (kJ/degree)		Combustion duration (degree)	
Load =2.13 bar	COV (%)	Aver age	COV (%)	Aver age	COV (%)	Aver age	COV (%)	Aver age	COV (%)	Aver age
λ= 0.95	7.33	23.5	5.42	7.03	22.12	0.51	10.92	0.046	6.26	97.45
λ= 1.09	10.3	21.1	5.48	6.63	33.05	0.42	15.34	0.040	9.37	98.5
λ= 1.23	8.08	20.5	3.06	6.59	12.81	0.36	13.95	0.035	4.74	102
λ= 1.36	10.9	22.9	4.54	7.23	34.13	0.47	15.49	0.045	6.63	101.7
λ= 1.50	11.2	19.6	4.49	6.96	32.89	0.33	17.31	0.037	5.70	102.5

Table 4: Variation of COV and Mean values of combustion related parameters with excess air ratio at 2.13 bar.

The Figures (13&14) show that there is a reduction in peak pressure and maximum net heat release rate values with the increase in excess air ratio. It suggests that lean mixture slowdowns the combustion process by reducing propagating flame speed. There are few cycles in which value of these parameters drop suddenly from their average value. These cycles are identified as partial burn cycles.

The cycle to cycle variations in these parameters are observed to be random variations about their mean value in the Figures (13&14) but frequency distribution plot (15) shows that it is close to skewed normal distribution for EAR 1.50. Under robust and fast combustion these distributions are close to normal distributions. When the combustion process is much slower, the cyclic variability becomes large and the distribution becomes skewed towards the slower burning cycles [10].
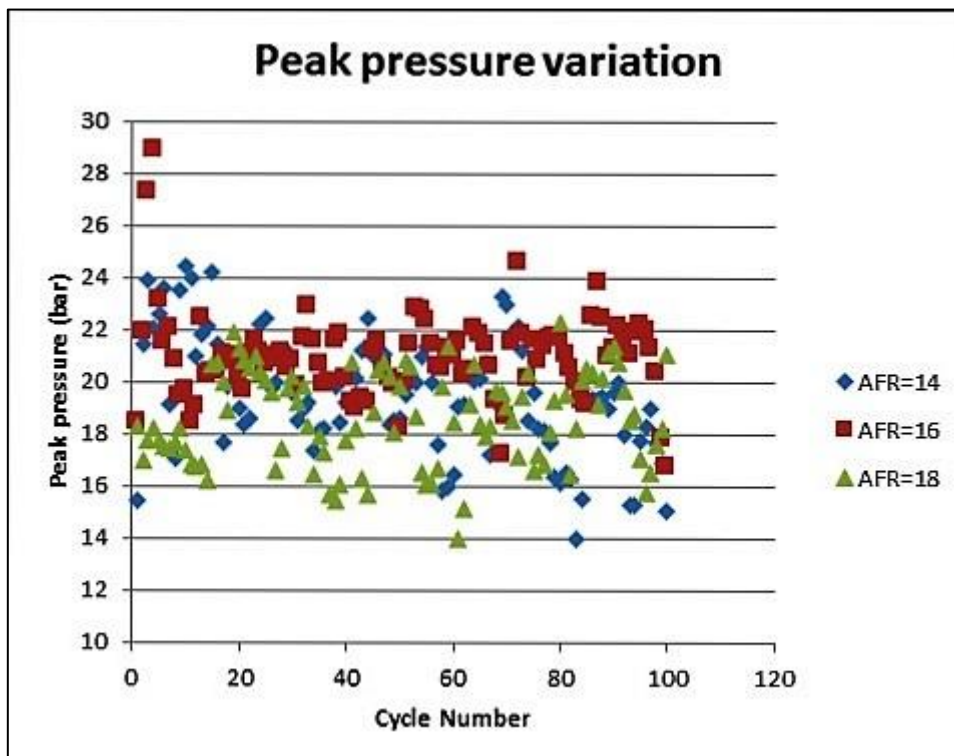

Figure 13: Cyclic variation of peak pressure for different air fuel ratios at 2.13 bar load.
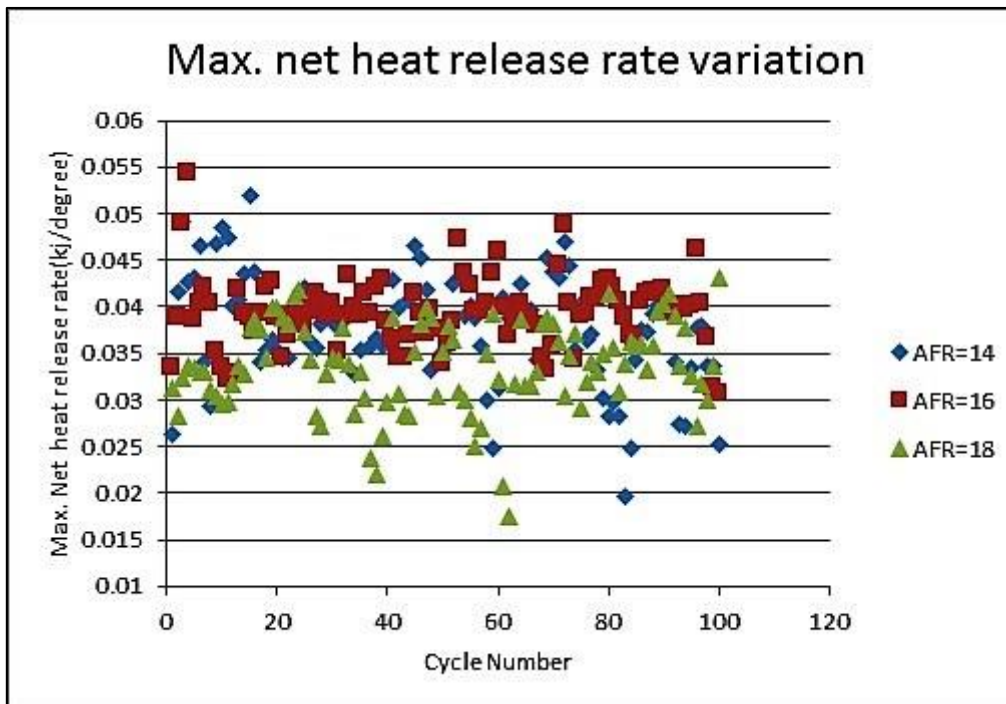
Figure 14: Cyclic variation of maximum net heat release rate for different air fuel ratios at 2.13 bar load.
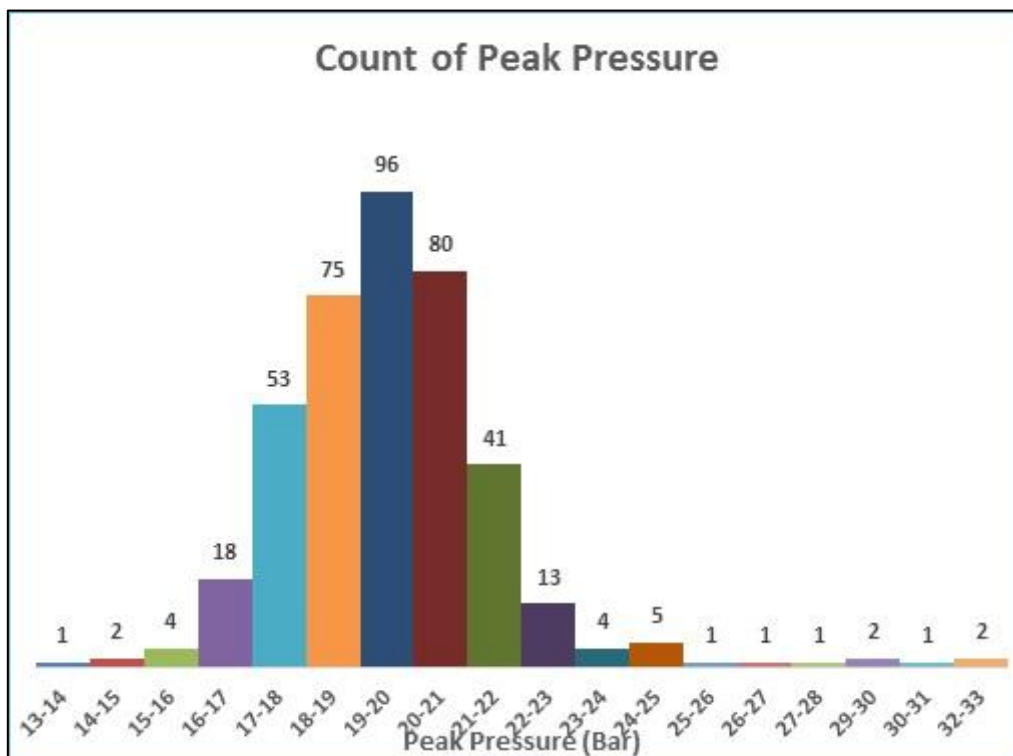

Figure 15: Frequency distribution of peak pressure for excess air ratio=1.50 at 2.13 bar.

The Figures (16&17) illustrate the relationship between p_{max}, θ_{pmax} and $nhrr_{max}, \theta_{nhrrmax}$ respectively for three different AFR. The vertical spread in p_{max} & $nhrr_{max}$ is due to variations in the amount of fuel entering the cylinder each cycle. The early θ_{pmax} & $\theta_{nhrrmax}$ with high magnitude of p_{max} & $nhrr_{max}$ indicate the faster burning cycles with the most advanced phasing. The early θ_{pmax} & $\theta_{nhrrmax}$ with low magnitude of p_{max} & $nhrr_{max}$ indicate the slower burning cycles with the most retarded phasing. [11] These cycles can be termed as partial burn cycles. This occurs when the rate of pressure rise due to combustion becomes so low that it is more than offset by the pressure decrease due to volume increase; eventually for extremely slow and late burning, the peak pressure approaches the motored pressure close to TDC. The higher θ_{pmax} & $\theta_{nhrrmax}$ with low magnitude of p_{max} & $nhrr_{max}$ indicate the slower burning cycles with the most retarded phasing. But in this kind of cycles, combustion lasts late in the expansion process without partial burn.

The similar results have been found for higher loads i.e. 2.5 bar and 3.36 bar, but with reduced cycle to cycle variations and a number of partial burn cycles. At higher loads, the engine operates with wide opening of throttle valve which increases intake pressure and inducted mass of charge. This leads to decrease in burn mass fraction of residual gases. It increases charge energy density and leads to increase in propagating flame speed. It can be seen in average value column of combustion duration in the Tables (4-6). Thus, it promotes faster burning and reduces cyclic variability. The findings also show that the average pressure at the time of spark discharge increases with the increase in air-fuel ratio. It is one of the reasons of increasing IMEP and thereby brake thermal efficiency of the engine under lean mixture condition.

The Figure (18) indicates box plots of peak pressure for different excess air ratios. The bottom and top of the box are first and third quartiles, and the band inside the box is second quartile (median). The end of the whisker represents minimum and maximum values of the peak pressures belonging to 400 consecutive cycles. The vertical length of the box represents the spread in the peak pressure data. The asymmetrical location of the box indicates the skewness in the data. With increase in EAR, the spread and skewness in peak pressure data should have increased but that has happened for only EAR 1.50. This is the result of errors in the measurement system. Figure (19) also supports the skewed behaviour of peak pressure variation for EAR 1.50 at 2.50 bar load.
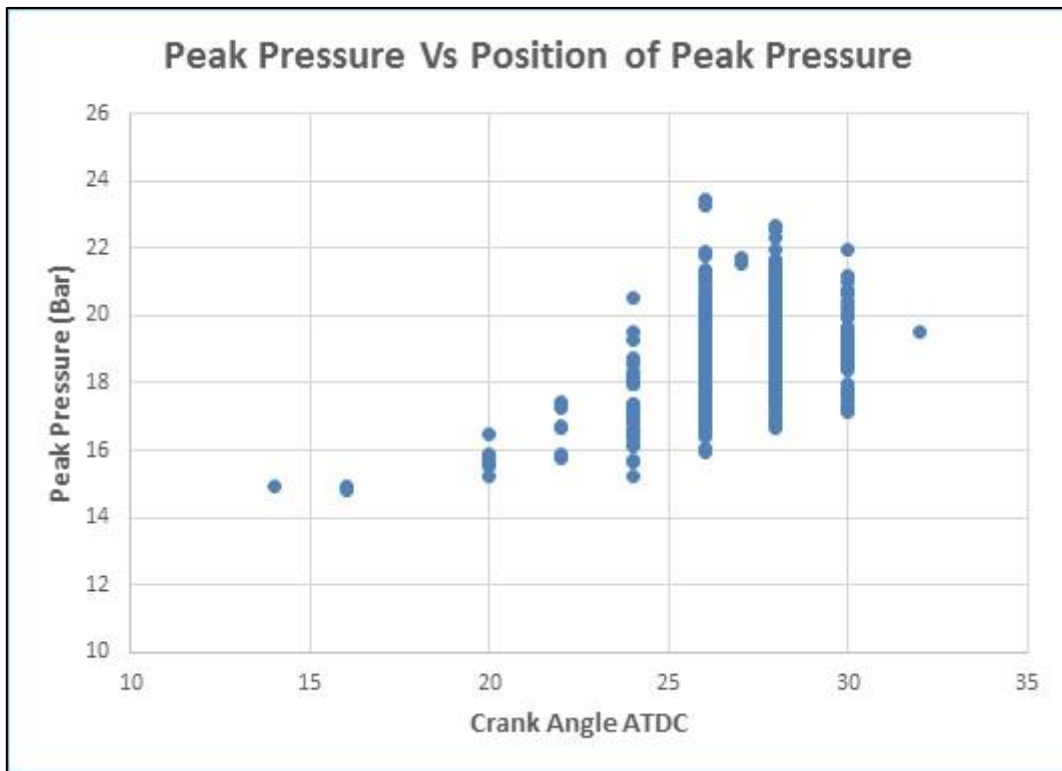
Figure 16: Variation in peak cylinder pressure and crank angle at which it occurs for EAR=1.23 at 2.13 bar.
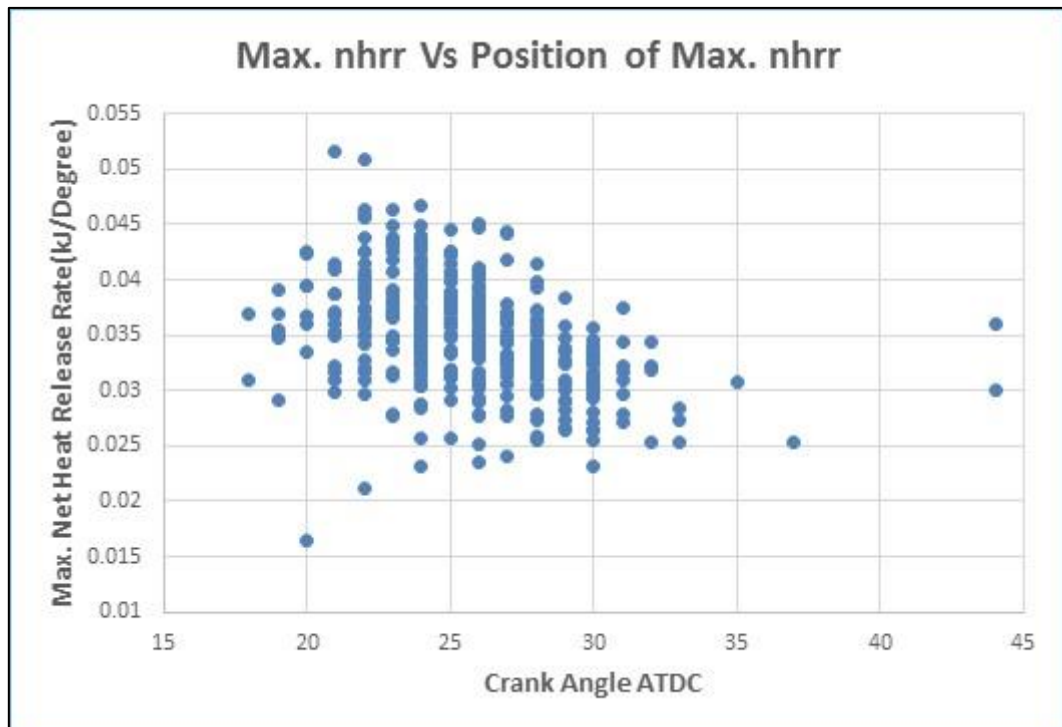
Figure 17: Variation in maximum net heat release rate and crank angle at which it occurs for EAR=1.23 at 2.13 bar.

C.R =10	Peak pressure (bar)		Spark timing pressure (bar)		Max. Rate of pressure rise (bar/degree)		Max. Rate of net heat release (kJ/degree)		Combustion duration (degree)	
Load=2.5 bar	COV (%)	Average	COV (%)	Average	COV (%)	Average	COV (%)	Average	COV (%)	Average
$\lambda=$ 0.95	5.99	24.06	5.20	7.18	16.48	0.56	9.68	0.051	10.9	80.79
$\lambda=$ 1.09	7.41	24.88	5.48	7.47	20.28	0.61	10.66	0.052	12.5	86.97
$\lambda=$ 1.23	8.25	23.29	5.89	7.03	20.28	0.55	11.46	0.048	10.2	81.86
$\lambda=$ 1.36	6.99	22.83	6.83	7.62	22.13	0.46	10.95	0.047	13.0	91.94
$\lambda=$ 1.50	9.13	20.75	6.98	7.30	25.15	0.37	13.92	0.043	8.5	89.92

Table 5: Variation of COV and Mean values of combustion related parameters with air-fuel ratio at 2.5 bar.
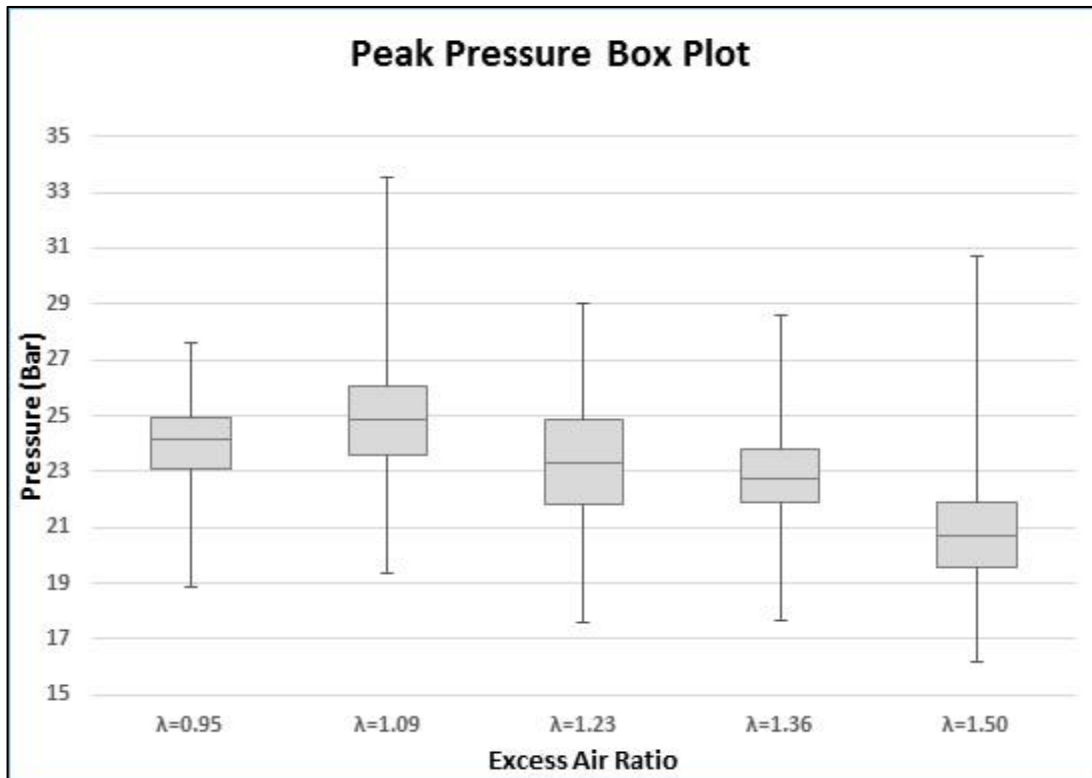
Figure 18: Box Plot of Peak pressure for different EAR at 2.5 bar load..
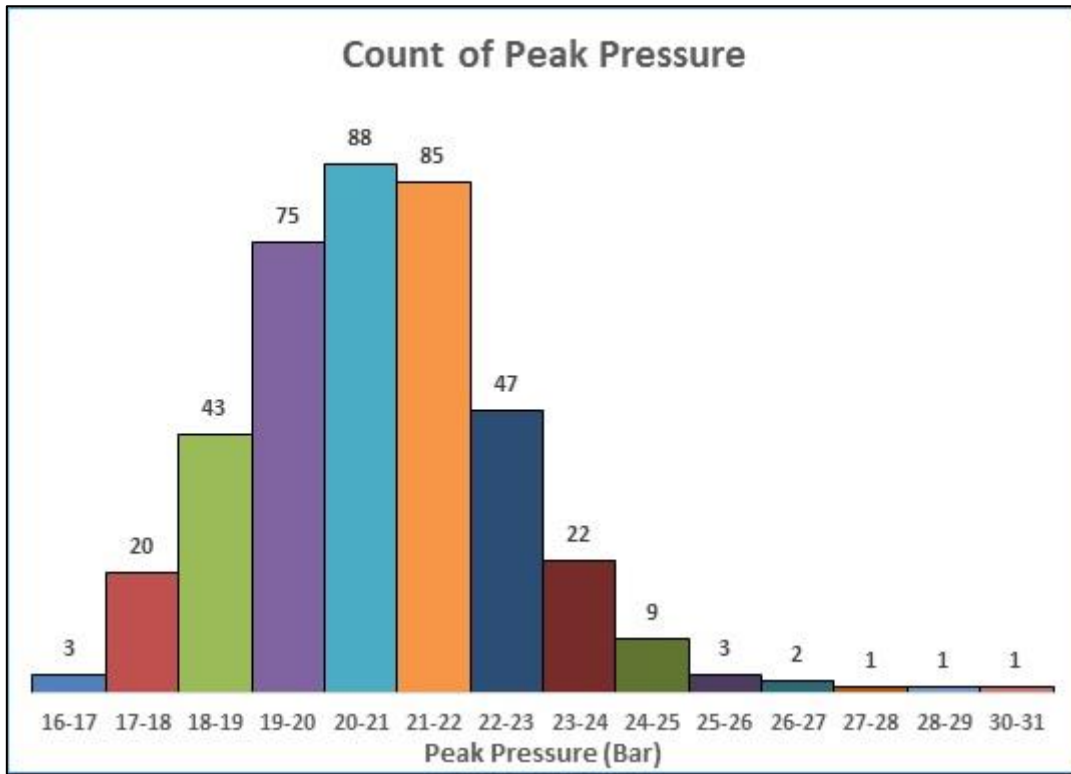
Figure 19: Frequency distribution of peak pressure for EAR=1.50 at 2.50 bar load.

It has been found in the table [6] that cyclic variations in the combustion process have been reduced considerably at 3.36 bar brake load, but average values of these combustion related parameters are varying significantly with lean mixtures. This might be the result of entrapment of less burn mass fraction of residual gases at high loads. Also, higher charge energy density increases burning speed and limits cyclic variability. Figures (21&22) shows probability density functions of peak pressure data for two different EARs 0.95& 1.50. The more spread and outliers are noticeable in the curve for EAR 1.50 because almost all data points fall within ±2σ.

C.R =10	Peak pressure (bar)		Spark timing pressure (bar)		Max. Rate of pressure rise (bar/degree)		Max. Rate of net heat release (kJ/degree)		Combustion duration (degree)	
Load=3.36 bar	COV (%)	Average	COV (%)	Average	COV (%)	Average	COV (%)	Average	COV (%)	Average
λ= 0.95	3.06	35.85	2.94	8.67	6.92	1.30	5.50	0.074	7.46	69.37
λ= 1.09	4.06	36.51	3.14	8.47	8.60	1.34	6.25	0.076	8.54	67.20
λ= 1.23	3.54	36.94	3.31	8.31	9.86	1.38	11.93	0.086	6.69	65.97
λ= 1.36	4.83	36.01	3.90	8.12	15.10	1.45	11.30	0.098	7.34	61.21
λ= 1.50	6.68	30.62	3.86	8.35	16.40	0.83	12.61	0.072	8.83	67.54

Table 6: Variation of COV and Mean values of combustion related parameters with EAR at 3.36 bar.
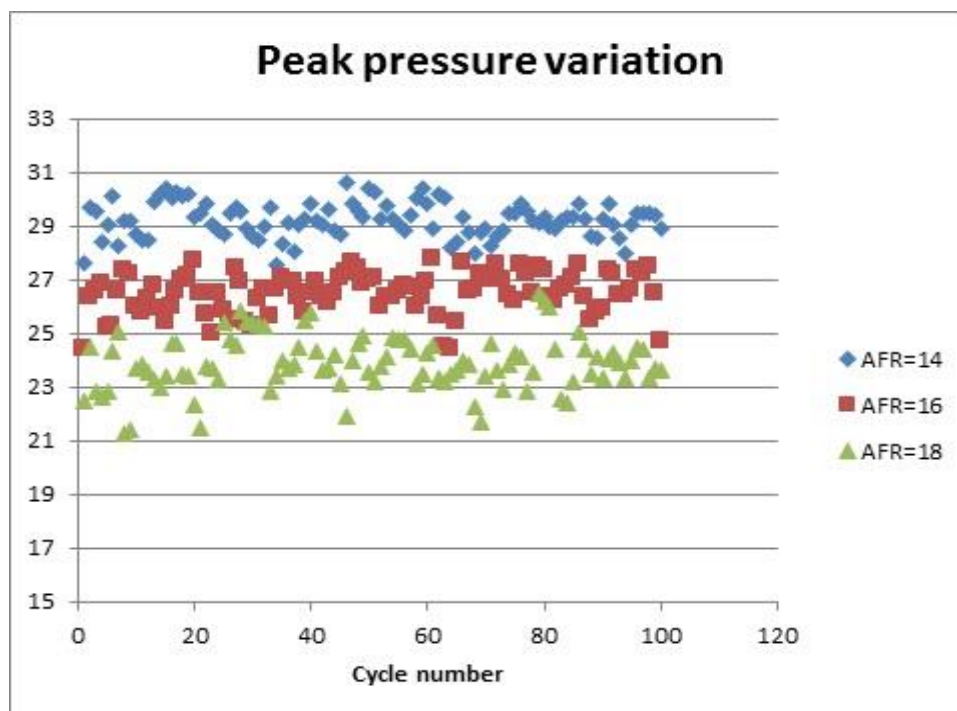
Figure 20: Cyclic variation of peak pressure for different air fuel ratio at 3.36 bar.
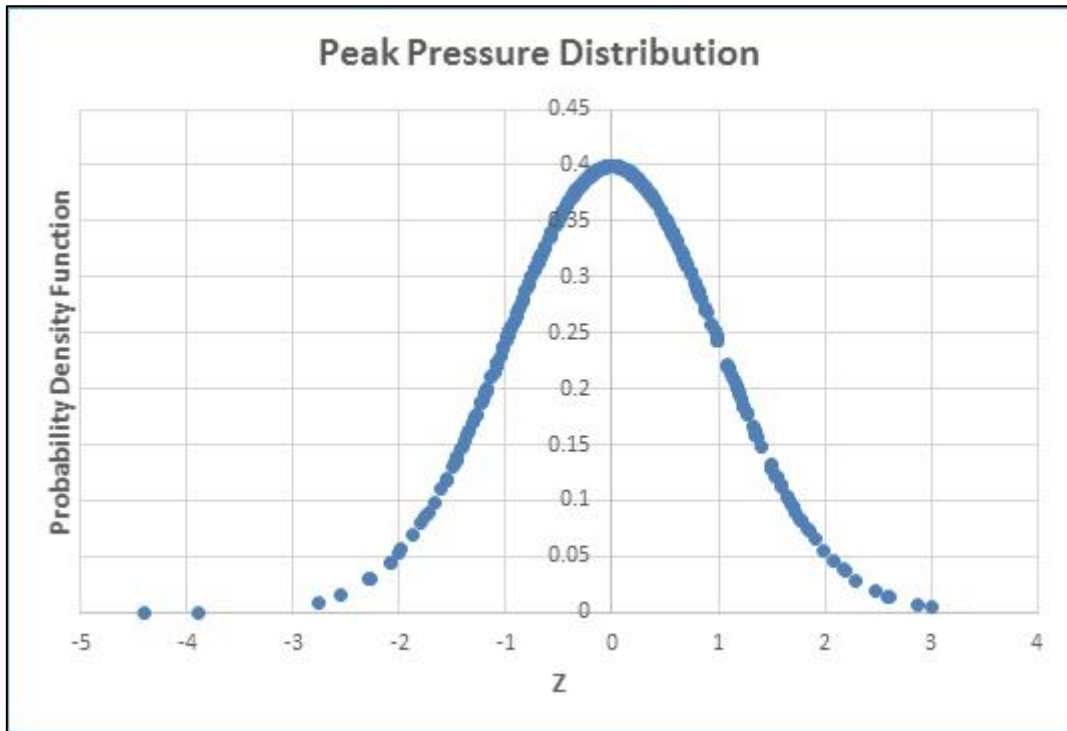
Figure 21: Standard normal distribution of peak pressure for EAR=0.95 at 3.36 bar load.
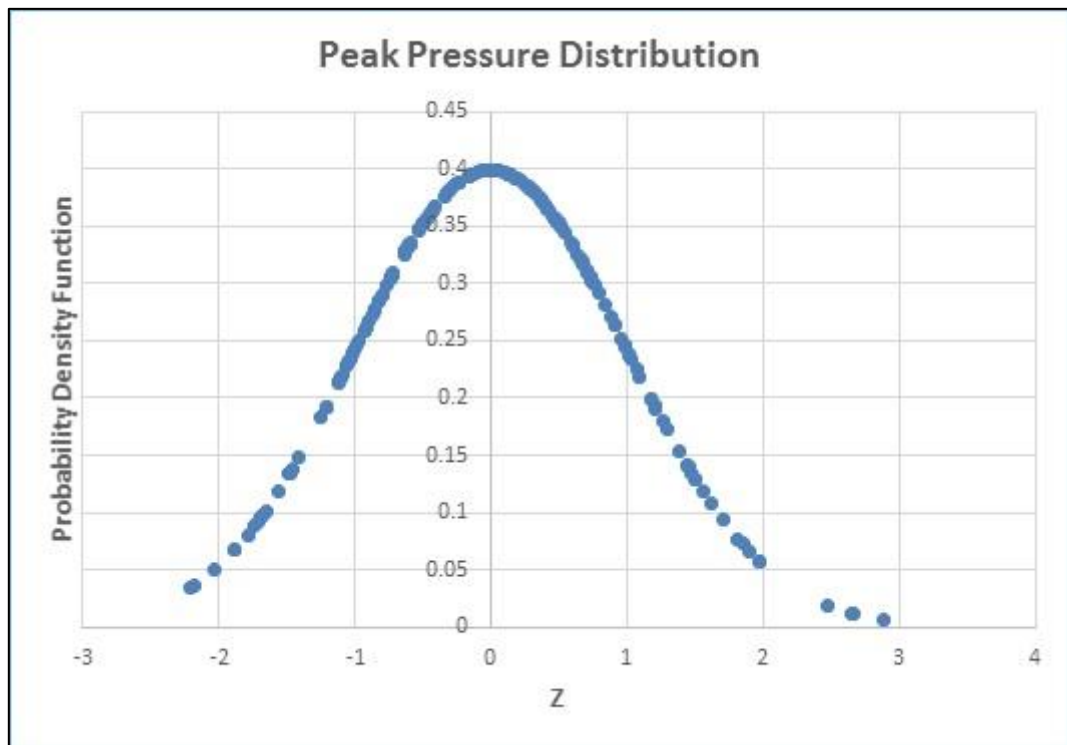
Figure 22: Standard normal distribution of peak pressure for EAR=1.50 at 3.36 bar load.

By comparing the table (5) and table (7), it is quite evident that there is a decrement in COV of almost all parameters with increase in compression ratio from 10 to 12. This suggests that increase in compression ratio not only improves the performance of the engine (Figure (23)) but also reduce the cyclic variability of the combustion process. Thus, lean stable limit of the engine can be extended with the increase in compression ratio. The increase in C.R reduces burn mass fraction of residual gases and increases the charge energy density. This makes the combustion chamber compact &fast burning. Thus, it tends to reduce the cyclic variation in the combustion process.

C.R =12	Peak pressure (bar)		Spark timing pressure (bar)		Max. Rate of pressure rise (bar/degree)		Max. Rate of net heat release (kJ/degree)		Combustion duration (degree)	
Load=2.5 bar	COV (%)	Average	COV (%)	Average	COV (%)	Average	COV (%)	Average	COV (%)	Average
λ= 0.95	9.08	33.24	5.25	9.33	29.92	1.24	19.97	0.083	9.96	87.8
λ= 1.09	10.4	25.64	5.36	9.26	28.16	0.53	17.67	0.051	7.05	95.42
λ= 1.23	10.8	26.2	5.84	9.26	26.83	0.54	19.78	0.053	9.55	96.69
λ= 1.36	11.1	25.5	6.29	9.34	28.29	0.51	19.25	0.051	10.3	96.4
λ= 1.50	11.4	23.95	6.74	9.0	27.82	0.47	20.2	0.046	12.4	93.4

Table 7: Variation of COV and Mean values of combustion related parameters with EAR at 2.5 bar &C.R=12.
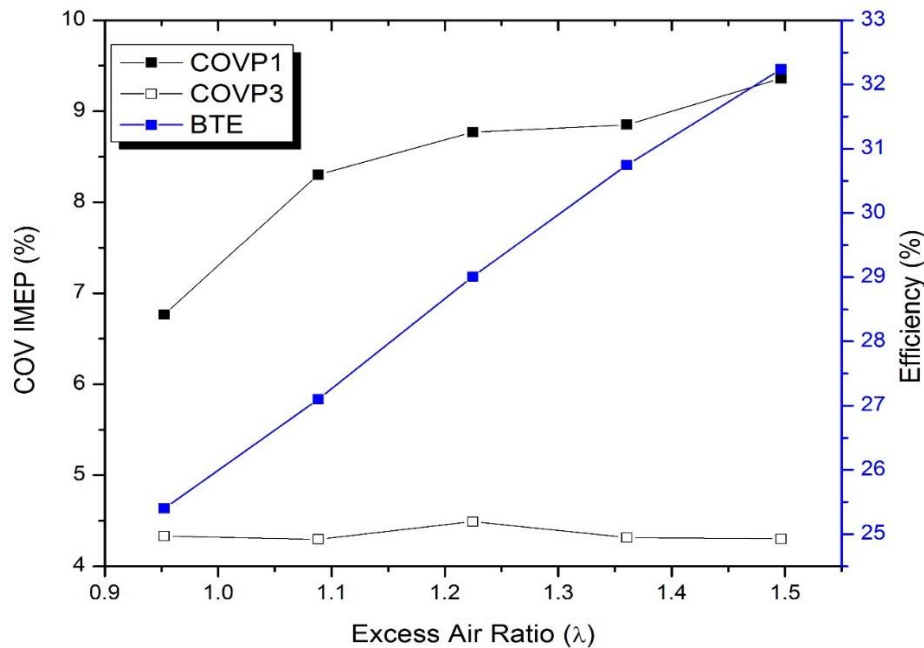
Figure 23: Variation of cyclic variability parameters and brake thermal efficiency with EAR at 2.5 bar & CR=12 .

6.2 Exhaust Emission Results

The Figures (24&25) show the trend and variation in magnitudes of exhaust emissions with air fuel mixture becoming progressively lean. The NOx emissions increase with the EARs under both loads. This result is quite contradictory to that found in the literature. But here it is important to note that the air fuel swing is carried out on each load by keeping the spark timing fixed at stoichiometric spark timing, so under lean mixture conditions, engine cycles are operated as a retarded cycles. The retarded cycles often result in incomplete burned cycles which lead to reduction in expansion work and increment in exhaust temperature. The NOx formation is strongly depend on burned gas temperature and oxygen content in the burned gas. It varies exponentially with gas temperature and oxygen content. This justifies the increment of NOx formation with increase in EARs.

CO emissions are reducing with lean mixtures for each load. The excess oxygen content in the lean mixtures helps to reduce CO formation. The high exhaust temperature also contributes towards converting exhaust CO into CO_2. At 3.36 bar load, fuel content in the cylinder is higher than that for 2.5 bar load, which result in higher CO formation at higher loads. The CO emission values for load 2.5 bar seem inaccurate and unreliable.
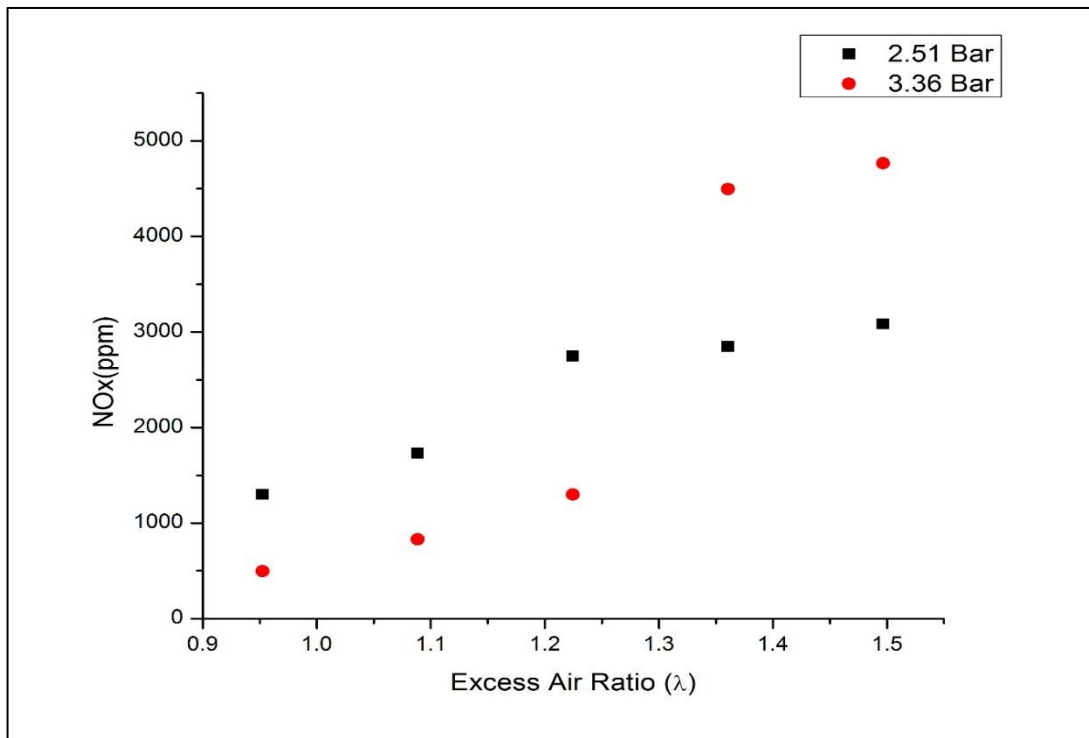
Figure 24: Variation of NOx emission with EAR for 2.5 &3.36 bar loads.
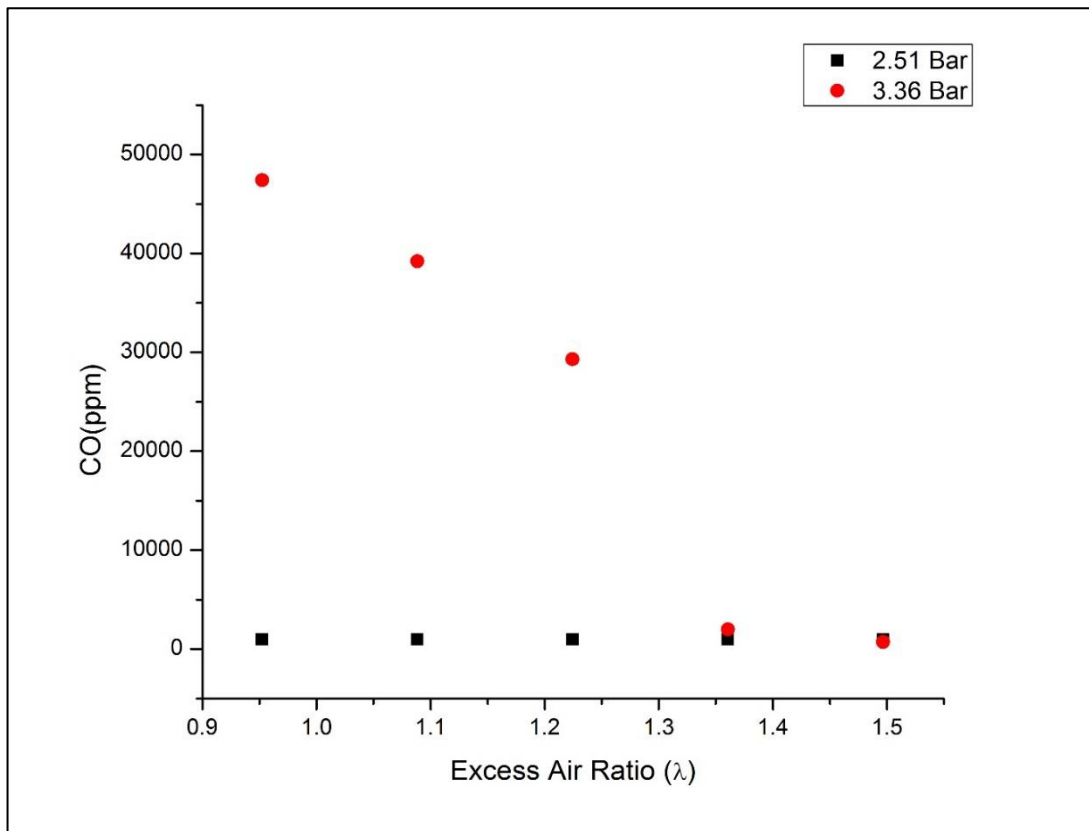
Figure 25: Variation of CO emission with EAR for 2.5 &3.36 bar loads.

6.3   Availability Results

Figure (26) shows that exergetic efficiency is increasing with leaner mixtures and also with loads. As mentioned in the subsection (2.2.3.1), exergy destruction during combustion increases with leaner mixture. It is the result of irreversibilities associated with the lean chemical reaction and mixing of excess air with burned gases. But this destruction in exergy is compensated by the exergy transfer during compression and expansion and loss in exhaust gases. Thus, net result is improvement in exergetic efficiency. Figure (27) indicates different process availabilities variation with leaner mixture. Here, availability destruction curve includes destruction during all processes and so it is decreasing with leaner mixtures.
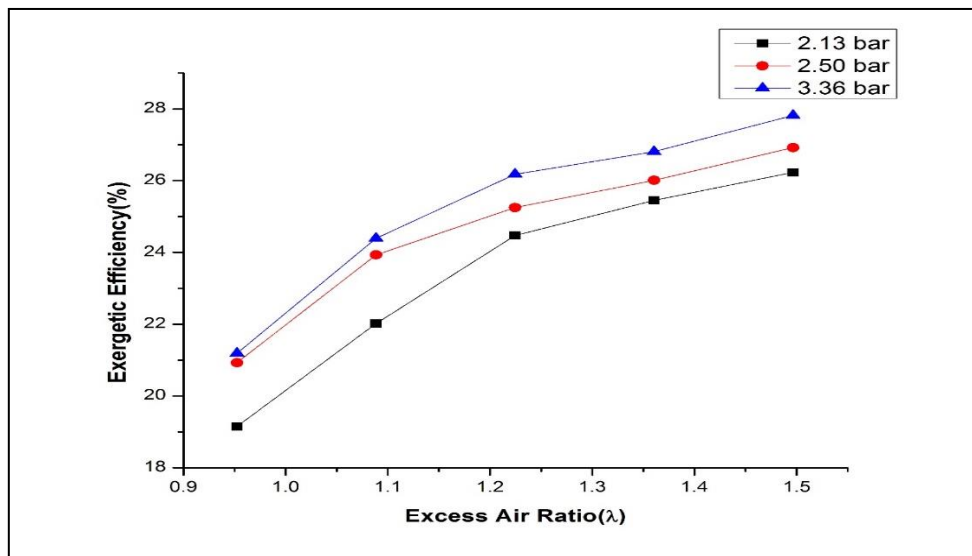
Figure 26: Plot of exergetic efficiency against EAR for different loads
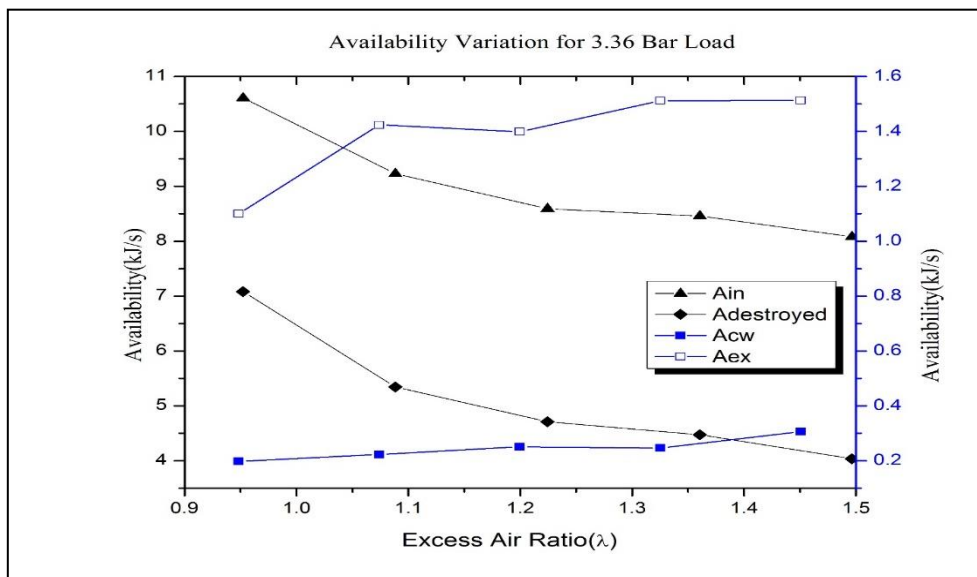
Figure 27: Different process availabilities variation against EAR for 3.36 bar load.

63

6.4   Simulation Results

The feasibility of any simulating mathematical model is proved through its validation. The validation is a process of comparing results of the model with that of standard experiments carried under the same operating conditions. The closeness of the results indicates the accuracy and operating range within which model is reasonably accurate. Thus, the validation highlights the shortcomings in the model which is in reverse used to overcome them. In the present study also, the developed model is validated against the several experimental data given in the literature. The mass fraction burned, cylinder pressure trace, and performance parameters (brake power and torque) were chosen as comparison parameters.
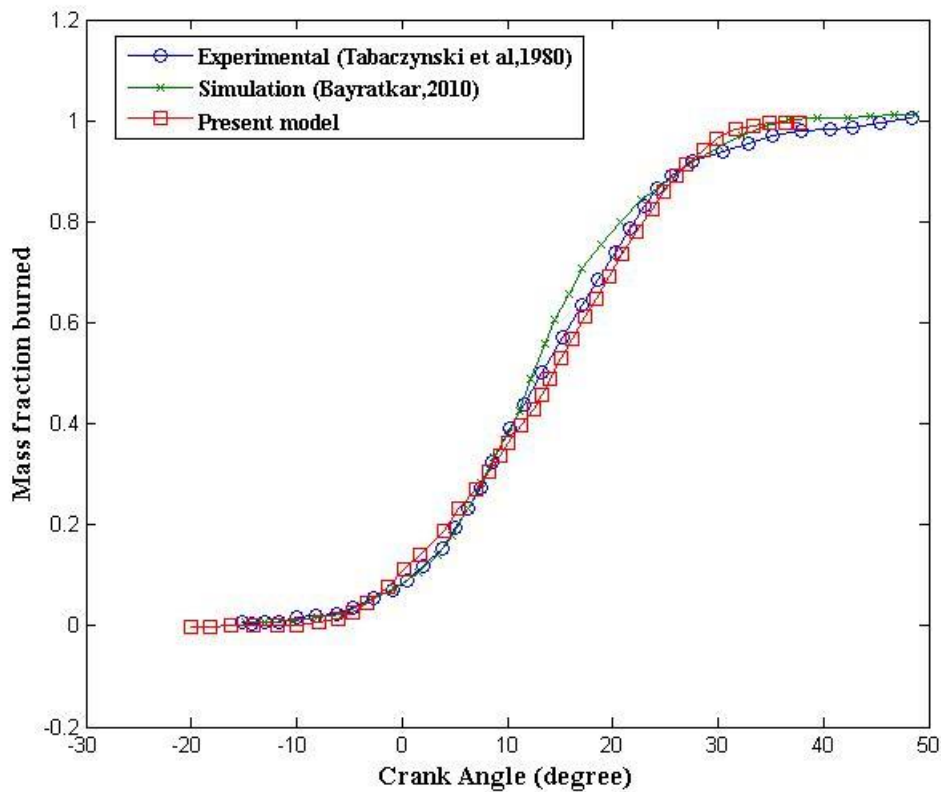
Figure 28: Comparison of predicted and experimental [18] mass fractions burned.

Figure (28) shows mass fraction burned curves obtained from experiment and two different simulations. Tabaczynski et al measured mass fraction burned in an SI engine operating at 2370 rpm with ø=0.91. The present model over predicts the mass fraction after initial flame development until around 10 degrees after TDC. It might be the result of inaccurate prediction of flame front surface and turbulent scales. The combustion seems to finish 10 degrees earlier

than the experimental one, because the flame termination process has not been modelled in the present model and also constraint has been imposed on the rapid burn duration.
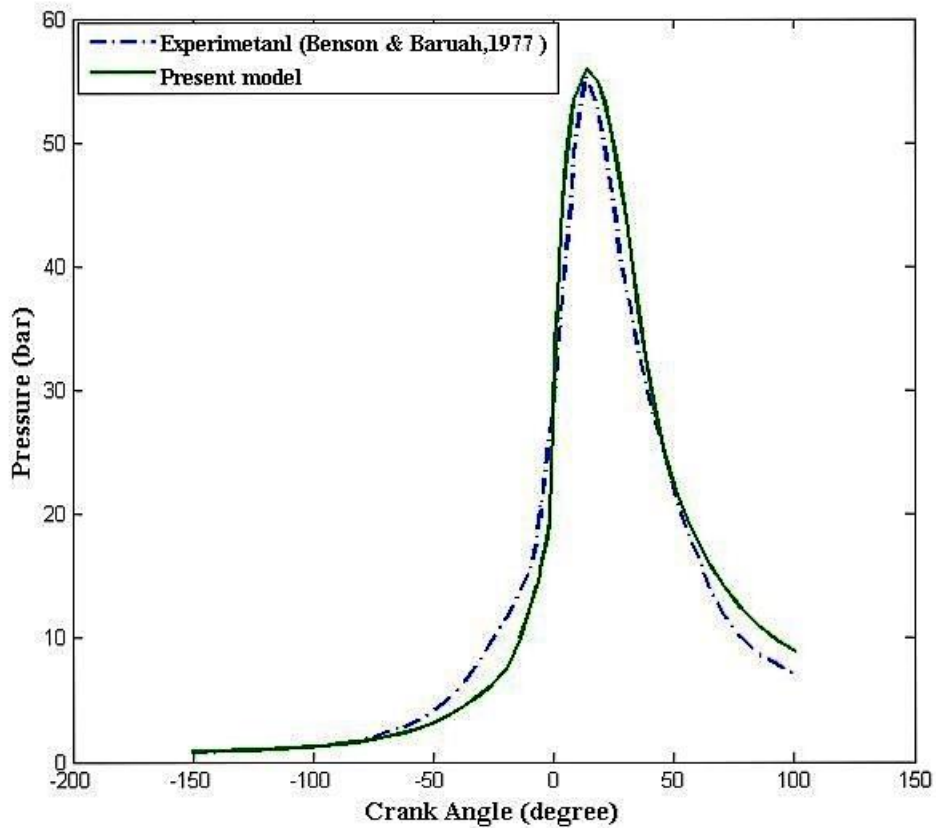
Figure 29: Comparison of Experimental [18] and Simulated pressure trace in an SI engine.

The in cylinder pressure trace curve obtained from simulation does not follow the experimental curve precisely, but still show reasonably good match. The discrepancy in pressure trace might be the result of inaccuracies in the empirical formula for heat loss to chamber wall. The formula contains several different constants and parameters, which are influenced by many factors like engine geometry, in-cylinder flow field, wall temperature etc. Also, inaccurate prediction of mass fraction burned yields error in pressure trace during combustion. Figure (29) indicates that the heat losses are under predicted in all processes.

The performance parameters are compared with that given for Mercedes Benz 250SE engine model. The specifications of the engine are given in the Table 8.
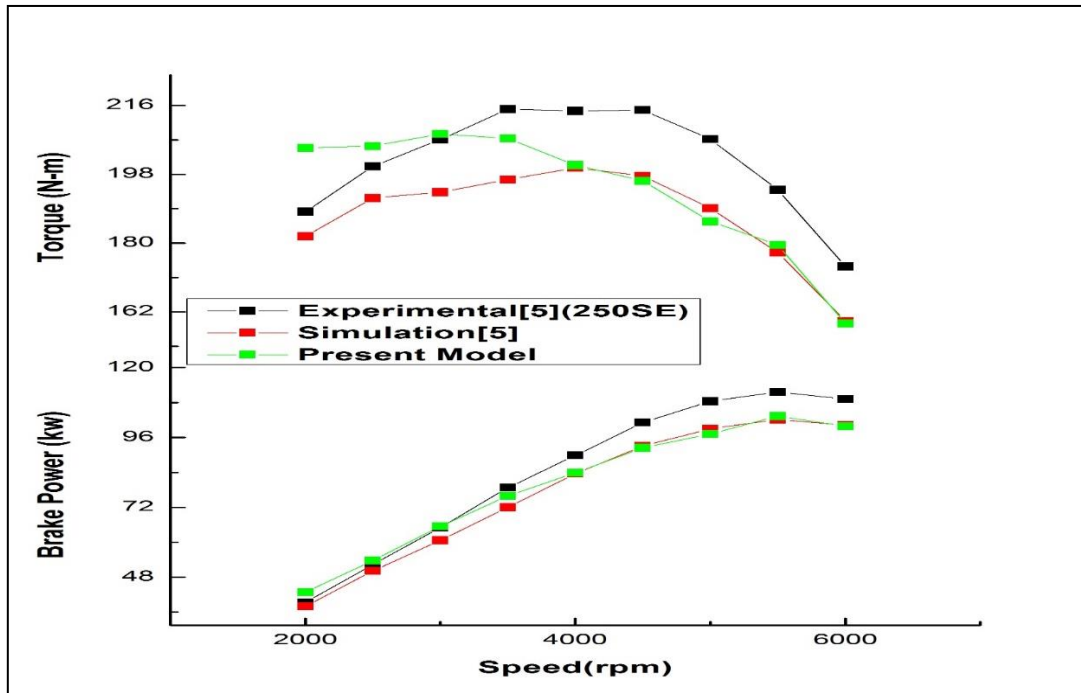
Figure 30: Comparison of predicted Break power and torque variation against speed with experimental data (Benz 250 SE) [19].

Figure (30) consists of two graphs, bottom one demonstrates the variation of brake torque with speed and the top one shows the variation of brake power with speed, for three different cases. The present simulation case exhibits close match with the existing simulation case for higher speeds i.e. after 4000rpm. The experimental values are still far from the simulated values. This is because power and torque values are directly proportional to amount of mass of charge inducted per cycle i.e. volumetric efficiency. The volumetric efficiency depends on many phenomena that occur inside the intake manifold during intake process. Theses phenomenon are charge heating, backflow, flow friction, tuning, chocking, and ram effects and almost all of these get influenced by engine speed substantially. So unless all these phenomena are included in the simulation model precisely, there would be variations in the trend as well as in the magnitudes of the parameters. The present model is equipped with charge heating, backflow, and chocking only and so it is unable to predict the trend and magnitudes of the performance parameters with speed.

The experimental data used for validation of the present simulation model were obtained through performing experiments on following engines by respective researchers.

Parameters	Mercedes Benz Model Year 1969 Series	Tabaczynski el al, engine	Benson & Baruah engine
	250 SE	-	-
No. of Cylinders	6	1	1
No. of Valves per Cylinder	2	2	2
Displacement (cc)	2500	400	493
Bore × Stroke (mm)	82×78.8	83×74	95.25×69.24
Compression Ratio	9.3:1	9.9:1	8.5:1
Connecting Rod (mm)	-	122.1	136.5
IVO before TDC (degree)	11	-	-
IVC after BDC (degree)	53	-	-
Maximum Valve Lift (mm)	8.5	5.3	4.5
Inlet Valve Diameter (mm)	41.2	-	-
Spark Angle BTDC (degree)	MBT	27	25

Table 8: The Specifications of the engines used for validation.

[Type text]

7 Conclusion

The lean burn operation of the engine is investigated under different parameters through cyclic variability, availability balance and exhaust emissions. The findings show that lean burn improves the performance by improving energetic and exergetic efficiencies and reduces exhaust emissions by providing excess air for complete reactions. On the other hand, it is found that engine operation becomes erratic under lean burn, which makes drivability difficult. Higher loads and compression ratios allow more lean operation with improved performance and reduced cyclic variations, up to the lean limit of operation. In the study, lean stable limit of the engine has not been achieved and so further experimentation is required to define operational envelop of the lean burn.

The second part of the study focused on developing simplified thermodynamic model for conventional SI engine. The SI engine processes have been modelled by applying first law of thermodynamics to cylinder volume. The auxiliary models are either analytical or empirical depending upon their simplicity and availability. The findings show that the model can predicts the performance and combustion parameters within certain accuracy under a fixed operating condition, by tweaking some parameters in the model. But dynamic prediction of the parameters with speed showed many discripencies in the results. For accurate predictions under any conditions, intake manifold needs to be modelled with inclunding all possible phenomena occurring in it. The turbulent scales and heat transfer models are required to upgrade to more sophisticated models.

Thus, this study is concluded with detailed investigation of different paramters on lean burn operation and development of quite accurate thermodynamic model and simulation procedure for SI engine simulation.

8 Future Scope

1. To continue with the experiments to determine the stable lean operating limit with MBT spark timing at each air fuel ratio.

2. To employ suitable strategies such as fuel blending, charge stratification to reduce cyclic variations and improve the performance of engine.

3. To check the performance and variability by employing different injection strategies in PFI and GDI fuelling mode.

4. Detailed modelling of intake and exhaust manifold flow considering friction, tuning and ram effect etc.

5. To adapt better heat transfer model and to include chemical equilibrium /kinetic model.

6. To extend the present model to simulate lean burn operations.

9 References

[1] Wang, S., Ji, C., Zhang, B., & Liu, X. (2014). Lean burn performance of a hydrogen-blended gasoline engine at the wide open throttle condition. *Applied Energy*, *136*, 43-50.

[2] Ceviz, M. A., & Yüksel, F. (2006). Cyclic variations on LPG and gasoline-fuelled lean burn SI engine. *Renewable Energy*, *31*(12), 1950-1960.

[3] Ismail, S., & Mehta, P. S. (2011). Evaluation of the effects of fuel and combustion-related processes on exergetic efficiency. *Fuel*, *90*(5), 1818-1825.

[4] Goldwitz, J. A. (2004). *Combustion optimization in a hydrogen-enhanced lean burn SI Engine* (Doctoral dissertation, Massachusetts Institute of Technology).

[5] Mahato, C. (2010). *Lean burn and stratified combustion strategies for small utility engines* (Doctoral dissertation, The University of Alabama TUSCALOOSA).

[6] Peres Lourenco Cardosa, T. J. (2011). *Port fuel injection strategies for a lean burn gasoline engine* (Doctoral dissertation, University of Brighton).

[7] Badr, O., Alsayed, N., & Manaf, M. (1998). A parametric study on the lean misfiring and knocking limits of gas-fueled spark ignition engines. *Applied thermal engineering*, *18*(7), 579-594.

[8] Ayala, F. A., Gerty, M. D., & Heywood, J. B. (2006). *Effects of combustion phasing, relative air-fuel ratio, compression ratio, and load on SI engine efficiency* (No. 2006-01-0229). SAE Technical Paper.

[9] Dunn-Rankin, D. (Ed.). (2011). *Lean combustion: technology and control*. Academic Press.

[10] Heywood, J. B. (2013). Internal combustion engine fundamentals. New York: Mcgraw-hill.

[11] Rakopoulos, C. D., & Giakoumis, E. G. (2006). Second-law analyses applied to internal combustion engines operation. *Progress in Energy and Combustion science*, *32*(1), 2-47.

[12] Rezapour, K. (2012). Availability analysis of a bi-fuel SI engine model for improvement its performance. *International Journal on "Technical and Physical Problems of Engineering*, *4*(2), 115-21.

[13] Annand, W. J. D. (1963). Heat transfer in the cylinders of reciprocating internal combustion engines. *Proceedings of the Institution of Mechanical Engineers*, *177*(1), 973-996.

[14] Annand, W. J. D. (1970). Geometry of spherical flame propagation in a disc-shaped combustion chamber. *Journal of mechanical engineering science*,*12*(2), 146-149.

[Type text]

[15] Benson, R. S., Annand, W. J. D., & Baruah, P. C. (1975). A simulation model including intake and exhaust systems for a single cylinder four-stroke cycle spark ignition engine. *International Journal of Mechanical Sciences*,*17*(2), 97-124.

[16] Benson, R. S., & Baruah, P. C. (1977). Performance and emission predictions for a multi-cylinder spark ignition engine. *Proceedings of the Institution of Mechanical Engineers*, *191*(1), 339-354.

[17] Blizard, N. C., & Keck, J. C. (1974). *Experimental and theoretical investigation of turbulent burning model for internal combustion engines* (No. 740191). SAE Technical Paper.

[18] Bayraktar, H. (2003). Mathematical modeling of spark-ignition engine cycles.*Energy sources*, *25*(5), 439-455.

[19] Sitthiracha, S., Patumsawad, S., & Koetniyom, S. (2006, October). An analytical model of spark ignition engine for performance prediction. In *The 20th Conference of Mechanical Engineering Network of Thailand. Nakhon Ratchasima, Thailand*.

[20] Georgios, Z. (2005). Mathematical and numerical modelling of flow and combustion processes in a spark ignition engine. *Department of Applied Mathematics*.

[21] Lumley, J. L. (1999). *Engines: an introduction*. Cambridge University Press.

[22] Karimi, M. N., & Kamboj, S. K. (2012). Effect of Fuel, Compression ratios on Energetic and Exergetic efficiency of Spark Ignition (SI) Engine. In *Proceedings of the World Congress on Engineering* (Vol. 3).

[23] Sahoo, B. B., Saha, U. K., Sahoo, N., & Prusty, P. (2009, January). Analysis of throttle opening variation impact on a diesel engine performance using second law of thermodynamics. In *ASME 2009 internal combustion engine division spring technical conference* (pp. 703-710). American Society of Mechanical Engineers.

[Type text]

10 Appendix

The developed MATLAB code for SI engine simulation is attached here. The output of the code is presented in Pressure Vs crank angle diagram for reference. The input parameters are given in code directly.

```matlab
clc
R=287;
g=9.81;
Ru=8314;
LHV=44.42*10^6;   %in J/kg
P_atm=1E-5;
rho_atm=1.2;
gamma=1.3;
T_atm=300;
xr=0.063;          %input('enter the residual gas fraction');
display('Enter dimensions in m')
Rad=34.62*10^-3;        % radius of crank
L=136.5*10^-3;                  % length of connecting rod
r=8.5;                          % compression ratio
Bore=95.25*10^-3;       % bore of cylinder
LIFT_MAX=4.5*10^-3;            % Maximum Lift
Vd=(pi*(Bore^2)*Rad)/2;
VOL_CLEARANCE=Vd/(r-1);
display('Enter any speed between 2000 to 4500 RPM')
N=input('Speed of Engine=');
W=(2*pi*N)/60;
CM=(N*2*Rad)/30;    % Mean Piston Speed
IVO=30;                  % IVO Before TDC
IVC=60;                  % IVC After BDC
EVO=0;
EVC=IVO;
D=41.2*10^-3;    % Inlet Valve Diameter
D2=2*D;           % Inlet manifold diameter
A1=pi*0.25*D^2;
A2=pi*0.25*D2^2;
T_m=((-0.043624*(N/1000))+1.2953)*T_atm;   % Charge Heating
P_m=90000                                  % manifold pressure
SA=335                                     % Spark Timing angle
%-------------------------Global Chemical Reaction---------------%
 fi=0.91;       % Equivalence ratio
   x=8;y=18;   %x=no of carbon atoms in a mole of fuel & y=no of        hydrogen atoms in a mole of fuel
   Nrfuel=1;
   Nro2=1*((x+(y/4))/fi);
   Nrn2=3.76*((x+(y/4))/fi);
   Npco2=x;
   Nph2o=y/2;
   Npo2=((x+(y/4))/fi)-x-(y/4);
```

[Type text]

```matlab
    Npn2=3.76*((x+(y/4))/fi);
    Nr=Nrfuel+ Nro2+ Nrn2;  % Number of moles of reactant
    Np=Npco2+ Nph2o+Npo2+ Npn2;
    Xrfuel=Nrfuel/Nr;       % mole fraction of fuel
    Xro2= Nro2/Nr;
    Xrn2=Nrn2/Nr;
    Xpco2=Npco2/Np;
    Xph2o=Nph2o/Np;
    Xpo2=Npo2/Np;
    Xpn2=Npn2/Np;
    MWc=12; MWh=1; MWo2=32; MWn2=28;MWrfuel=(x*MWc+y*MWh);

MWr=sqrt(Xrfuel*power((x*MWc+y*MWh),2)+Xro2*power(MWo2,2)+Xrn2*power(MW
n2,2));   % Molecular weight of reactant in kg/kmol

MWp=sqrt(Xpco2*power((MWc+MWo2),2)+Xph2o*power(((2*MWh)+(MWo2/2)),2)+X
po2*power(MWo2,2)+Xpn2*power(MWn2,2));
    cprfuel=0.85;                         cpro2=0.918;                    cprn2=1.040;
cppco2=0.85;cpph2o=4.18;cppo2=0.918;cppn2=1.042;

cpr=((Xrfuel*(x*MWc+y*MWh)*cprfuel+Xro2*MWo2*cpro2+Xrn2*MWn2*cprn2))*10^
3 ;  % specific heat of reactant in J/kmol-K
    cvr=cpr-Ru;

cpp=((Xpco2*(MWc+MWo2)*cppco2+Xph2o*((2*MWh)+(MWo2/2))*cpph2o+Xpo2*M
Wo2*cppo2+Xpn2*MWn2*cppn2))*10^3; % specific heat of product in J/kmol-K
    cvp=cpp-Ru;

%--------------------------------------------------------------------------%
%--------------Modelling of Intake Stroke---------------------------------%
%--------------------------------------------------------------------------%
gamma1=cpr/cvr;
U_m=((pi/4)*Bore^2*CM)/(A2);   % Approximate velocity of air in inlet manifold
U_v=((pi/4)*Bore^2*CM)/(A1);   % Approximate velocity of air at inlet Valve
U_Sound=sqrt(gamma1*(Ru/MWr)*T_m);
Mat=U_v/U_Sound;
Mam=U_m/U_Sound;
Pexhaust=101325;%input('Enter the exhaust manifold pressure=');
rho_m=rho_atm/((1+((gamma1-1)*0.5*Mam^2))^(1/(gamma1-1)));
rhot=rho_atm/((1+((gamma1-1)*0.5*Mat^2))^(1/(gamma1-1)));
SP_m=P_m+(0.5*rho_m*U_m^2); % Stagnation pressure
ST_m=T_m+((0.5*U_m^2)/(cpr/MWr)); % Stagnation Temperature
dtheta=0.0008;
if IVO>=0
theta1=(0-IVO):dtheta:0;
theta2=dtheta:dtheta:(180+IVC);
N1=floor((IVO/dtheta)+1);
N2=floor(((180+IVC-dtheta)/dtheta))+(N1+1);
else
theta1=0:dtheta:abs(IVO);
theta2=(abs(IVO)+dtheta):dtheta:(180+IVC);
N1=floor((abs(IVO)/dtheta)+1);
```

```matlab
N2=floor((((180+IVC)-((abs(IVO)+dtheta)))/dtheta))+(N1+1);
end
theta(1,1:N1)=theta1;
theta(1,N1+1:N2)=theta2;
V_v=zeros(N2,1);
dV=zeros(N2,1);

for i=1:N1      % crank angle from IVO to TDC
V_v(i,1)=((Vd/(r-1))+((Vd/2)*(1+(L/Rad)-cosd(theta1(1,i))-((L/Rad)^2-
(sind(theta1(1,i)))^2)^0.5)));  % Incylinder volume (Cubic meter ) calculation
end
for i=(N1+1):N2  % crank angle from TDC to IVC
V_v(i,1)=((Vd/(r-1))+((Vd/2)*(1+(L/Rad)-cosd(theta2(1,(i-N1)))-((L/Rad)^2-
(sind(theta2(1,i-N1)))^2)^0.5)));
end
dV(1:N1,1)=gradient(V_v(1:N1,1),dtheta);
dV(N1+1:N2,1)=gradient(V_v(N1+1:N2,1),dtheta);
P_v=zeros(N2,1);
T_v=zeros(N2,1);
m=zeros(N2,1);
rho_v=zeros(N2,1);
dm=zeros(N2,1);
dP_v=zeros(N2,1);
P_v(1,1)=P_m;      % Initial Value
T_v(1,1)=T_m;
m(1,1)=(P_v(1,1)*V_v(1,1))/((Ru/MWr)*T_v(1,1));
rho_v(1,1)=m(1,1)/V_v(1,1);
Uavg_v=0;
CF_Avg=0;

for i=1:N2-1
   si=(pi*(IVO-IVC+540+(2*theta(1,i))))/(IVO+IVC+180);
   LIFT=LIFT_MAX*(1+cos(si))/2;
   CD=(107.78*((LIFT/D)^4))-(77.204*((LIFT/D)^3))+(14.1*((LIFT/D)^2))-
(1.01*(LIFT/D))+0.6687;
   CURTAREA=pi*D*LIFT;
   if LIFT>=D/4
      CURTAREA=(pi/4)*D^2;
   end
   PORTAREA=(pi/4)*D^2;
   CF=CURTAREA/PORTAREA;
   CF_Avg=(CF*dtheta)+CF_Avg;
   if (P_v(i,1)<=SP_m)
   if (P_v(i,1)/SP_m)>=(2/(gamma1+1))^(gamma1/(gamma1-1))  % subsonic condition

dm(i,1)=(((((CD*CURTAREA*SP_m)/(sqrt(R*ST_m)))*((P_v(i,1)/SP_m)^(1/gamma1))*(((
2*gamma1)/(gamma1-1))*(1-((P_v(i,1)/SP_m)^((gamma1-1)/gamma1))))^0.5)/W);
      m(i+1,1)=(dtheta*dm(i,1))+m(i,1);
      U_v=(dm(i,1)*W)/(rhot*A1);
      U_m=(dm(i,1)*W)/(rho_m*A2);
      Mat=U_v/U_Sound;
      Mam=U_m/U_Sound;
```

[Type text]

```matlab
        rhot=rho_atm/((1+((gamma1-1)*0.5*Mat^2))^(1/(gamma1-1)));
        rho_m=rho_atm/((1+((gamma1-1)*0.5*Mam^2))^(1/(gamma1-1)));
        SP_m=P_m+(0.5*rho_m*U_m^2);


    end
    if (P_v(i,1)/SP_m)<(2/(gamma1+1))^(gamma1/(gamma1-1))    %sonic condition

dm(i,1)=(((CD*CURTAREA*SP_m)/(sqrt(R*ST_m)))*((gamma1)^0.5)*(2/(gamma1+1))^(
(gamma1+1)/(2*(gamma1-1))))/W;
        m(i+1,1)=(dtheta*dm(i,1))+m(i,1);
        U_v=(dm(i,1)*W)/(rhot*A1);
        U_m=(dm(i,1)*W)/(rho_m*A2);
        Mat=U_v/U_Sound;
        Mam=U_m/U_Sound;
        rhot=rho_atm/((1+((gamma1-1)*0.5*Mat^2))^(1/(gamma1-1)));
        rho_m=rho_atm/((1+((gamma1-1)*0.5*Mam^2))^(1/(gamma1-1)));
        SP_m=P_m+(0.5*rho_m*U_m^2);
    end
        dP_v(i,1)=(((gamma1-1)*(dm(i,1)*(cpr/MWr)*T_v(i,1)))-
(gamma1*P_v(i,1)*dV(i,1)))/V_v(i,1);
        P_v(i+1,1)=(dtheta*dP_v(i,1))+P_v(i,1);
        T_v(i+1,1)=(P_v(i+1,1)*V_v(i+1,1))/(m(i+1,1)*(Ru/MWr));
        rho_v(i+1,1)= (P_v(i+1,1)*MWr)/(Ru*T_v(i+1,1));


    else

    if (SP_m/P_v(i,1))>=(2/(gamma1+1))^(gamma1/(gamma1-1))   % subsonic condition


dm(i,1)=((((CD*CURTAREA*P_v(i,1))/(sqrt(R*T_v(i,1))))*((SP_m/P_v(i,1))^(1/gamma1)
)*(((2*gamma1)/(gamma1-1))*(1-((SP_m/P_v(i,1))^((gamma1-1)/gamma1))))^0.5)/W);
        m(i+1,1)=(dtheta*-dm(i,1))+m(i,1);
        U_v=(-dm(i,1)*W)/(rhot*A1);
        U_m=(-dm(i,1)*W)/(rho_m*A2);
        Mat=U_v/U_Sound;
        Mam=U_m/U_Sound;
        rhot=rho_atm/((1+((gamma1-1)*0.5*Mat^2))^(1/(gamma1-1)));
        rho_m=rho_atm/((1+((gamma1-1)*0.5*Mam^2))^(1/(gamma1-1)));
        SP_m=P_m+(0.5*rho_m*U_m^2);
    end
    if (SP_m/P_v(i,1))<(2/(gamma1+1))^(gamma1/(gamma1-1))   %sonic condition

dm(i,1)=(((CD*CURTAREA*P_v(i,1))/(sqrt(R*T_v(i,1))))*((gamma1)^0.5)*(2/(gamma1+
1))^((gamma1+1)/(2*(gamma1-1))))/W;
        m(i+1,1)=(dtheta*-dm(i,1))+m(i,1);
        U_v=(-dm(i,1)*W)/(rhot*A1);
        U_m=(-dm(i,1)*W)/(rho_m*A2);
        Mat=U_v/U_Sound;
        Mam=U_m/U_Sound;
        rhot=rho_atm/((1+((gamma1-1)*0.5*Mat^2))^(1/(gamma1-1)));
```

[Type text]

```matlab
        rho_m=rho_atm/((1+((gamma1-1)*0.5*Mam^2))^(1/(gamma1-1)));
        SP_m=P_m+(0.5*rho_m*U_m^2);
    end
        dP_v(i,1)=(((gamma1-1)*(-dm(i,1)*(cpr/MWr)*T_v(i,1)))-
(gamma1*P_v(i,1)*dV(i,1)))/V_v(i,1);
        P_v(i+1,1)=(dtheta*dP_v(i,1))+P_v(i,1);
        T_v(i+1,1)=(P_v(i+1,1)*V_v(i+1,1))/(m(i+1,1)*(Ru/MWr));
        rho_v(i+1,1)= (P_v(i+1,1)*MWr)/(Ru*T_v(i+1,1));

    end
        Uavg_v=Uavg_v+U_v;
end
Uavg_v=Uavg_v/(N2-1);      % Average velocity at the inlet valve for turbulent velocity (Ut)
calculations.
CF_Avg=(1/(IVO+180+IVC))*CF_Avg;    % average flow coefficient.
MI=(CM/U_Sound)*(Bore/D)^2*(1/CF_Avg); % Mach Index
  mivc=m(N2,1);
  mf=(mivc)/((14.7/fi)+1);
  ma=mivc-mf;
  VOL_EFF=ma/(rho_atm*Vd);
%-------------------Modelling of Compression Stroke----------------------%
%------------------------------------------------------------------------%
  Tw=400;
  dtheta=0.005;      % dtheta value should not increase above 0.010
  thetac=180+IVC:dtheta:SA;
  Nc=floor((SA-(180+IVC))/dtheta)+1;
  V_comp=zeros(Nc,1);
  Aw=zeros(Nc,1);
  Ru=8314;
  for i=1:Nc      % crank angle from IVC to Spark Timing
  V_comp(i,1)=((Vd/(r-1))+((Vd/2)*(1+(L/Rad)-cosd(thetac(1,i))-((L/Rad)^2-
(sind(thetac(1,i)))^2)^0.5))); % Incylinder volume (Cubic meter ) calculation
  Aw(i,1)=(pi*0.5*Bore^2)+((pi*Bore*Rad)*((L/Rad)+1-cosd(thetac(1,i))+((L/Rad)^2-
(sind(thetac(1,i)))^2)^0.5));
  end
  dVc=gradient(V_comp,dtheta);  % gradient of cylinder volume
  P_comp=zeros(Nc,1);
  T_comp=zeros(Nc,1);
  rho=zeros(Nc,1);
  A_comp=zeros(Nc,1);
  Q_comp=zeros(Nc,1);
  Sr=zeros(Nc,1);
  rho(1,1)=mivc/V_comp(1,1);
  T_comp(1,1)=T_v(N2,1);
  P_comp(1,1)=rho(1,1)*(Ru/MWr)*T_comp(1,1);
for i=1:Nc-1     % Compression Loop
  if T_comp(i,1)<1000
    c1o2=0.03212936E2;c2o2=0.112748E-2;c3o2=-0.057561E-5;c4o2=0.131387E-
8;c5o2=-0.0876855E-11;c6o2=-0.1005249E4;c7o2=0.060347E2;
    c1n2=0.0329867E2;c2n2=0.140824E-2;c3n2=-0.0396322E-4;c4n2=0.0564151E-
7;c5n2=-0.0244485E-10;c6n2=-0.1020899E4;c7n2=0.0395037E2;
  else
```

[Type text]

```matlab
    c1o2=0.036975E2;c2o2=0.0613519E-2;c3o2=-0.1258842E-6;c4o2=0.0177528E-
9;c5o2=-0.1136435E-14;c6o2=-0.1233930E4;c7o2=0.0318916E2;
    c1n2=0.0292664E2;c2n2=0.1487976E-2;c3n2=-0.0568476E-5;c4n2=0.10097038E-
9;c5n2=-0.0675335E-13;c6n2=-0.0922797E4;c7n2=0.0598052E2;
  end
  if T_comp(i,1)<1396
    c1f=-4.20868893E+00;c2f=1.11440581E-01;c3f=-7.91346582E-05;c4f=2.92406242E-
08;c5f=-4.43743191E-12;c6f=-2.99446875E+04;c7f=4.49521701E+01;
  else
    c1f=2.71373590E+01;c2f=3.79004890E-02;c3f=-1.29437358E-05;c4f=2.00760372E-
09;c5f=-1.16400580E-13;c6f=-4.07958177E+04;c7f=-1.23277495E+02;
  end

cprfuel=Ru*(c1f+(c2f*T_comp(i,1))+(c3f*(T_comp(i,1))^2)+(c4f*(T_comp(i,1))^3)+(c5f*(
T_comp(i,1))^4));

cpro2=Ru*(c1o2+(c2o2*T_comp(i,1))+(c3o2*(T_comp(i,1))^2)+(c4o2*(T_comp(i,1))^3)+(
c5o2*(T_comp(i,1))^4));

cprn2=Ru*(c1n2+(c2n2*T_comp(i,1))+(c3n2*(T_comp(i,1))^2)+(c4n2*(T_comp(i,1))^3)+(
c5n2*(T_comp(i,1))^4));
  cpr=((Xrfuel*cprfuel+Xro2*cpro2+Xrn2*cprn2));    % specific heat of reactant in J/kmol-
K
  cvr=cpr-Ru;

Hrfuel=Ru*T_comp(i,1)*(c1f+((c2f/2)*T_comp(i,1))+((c3f/3)*(T_comp(i,1))^2)+((c4f/4)*(
T_comp(i,1))^3)+((c5f/5)*(T_comp(i,1))^4)+(c6f/T_comp(i,1)));

Hro2=Ru*T_comp(i,1)*(c1o2+((c2o2/2)*T_comp(i,1))+((c3o2/3)*(T_comp(i,1))^2)+((c4o
2/4)*(T_comp(i,1))^3)+((c5o2/5)*(T_comp(i,1))^4)+(c6o2/T_comp(i,1)));

Hrn2=Ru*T_comp(i,1)*(c1n2+((c2n2/2)*T_comp(i,1))+((c3n2/3)*(T_comp(i,1))^2)+((c4n
2/4)*(T_comp(i,1))^3)+((c5n2/5)*(T_comp(i,1))^4)+(c6n2/T_comp(i,1)));
  Hr=((Xrfuel*Hrfuel+Xro2*Hro2+Xrn2*Hrn2));

Srfuel=(Ru*((c1f*log(T_comp(i,1)))+(c2f*T_comp(i,1))+((c3f/2)*(T_comp(i,1))^2)+((c4f/
3)*(T_comp(i,1))^3)+((c5f/4)*(T_comp(i,1))^4)+c7f))-
(Ru*log((Xrfuel*P_comp(i,1))/P_atm));

Sro2=(Ru*((c1o2*log(T_comp(i,1)))+(c2o2*T_comp(i,1))+((c3o2/2)*(T_comp(i,1))^2)+((c
4o2/3)*(T_comp(i,1))^3)+((c5o2/4)*(T_comp(i,1))^4)+c7o2))-
(Ru*log((Xro2*P_comp(i,1))/P_atm));

Srn2=(Ru*((c1n2*log(T_comp(i,1)))+(c2n2*T_comp(i,1))+((c3n2/2)*(T_comp(i,1))^2)+((c
4n2/3)*(T_comp(i,1))^3)+((c5n2/4)*(T_comp(i,1))^4)+c7n2))-
(Ru*log((Xrn2*P_comp(i,1))/P_atm));
  Sr(i,1)=((Xrfuel*Srfuel+Xro2*Sro2+Xrn2*Srn2));
  drhoP=(MWr/(Ru*T_comp(i,1)))*(cvr/(cvr+Ru));
  drhoT=(rho(i,1)*cvr)/(Ru*T_comp(i,1));
  A=((1/rho(i,1))*(drhoT/drhoP))+(cpr/MWr);
  B=1/drhoP;
```

[Type text]

```matlab
    Ku=0.0243;   %thermal conductivity of air
    dQ_comp=(Aw(i,1)*(((0.45*Ku*((80000)^0.75)*(T_comp(i,1)-Tw))/Bore)+((4.3*10^-
9)*((T_comp(i,1))^4-Tw^4))))/W; % Heat loss in J/radian
    f_T1=((B/A)*((-dVc(i,1)/V_comp(i,1))-(dQ_comp/(B*mivc))));
    T_comp(i+1,1)=(f_T1*dtheta)+T_comp(i,1);              % Temperature during compression
    rho(i+1,1)=mivc/V_comp(i+1,1);
    P_comp(i+1,1)=(rho(i+1,1)*(Ru/MWr)*T_comp(i+1,1));              % Pressure during
compression

end

Srfuel=(Ru*((c1f*log(T_comp(Nc,1)))+(c2f*T_comp(Nc,1))+((c3f/2)*(T_comp(Nc,1))^2)
+((c4f/3)*(T_comp(Nc,1))^3)+((c5f/4)*(T_comp(Nc,1))^4)+c7f))-
(Ru*log((Xrfuel*P_comp(Nc,1))/P_atm));

Sro2=(Ru*((c1o2*log(T_comp(Nc,1)))+(c2o2*T_comp(Nc,1))+((c3o2/2)*(T_comp(Nc,1))
^2)+((c4o2/3)*(T_comp(Nc,1))^3)+((c5o2/4)*(T_comp(Nc,1))^4)+c7o2))-
(Ru*log((Xro2*P_comp(Nc,1))/P_atm));

Srn2=(Ru*((c1n2*log(T_comp(Nc,1)))+(c2n2*T_comp(Nc,1))+((c3n2/2)*(T_comp(Nc,1))
^2)+((c4n2/3)*(T_comp(Nc,1))^3)+((c5n2/4)*(T_comp(Nc,1))^4)+c7n2))-
(Ru*log((Xrn2*P_comp(Nc,1))/P_atm));
    Sr(Nc,1)=((Xrfuel*Srfuel+Xro2*Sro2+Xrn2*Srn2));


    %----------------------------------------------------------------%
    %---------------Modeling of combustion----------------------------%
    %----------------------------------------------------------------%
    dtheta=0.005;       %Step size for Combustion
    comb_dura=((-1.6189*(N/1000)^2)+(19.886*(N/1000))+39.951);
    thetaEOB=(SA)+comb_dura;
    thetacb=(SA):dtheta:thetaEOB;
    Ncb=floor((thetaEOB-(SA))/dtheta)+1;
    V_cb=zeros(Ncb,1);
    Aw_cb=zeros(Ncb,1);
    double(V_cb);
    double(Aw_cb);
    for i=1:Ncb
    V_cb(i,1)=((Vd/(r-1))+((Vd/2)*(1+(L/Rad)-cosd(thetacb(1,i))-((L/Rad)^2-
(sind(thetacb(1,i)))^2)^0.5))); % Incylinder volume (Cubic meter ) calculation
    Aw_cb(i,1)=(pi*0.5*Bore^2)+((pi*Bore*Rad)*((L/Rad)+1-
cosd(thetacb(1,i))+((L/Rad)^2-(sind(thetacb(1,i)))^2)^0.5));
    end
    dVcb=gradient(V_cb,dtheta); % gradient of cylinder volume
    f=zeros(Ncb,1);
    Vu_cb=zeros(Ncb,1);
    Vb_cb=zeros(Ncb,1);
    double(f);
    double(Vu_cb);
    double(Vb_cb);
    a=5; m1=3;j1=0;j2=0;        % for fixed com_dura m=2.1, for variable comb_dura m=2.2,
w/o HT m=2.0
    for i=1:Ncb
```

[Type text]

```
f(i,1)=1-(exp(-a*((thetacb(1,i)-(SA))/comb_dura)^m1));
Vu_cb(i,1)=(1-f(i,1))*V_cb(i,1);
Vb_cb(i,1)=f(i,1)*V_cb(i,1);

if f(i,1)<=0.1
   j1=j1+1;
end
if f(i,1)>0.1&&f(i,1)<=0.95
   j2=j2+1;
end
end

thetad=(j1-1)*dtheta;
thetab=(j2-1)*dtheta;
df=gradient(f,dtheta);
P_cb=zeros(Ncb,1);rhou=zeros(Ncb,1);
Pu_cb=zeros(Ncb,1);rhob=zeros(Ncb,1);
Tu_cb=zeros(Ncb,1);mu=zeros(Ncb,1);
Pb_cb=zeros(Ncb,1);mb=zeros(Ncb,1);
Tb_cb=zeros(Ncb,1);me=zeros(Ncb,1);
dmb=zeros(Ncb,1);f_Pu1=zeros(Ncb,1);
dmu=zeros(Ncb,1);f_Tu1=zeros(Ncb,1);
f_Pb1=zeros(Ncb,1);Af=zeros(Ncb,1);
f_Tb1=zeros(Ncb,1);Aw2=zeros(Ncb,1);
A_cb=zeros(Ncb,1);Au_cb=zeros(Ncb,1);
Ab_cb=zeros(Ncb,1);Vf=zeros(Ncb,1);
Sr=zeros(Ncb,1);Sp=zeros(Ncb,1);
double(P_cb); double(Pu_cb);double(Pb_cb);double(Tu_cb);
double(Tb_cb);double(rhou);double(rhob); double(mu);
double(mb); double(me);double(dmb); double(dmu);
double(f_Pu1); double(f_Pb1);double(f_Tu1); double(f_Tb1);
rhou(1,1)=rho(Nc,1);
rhob(1,1)=1E-10;
Pu_cb(1,1)=P_comp(Nc,1);
Pb_cb(1,1)=1.1E-10;
Tu_cb(1,1)=T_comp(Nc,1);
Tb_cb(1,1)=T_comp(Nc,1);
P_cb(1,1)=Pu_cb(1,1);
Au_cb(1,1)=A_comp(Nc,1);
Ab_cb(1,1)=1E-10;
A_cb(1,1)=A_comp(Nc,1);
mb(2,1)=f(2,1)*mivc;
mu(2,1)=mivc-mb(2,1);
me(2,1)=mb(2,1);
Tu_cb(2,1)=T_comp(Nc,1)+(1E-5);
Pr=0;
[Tad]=adiabaticTemp;
Tb_cb(2,1)=Tad;
Pu_cb(2,1)=((mu(2,1)*(Ru/MWr)*Tu_cb(2,1))/Vu_cb(2,1));
Pb_cb(2,1)=1.1E-5;
P_cb(2,1)=Pu_cb(2,1)+Pb_cb(2,1)+Pr;
Au_cb(2,1)=(1-f(2,1))*A_comp(Nc,1);
```

```matlab
Ab_cb(2,1)=f(2,1)*A_comp(Nc,1);
A_cb(2,1)=Au_cb(2,1)+Ab_cb(2,1);

for i=2:Ncb-1      %Starting from SA+dtheta
dVu_cb=((1-f(i,1))*dVcb(i,1))+(V_cb(i,1)*-df(i,1));
dVb_cb=(df(i,1)*V_cb(i,1))+(f(i,1)*dVcb(i,1));
double(dVu_cb); double(dVb_cb);
if mb(i,1)<=1E-9&&Vb_cb(i,1)<=1E-10
  rhob(i,1)=1E-8;
else if mb(i,1)<=1E-9
    rhob(i,1)=1E-8;
  else
    rhob(i,1)=(mb(i,1))/Vb_cb(i,1);
  end
end

if mu(i,1)<=1E-9&&Vu_cb(i,1)<=1E-10
  rhou(i,1)=1E-8;
else if mu(i,1)<=1E-9
    rhou(i,1)=1E-8;
  else
    rhou(i,1)=mu(i,1)/Vu_cb(i,1);
  end
end


Vf(i,1)=Vb_cb(i,1)+((me(i,1)-mb(i,1))/rhou(i,1));
if Vf<=0.0
  Vf=1E-10;
end
hz=(V_cb(i,1)*4)/(pi*Bore^2);    % Chamber height
rc=51.5*10^-3;                   % spark plug location from the edge of the cylinder.
rf=((thetacb(1,i)-SA-thetad*(1-exp((-(thetacb(1,i)-SA)/thetad))))/thetab)*(Bore/2);        %
Flame front radius
if rf<=hz
  x=rf;                   % Flame depth
else
  x=hz;
end
if rf<=rc
  Af(i,1)=2*pi*rf*x;
  Aw2(i,1)=0;
end

if rf>rc
  y=0:x/100:x;
  S=zeros(101,1);
  Aw2c=zeros(101,1);
  for j=1:101
    fy=sqrt(rf^2-(y(1,j))^2);
  if fy<=rc
    p=2*pi*fy;
```

[Type text]

```matlab
    q=0;
    S(j,1)=((rf*p)/fy)*(x/100);
    Aw2c(j,1)=q*(x/100);
    end
  if fy>=(Bore-rc)
     p=0;
     q=pi*Bore;
     S(j,1)=((rf*p)/fy)*(x/100);
     Aw2c(j,1)=q*(x/100);
   end
  if fy>rc&&fy<(Bore-rc)
     p=2*(pi-Bore)*fy;
     beta1=acos(1+(((rc/Bore)^2-(fy/Bore)^2)/(0.5-(rc/Bore))));
     q=Bore*beta1;
     S(j,1)=((rf*p)/fy)*(x/100);
     Aw2c(j,1)=q*(x/100);
   end
   end
   Af(i,1)=sum(S);
   Aw2(i,1)=sum(Aw2c);
end
Awb_cb=Aw2(i,1);
Awu_cb=Aw_cb(i,1)-Aw2(i,1);
double(Awu_cb);double(Awb_cb);
   alpha=2.18-(0.8*(fi-1));
   beta=-0.16+(0.22*(fi-1));
   Sl0=0.305+(-0.549*(fi-1.21)^2);
    if i<=j1
      Sl=0.13;
    else
      Sl=Sl0*((Tu_cb(i,1)/298)^alpha)*((P_cb(i,1)/101300)^beta);
    end

   if i<=j1
     Ut=1E-5;
     Lt=1E-5;
   else
     Ut=0.08*Uavg_v*sqrt((rhou(i,1)*N2)/sum(rho_v));
     Lt=0.8*LIFT_MAX*((sum(rho_v)/(N2*rhou(i,1)))^(3/4));
   end

   dmb(i,1)=((rhou(i,1)*Af(i,1)*Sl)+(((me(i,1)-mb(i,1))*Sl)/Lt))/W;
   dme=(rhou(i,1)*Af(i,1)*(Ut+Sl))/W;

   mb(i+1,1)=(dmb(i,1)*dtheta)+mb(i,1);
   me(i+1,1)=(dme*dtheta)+me(i,1);
   dmu(i,1)=-dmb(i,1);
   mu(i+1,1)=mu(i,1)+(dmu(i,1)*dtheta);

   if mb(i+1,1)<=1E-9&&Vb_cb(i+1,1)<=1E-10
     rhob(i+1,1)=1E-8;
   else if mb(i+1,1)<=1E-9
```

[Type text]

```matlab
                rhob(i+1,1)=1E-8;
            else
                rhob(i+1,1)=(mb(i+1,1))/Vb_cb(i+1,1);
            end
        end


    if mu(i+1,1)<=1E-9&&Vu_cb(i+1,1)<=1E-10
        rhou(i+1,1)=1E-8;
    else if mu(i+1,1)<=1E-9
            rhou(i+1,1)=1E-8;
        else
            rhou(i+1,1)=mu(i+1,1)/Vu_cb(i+1,1);
        end
    end

        % Unburned Mixture calculation

    if Tu_cb(i,1)<1000
        c1o2=0.03212936E2;c2o2=0.112748E-2;c3o2=-0.057561E-5;c4o2=0.131387E-
8;c5o2=-0.0876855E-11;c6o2=-0.1005249E4;c7o2=0.060347E2;
        c1n2=0.0329867E2;c2n2=0.140824E-2;c3n2=-0.0396322E-4;c4n2=0.0564151E-
7;c5n2=-0.0244485E-10;c6n2=-0.1020899E4;c7n2=0.0395037E2;
    else
        c1o2=0.036975E2;c2o2=0.0613519E-2;c3o2=-0.1258842E-6;c4o2=0.0177528E-
9;c5o2=-0.1136435E-14;c6o2=-0.1233930E4;c7o2=0.0318916E2;
        c1n2=0.0292664E2;c2n2=0.1487976E-2;c3n2=-0.0568476E-5;c4n2=0.10097038E-
9;c5n2=-0.0675335E-13;c6n2=-0.0922797E4;c7n2=0.0598052E2;
    end
    if Tu_cb(i,1)<1396
        c1f=-4.20868893E+00;c2f=1.11440581E-01;c3f=-7.91346582E-05;c4f=2.92406242E-
08;c5f=-4.43743191E-12;c6f=-2.99446875E+04;c7f=4.49521701E+01;
    else
        c1f=2.71373590E+01;c2f=3.79004890E-02;c3f=-1.29437358E-05;c4f=2.00760372E-
09;c5f=-1.16400580E-13;c6f=-4.07958177E+04;c7f=-1.23277495E+02;
    end

cprfuel=Ru*(c1f+(c2f*Tu_cb(i,1))+(c3f*(Tu_cb(i,1))^2)+(c4f*(Tu_cb(i,1))^3)+(c5f*(Tu_c
b(i,1))^4));

cpro2=Ru*(c1o2+(c2o2*Tu_cb(i,1))+(c3o2*(Tu_cb(i,1))^2)+(c4o2*(Tu_cb(i,1))^3)+(c5o2
*(Tu_cb(i,1))^4));

cprn2=Ru*(c1n2+(c2n2*Tu_cb(i,1))+(c3n2*(Tu_cb(i,1))^2)+(c4n2*(Tu_cb(i,1))^3)+(c5n2
*(Tu_cb(i,1))^4));
    cpr=((Xrfuel*cprfuel+Xro2*cpro2+Xrn2*cprn2));   % specific heat of reactants in J/kmol-
K
    cvr=cpr-Ru;

Hrfuel=Ru*Tu_cb(i,1)*(c1f+((c2f/2)*Tu_cb(i,1))+((c3f/3)*(Tu_cb(i,1))^2)+((c4f/4)*(Tu_c
b(i,1))^3)+((c5f/5)*(Tu_cb(i,1))^4)+(c6f/Tu_cb(i,1)));
```

[Type text]

```matlab
Hro2=Ru*Tu_cb(i,1)*(c1o2+((c2o2/2)*Tu_cb(i,1))+((c3o2/3)*(Tu_cb(i,1))^2)+((c4o2/4)*(
Tu_cb(i,1))^3)+((c5o2/5)*(Tu_cb(i,1))^4)+(c6o2/Tu_cb(i,1)));

Hrn2=Ru*Tu_cb(i,1)*(c1n2+((c2n2/2)*Tu_cb(i,1))+((c3n2/3)*(Tu_cb(i,1))^2)+((c4n2/4)*(
Tu_cb(i,1))^3)+((c5n2/5)*(Tu_cb(i,1))^4)+(c6n2/Tu_cb(i,1)));
    Hr=((Xrfuel*Hrfuel+Xro2*Hro2+Xrn2*Hrn2));        % specific enthalpy of reactants in
J/kmol

Srfuel=(Ru*((c1f*log(Tu_cb(i,1)))+(c2f*Tu_cb(i,1))+((c3f/2)*(Tu_cb(i,1))^2)+((c4f/3)*(T
u_cb(i,1))^3)+((c5f/4)*(Tu_cb(i,1))^4)+c7f))-(Ru*log((Xrfuel*Pu_cb(i,1))/P_atm));

Sro2=(Ru*((c1o2*log(Tu_cb(i,1)))+(c2o2*Tu_cb(i,1))+((c3o2/2)*(Tu_cb(i,1))^2)+((c4o2/3
)*(Tu_cb(i,1))^3)+((c5o2/4)*(Tu_cb(i,1))^4)+c7o2))-(Ru*log((Xro2*Pu_cb(i,1))/P_atm));

Srn2=(Ru*((c1n2*log(Tu_cb(i,1)))+(c2n2*Tu_cb(i,1))+((c3n2/2)*(Tu_cb(i,1))^2)+((c4n2/3
)*(Tu_cb(i,1))^3)+((c5n2/4)*(Tu_cb(i,1))^4)+c7n2))-(Ru*log((Xrn2*Pu_cb(i,1))/P_atm));
    Sr(i,1)=((Xrfuel*Srfuel+Xro2*Sro2+Xrn2*Srn2));        % specific entropy of reactants in
J/kmol-k



if i==1
    drhoPu=(rho(Nc,1)-rho((Nc-1),1))/(P_comp(Nc,1)-P_comp((Nc-1),1));
    drhoTu=(rho(Nc,1)-rho((Nc-1),1))/(T_comp(Nc,1)-T_comp((Nc-1),1));

else
  if abs(rhou(i,1)-rhou(i-1,1))<=1E-20
     drhoPu=1E-10;
     drhoTu=1E-10;
  else

     drhoPu=(rhou(i,1)-rhou((i-1),1))/(Pu_cb(i,1)-Pu_cb((i-1),1));
     drhoTu=(rhou(i,1)-rhou((i-1),1))/(Tu_cb(i,1)-Tu_cb((i-1),1));
  end
end



  A=((1/rhou(i,1))*(drhoTu/drhoPu))+(cpr/MWr);
  B=1/drhoPu;
  if A>=1E20
     A=1E20;
  end
  if A<=-1E20
     A=-1E20;
  end
  if B>=1E20
     B=1E20;
  end
  if B<=-1E20
     B=-1E20;
```

[Type text]

```
    end


    hu=Hr/MWr;          %Specific enthalpy of unburned gases in J/kg
    Ku=0.0243;   %thermal conductivity of air
    dQu=(Awu_cb*(((0.45*Ku*((80000)^0.75)*(Tu_cb(i,1)-Tw))/Bore)+((4.3*10^-
9)*((Tu_cb(i,1))^4-Tw^4))))/W; % Heat loss in J/radian
    f_Tu1(i,1)=((B/A)*((-dVu_cb/Vu_cb(i,1))+((-dQu)/(B*mu(i,1)))+(dmu(i,1)/mu(i,1))));
    Tu_cb(i+1,1)=(f_Tu1(i,1)*dtheta)+Tu_cb(i,1);      % Temperature of unburned gases
    Pu_cb(i+1,1)=rhou(i+1,1)*(Ru/MWr)*Tu_cb(i+1,1);    % Pressure of unburned gases

    % Burned Mixture Calculation

    if Tb_cb(i,1)<1000
      c1o2=0.03212936E2;c2o2=0.112748E-2;c3o2=-0.057561E-5;c4o2=0.131387E-
8;c5o2=-0.0876855E-11;c6o2=-0.1005249E4;c7o2=0.060347E2;
      c1n2=0.0329867E2;c2n2=0.140824E-2;c3n2=-0.0396322E-4;c4n2=0.0564151E-
7;c5n2=-0.0244485E-10;c6n2=-0.1020899E4;c7n2=0.0395037E2;
      c1co2=0.0227572E2;c2co2=0.0992207E-1;c3co2=-0.1040911E-
4;c4co2=0.06866686E-7;c5co2=-0.0211728E-10;c6co2=-
0.0483731E6;c7co2=0.1018848E2;
      c1h2o=0.0338684E2;c2h2o=0.0347498E-1;c3h2o=-0.0635469E-4;c4h2o=0.0696858E-
7;c5h2o=-0.0250658E-10;c6h2o=-0.0302081E6;c7h2o=0.0259023E2;
    else
      c1o2=0.036975E2;c2o2=0.0613519E-2;c3o2=-0.1258842E-6;c4o2=0.0177528E-
9;c5o2=-0.1136435E-14;c6o2=-0.1233930E4;c7o2=0.0318916E2;
      c1n2=0.0292664E2;c2n2=0.1487976E-2;c3n2=-0.0568476E-5;c4n2=0.10097038E-
9;c5n2=-0.0675335E-13;c6n2=-0.0922797E4;c7n2=0.0598052E2;
      c1co2=0.0445362E2;c2co2=0.0314016E-1;c3co2=-0.1278410E-5;c4co2=0.0239399E-
8;c5co2=-0.1669033E-13;c6co2=-0.0489669E6;c7co2=-0.0955395E1;
      c1h2o=0.02672145E2;c2h2o=0.0305629E-1;c3h2o=-0.0873026E-
5;c4h2o=0.1200996E-9;c5h2o=-0.06391618E-13;c6h2o=-
0.02989921E6;c7h2o=0.06862817E2;
    end

cppco2=Ru*(c1co2+(c2co2*Tb_cb(i,1))+(c3co2*(Tb_cb(i,1))^2)+(c4co2*(Tb_cb(i,1))^3)+(
c5co2*(Tb_cb(i,1))^4));

cpph2o=Ru*(c1h2o+(c2h2o*Tb_cb(i,1))+(c3h2o*(Tb_cb(i,1))^2)+(c4h2o*(Tb_cb(i,1))^3)+
(c5h2o*(Tb_cb(i,1))^4));

cppo2=Ru*(c1o2+(c2o2*Tb_cb(i,1))+(c3o2*(Tb_cb(i,1))^2)+(c4o2*(Tb_cb(i,1))^3)+(c5o2
*(Tb_cb(i,1))^4));

cppn2=Ru*(c1n2+(c2n2*Tb_cb(i,1))+(c3n2*(Tb_cb(i,1))^2)+(c4n2*(Tb_cb(i,1))^3)+(c5n2
*(Tb_cb(i,1))^4));
    cpp=((Xpco2*cppco2+Xph2o*cpph2o+Xpo2*cppo2+Xpn2*cppn2));  % specific heat of
product in J/kmol-K
    cvp=cpp-Ru;

Hpo2=Ru*Tb_cb(i,1)*(c1o2+((c2o2/2)*Tb_cb(i,1))+((c3o2/3)*(Tb_cb(i,1))^2)+((c4o2/4)*(
Tb_cb(i,1))^3)+((c5o2/5)*(Tb_cb(i,1))^4)+(c6o2/Tb_cb(i,1)));
```

[Type text]

```
Hpn2=Ru*Tb_cb(i,1)*(c1n2+((c2n2/2)*Tb_cb(i,1))+((c3n2/3)*(Tb_cb(i,1))^2)+((c4n2/4)*(
Tb_cb(i,1))^3)+((c5n2/5)*(Tb_cb(i,1))^4)+(c6n2/Tb_cb(i,1)));

Hpco2=Ru*Tb_cb(i,1)*(c1co2+((c2co2/2)*Tb_cb(i,1))+((c3co2/3)*(Tb_cb(i,1))^2)+((c4co
2/4)*(Tb_cb(i,1))^3)+((c5co2/5)*(Tb_cb(i,1))^4)+(c6co2/Tb_cb(i,1)));

Hph2o=Ru*Tb_cb(i,1)*(c1h2o+((c2h2o/2)*Tb_cb(i,1))+((c3h2o/3)*(Tb_cb(i,1))^2)+((c4h2
o/4)*(Tb_cb(i,1))^3)+((c5h2o/5)*(Tb_cb(i,1))^4)+(c6h2o/Tb_cb(i,1)));
   Hp=((Xpco2*Hpco2+Xph2o*Hph2o+Xpo2*Hpo2+Xpn2*Hpn2));          % specific
enthalpy of products in J/kmol

Spo2=(Ru*((c1o2*log(Tb_cb(i,1)))+(c2o2*Tb_cb(i,1))+((c3o2/2)*(Tb_cb(i,1))^2)+((c4o2/
3)*(Tb_cb(i,1))^3)+((c5o2/4)*(Tb_cb(i,1))^4)+c7o2))-(Ru*log((Xpo2*Pb_cb(i,1))/P_atm));

Spn2=(Ru*((c1n2*log(Tb_cb(i,1)))+(c2n2*Tb_cb(i,1))+((c3n2/2)*(Tb_cb(i,1))^2)+((c4n2/
3)*(Tb_cb(i,1))^3)+((c5n2/4)*(Tb_cb(i,1))^4)+c7n2))-(Ru*log((Xpn2*Pb_cb(i,1))/P_atm));

Spco2=(Ru*((c1co2*log(Tb_cb(i,1)))+(c2co2*Tb_cb(i,1))+((c3co2/2)*(Tb_cb(i,1))^2)+((c
4co2/3)*(Tb_cb(i,1))^3)+((c5co2/4)*(Tb_cb(i,1))^4)+c7co2))-
(Ru*log((Xpco2*Pb_cb(i,1))/P_atm));

Sph2o=(Ru*((c1h2o*log(Tb_cb(i,1)))+(c2h2o*Tb_cb(i,1))+((c3h2o/2)*(Tb_cb(i,1))^2)+((c
4h2o/3)*(Tb_cb(i,1))^3)+((c5h2o/4)*(Tb_cb(i,1))^4)+c7h2o))-
(Ru*log((Xph2o*Pb_cb(i,1))/P_atm));
   Sp(i,1)=((Xpco2*Spco2+Xph2o*Sph2o+Xpo2*Spo2+Xpn2*Spn2));          % specific
entropy of products in J/kmol-K


    if (Tb_cb(i,1)-Tb_cb((i-1),1))<=1E-5
       DTb=1E-5;
    else if(Tb_cb(i,1)-Tb_cb((i-1),1))<=-1E-5
         DTb=-1E-5;
       else
         DTb=(Tb_cb(i,1)-Tb_cb((i-1),1));
       end
    end
if i==1
  drhoPb=1E-10;
  drhoTb=1E-10;
else
  if abs(rhob(i,1)-rhob(i-1,1))<=1E-20
     drhoPb=1E-10;
     drhoTb=1E-10;
  else

     drhoPb=(rhob(i,1)-rhob((i-1),1))/(Pb_cb(i,1)-Pb_cb((i-1),1));
     drhoTb=(rhob(i,1)-rhob((i-1),1))/DTb;
  end
end

    A=((1/rhob(i,1))*(drhoTb/drhoPb))+(cpp/MWp);  % modification is done
```

[Type text]

```matlab
    B=1/drhoPb;
    if A>=1E20
      A=1E20;
    end
    if A<=-1E20
      A=-1E20;
    end
    if B>=1E20
      B=1E20;
    end
    if B<=-1E20
      B=-1E20;
    end


    hb=Hp/MWp;      %Specific enthalpy of burned gases in J/kg
    Ku=0.0243;   %thermal conductivity of air
    dQb=(Awb_cb*(((0.45*Ku*((80000)^0.75)*(Tb_cb(i,1)-Tw))/Bore)+((4.3*10^-
9)*((Tb_cb(i,1))^4-Tw^4))))/W; % Heat loss in J/radian
    f_Tb1(i,1)=((B/A)*((-dVb_cb/Vb_cb(i,1))+((-dQb+(dmb(i,1)*(hu-
hb)))/(B*mb(i,1)))+(dmb(i,1)/mb(i,1))));
    Tb_cb(i+1,1)=(f_Tb1(i,1)*dtheta)+Tb_cb(i,1);          % Burned gas Temperature during
combustion.
    Pb_cb(i+1,1)=rhob(i+1,1)*(Ru/MWp)*Tb_cb(i+1,1);       % Burned gas Pressure during
combustion.
    P_cb(i+1,1)=Pu_cb(i+1,1)+Pb_cb(i+1,1);            % Total cylinder pressure.
    xb=mb(i+1,1)/mivc;
    rhoT=(xb*rhob(i+1,1))+((1-xb)*rhou(i+1,1));
    MWT=((Np*MWp)+(Nr*MWr))/(Nr+Np);
    T_cb=(P_cb(i+1,1)*(MWT))/(rhoT*Ru);            % total cylinder temperature.
    if i>(j1+j2)
    thetarEOB=(i-1)*dtheta;
    Nrcb=i;
    break;
    end
    end


%----------------------------------------%
%        Start of Expansion        %
%----------------------------------------%
thetaexp=(SA+thetarEOB):dtheta:(540-EVO);
Nexp=floor(((540-EVO-SA-thetarEOB)/dtheta)+1);
V_exp=zeros(Nexp,1);
Aw=zeros(Nexp,1);
Tw=1300;
    for i=1:Nexp
    V_exp(i,1)=((Vd/(r-1))+((Vd/2)*(1+(L/Rad)-cosd(thetaexp(1,i))-((L/Rad)^2-
(sind(thetaexp(1,i)))^2)^0.5))); % Incylinder volume (Cubic meter ) calculation
    Aw(i,1)=(pi*0.5*Bore^2)+((pi*Bore*Rad)*((L/Rad)+1-cosd(thetaexp(1,i))+((L/Rad)^2-
(sind(thetaexp(1,i)))^2)^0.5));
    end
    dVexp=gradient(V_exp,dtheta); % gradient of cylinder volume
    P_exp=zeros(Nexp,1);
```

[Type text]

```
    T_exp=zeros(Nexp,1);
    rho_exp=zeros(Nexp,1);
    Sp=zeros(Nexp,1);
    A_exp=zeros(Nexp,1);
    P_exp(1,1)=P_cb(Nrcb,1);
    T_exp(1,1)=T_cb;
    rho_exp(1,1)=rhoT;
    A_exp(1,1)=A_cb(Nrcb,1);
    cvpavg=0;
    for i=1:Nexp-1     % expansion Loop
    if T_exp(i,1)<1000
        c1o2=0.03212936E2;c2o2=0.112748E-2;c3o2=-0.057561E-5;c4o2=0.131387E-
8;c5o2=-0.0876855E-11;c6o2=-0.1005249E4;c7o2=0.060347E2;
        c1n2=0.0329867E2;c2n2=0.140824E-2;c3n2=-0.0396322E-4;c4n2=0.0564151E-
7;c5n2=-0.0244485E-10;c6n2=-0.1020899E4;c7n2=0.0395037E2;
        c1co2=0.0227572E2;c2co2=0.0992207E-1;c3co2=-0.1040911E-
4;c4co2=0.06866686E-7;c5co2=-0.0211728E-10;c6co2=-
0.0483731E6;c7co2=0.1018848E2;
        c1h2o=0.0338684E2;c2h2o=0.0347498E-1;c3h2o=-0.0635469E-4;c4h2o=0.0696858E-
7;c5h2o=-0.0250658E-10;c6h2o=-0.0302081E6;c7h2o=0.0259023E2;
      else
        c1o2=0.036975E2;c2o2=0.0613519E-2;c3o2=-0.1258842E-6;c4o2=0.0177528E-
9;c5o2=-0.1136435E-14;c6o2=-0.1233930E4;c7o2=0.0318916E2;
        c1n2=0.0292664E2;c2n2=0.1487976E-2;c3n2=-0.0568476E-5;c4n2=0.10097038E-
9;c5n2=-0.0675335E-13;c6n2=-0.0922797E4;c7n2=0.0598052E2;
        c1co2=0.0445362E2;c2co2=0.0314016E-1;c3co2=-0.1278410E-5;c4co2=0.0239399E-
8;c5co2=-0.1669033E-13;c6co2=-0.0489669E6;c7co2=-0.0955395E1;
        c1h2o=0.02672145E2;c2h2o=0.0305629E-1;c3h2o=-0.0873026E-
5;c4h2o=0.1200996E-9;c5h2o=-0.06391618E-13;c6h2o=-
0.02989921E6;c7h2o=0.06862817E2;
      end

cppco2=Ru*(c1co2+(c2co2*T_exp(i,1))+(c3co2*(T_exp(i,1))^2)+(c4co2*(T_exp(i,1))^3)+(
c5co2*(T_exp(i,1))^4));

cpph2o=Ru*(c1h2o+(c2h2o*T_exp(i,1))+(c3h2o*(T_exp(i,1))^2)+(c4h2o*(T_exp(i,1))^3)+
(c5h2o*(T_exp(i,1))^4));

cppo2=Ru*(c1o2+(c2o2*T_exp(i,1))+(c3o2*(T_exp(i,1))^2)+(c4o2*(T_exp(i,1))^3)+(c5o2
*(T_exp(i,1))^4));

cppn2=Ru*(c1n2+(c2n2*T_exp(i,1))+(c3n2*(T_exp(i,1))^2)+(c4n2*(T_exp(i,1))^3)+(c5n2
*(T_exp(i,1))^4));
    cpp=((Xpco2*cppco2+Xph2o*cpph2o+Xpo2*cppo2+Xpn2*cppn2));  % specific heat of
product in J/kmol-K
    cvp=cpp-Ru;


Hpo2=Ru*T_exp(i,1)*(c1o2+((c2o2/2)*T_exp(i,1))+((c3o2/3)*(T_exp(i,1))^2)+((c4o2/4)*(
T_exp(i,1))^3)+((c5o2/5)*(T_exp(i,1))^4)+(c6o2/T_exp(i,1)));
```

[Type text]

```matlab
Hpn2=Ru*T_exp(i,1)*(c1n2+((c2n2/2)*T_exp(i,1))+((c3n2/3)*(T_exp(i,1))^2)+((c4n2/4)*(
T_exp(i,1))^3)+((c5n2/5)*(T_exp(i,1))^4)+(c6n2/T_exp(i,1)));

Hpco2=Ru*T_exp(i,1)*(c1co2+((c2co2/2)*T_exp(i,1))+((c3co2/3)*(T_exp(i,1))^2)+((c4co
2/4)*(T_exp(i,1))^3)+((c5co2/5)*(T_exp(i,1))^4)+(c6co2/T_exp(i,1)));

Hph2o=Ru*T_exp(i,1)*(c1h2o+((c2h2o/2)*T_exp(i,1))+((c3h2o/3)*(T_exp(i,1))^2)+((c4h2
o/4)*(T_exp(i,1))^3)+((c5h2o/5)*(T_exp(i,1))^4)+(c6h2o/T_exp(i,1)));
    Hp=((Xpco2*Hpco2+Xph2o*Hph2o+Xpo2*Hpo2+Xpn2*Hpn2));          % specific
enthalpy of products in J/kmol


Spo2=(Ru*((c1o2*log(T_exp(i,1)))+(c2o2*T_exp(i,1))+((c3o2/2)*(T_exp(i,1))^2)+((c4o2/
3)*(T_exp(i,1))^3)+((c5o2/4)*(T_exp(i,1))^4)+c7o2))-(Ru*log((Xpo2*P_exp(i,1))/P_atm));

Spn2=(Ru*((c1n2*log(T_exp(i,1)))+(c2n2*T_exp(i,1))+((c3n2/2)*(T_exp(i,1))^2)+((c4n2/
3)*(T_exp(i,1))^3)+((c5n2/4)*(T_exp(i,1))^4)+c7n2))-(Ru*log((Xpn2*P_exp(i,1))/P_atm));

Spco2=(Ru*((c1co2*log(T_exp(i,1)))+(c2co2*T_exp(i,1))+((c3co2/2)*(T_exp(i,1))^2)+((c
4co2/3)*(T_exp(i,1))^3)+((c5co2/4)*(T_exp(i,1))^4)+c7co2))-
(Ru*log((Xpco2*P_exp(i,1))/P_atm));

Sph2o=(Ru*((c1h2o*log(T_exp(i,1)))+(c2h2o*T_exp(i,1))+((c3h2o/2)*(T_exp(i,1))^2)+((c
4h2o/3)*(T_exp(i,1))^3)+((c5h2o/4)*(T_exp(i,1))^4)+c7h2o))-
(Ru*log((Xph2o*P_exp(i,1))/P_atm));
    Sp(i,1)=((Xpco2*Spco2+Xph2o*Sph2o+Xpo2*Spo2+Xpn2*Spn2));   % specific entropy
of products in J/kmol


    drhoP=(MWp/(Ru*T_exp(i,1)))*(cvp/(cvp+Ru));
    drhoT=(rho_exp(i,1)*cvp)/(Ru*T_exp(i,1));
    A=((1/rho_exp(i,1))*(drhoT/drhoP))+(cpp/MWp);
    B=1/drhoP;
    Ka=0.0243;   %thermal conductivity of air
    dQ_exp=(Aw(i,1)*(((0.45*Ka*((80000)^0.75)*(T_exp(i,1)-Tw))/Bore)+((4.3*10^-
9)*((T_exp(i,1))^4-Tw^4))))/W; % Heat loss in J/degree
    f_T1=((B/A)*((-dVexp(i,1)/V_exp(i,1))-(dQ_exp/(B*mivc))));
    T_exp(i+1,1)=(f_T1*dtheta)+T_exp(i,1);                % Temperature during expansion
    P_exp(i+1,1)=(mivc*(Ru/MWp)*T_exp(i+1,1))/V_exp(i+1,1);
    rho_exp(i+1,1)=(P_exp(i+1,1)*MWp)/(Ru*T_exp(i+1,1));
    end
Spo2=(Ru*((c1o2*log(T_exp(Nexp,1)))+(c2o2*T_exp(Nexp,1))+((c3o2/2)*(T_exp(Nexp,1
))^2)+((c4o2/3)*(T_exp(Nexp,1))^3)+((c5o2/4)*(T_exp(Nexp,1))^4)+c7o2))-
(Ru*log((Xpo2*P_exp(Nexp,1))/P_atm));

Spn2=(Ru*((c1n2*log(T_exp(Nexp,1)))+(c2n2*T_exp(Nexp,1))+((c3n2/2)*(T_exp(Nexp,1
))^2)+((c4n2/3)*(T_exp(Nexp,1))^3)+((c5n2/4)*(T_exp(Nexp,1))^4)+c7n2))-
(Ru*log((Xpn2*P_exp(Nexp,1))/P_atm));

Spco2=(Ru*((c1co2*log(T_exp(Nexp,1)))+(c2co2*T_exp(Nexp,1))+((c3co2/2)*(T_exp(Ne
xp,1))^2)+((c4co2/3)*(T_exp(Nexp,1))^3)+((c5co2/4)*(T_exp(Nexp,1))^4)+c7co2))-
(Ru*log((Xpco2*P_exp(Nexp,1))/P_atm));
```
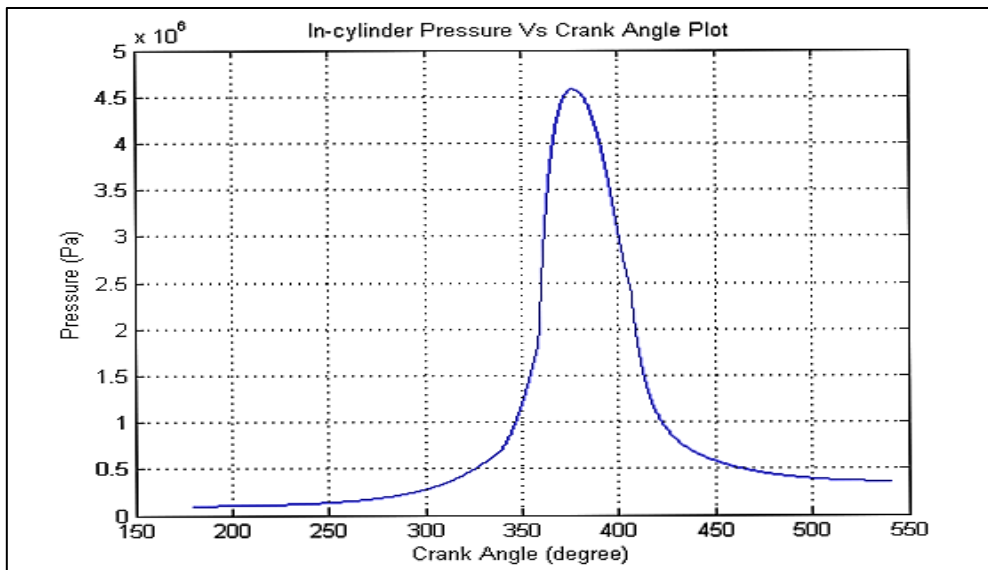
```matlab
Sph2o=(Ru*((c1h2o*log(T_exp(Nexp,1)))+(c2h2o*T_exp(Nexp,1))+((c3h2o/2)*(T_exp(Nexp,1))^2)+((c4h2o/3)*(T_exp(Nexp,1))^3)+((c5h2o/4)*(T_exp(Nexp,1))^4)+c7h2o))-(Ru*log((Xph2o*P_exp(Nexp,1))/P_atm));
    Sp(Nexp,1)=((Xpco2*Spco2+Xph2o*Sph2o+Xpo2*Spo2+Xpn2*Spn2));
 %-------------------------------------------------------%
    theta=180+IVC:dtheta:540-EVO;
    NT=floor(((540-EVO)-(180+IVC))/dtheta)+1;
    V=zeros(NT,1);
    for i=1:NT
    V(i,1)=((Vd/(r-1))+((Vd/2)*(1+(L/Rad)-cosd(theta(1,i))-((L/Rad)^2-(sind(theta(1,i)))^2)^0.5))); % Incylinder volume (Cubic meter ) calculation
    end
    DV=gradient(V,dtheta);
    P=zeros(NT,1);
    P(1:Nc,1)=P_comp(:,1);
    P(Nc+1:(Nc+Nrcb-1),1)=P_cb(2:Nrcb,1);
    P((Nc+Nrcb):(Nrcb+Nc+Nexp-2),1)=P_exp(2:Nexp,1);
    figure;plot(theta',P);grid on;
%---Modelling of Exhaust Process------------------%
Pr=(1.05/1.25)*P_atm;
Tr=T_exp(Nexp,1)/((P_exp(Nexp,1)/Pr)^(1/3));
%------------------Power and Torque Calculations------------%
IWD=0;
for i=1:NT
IWD=IWD+(P(i,1)*DV(i,1)*dtheta);
end
IMEP=(IWD/Vd)*10^-5;
FMEP=(0.05*(N/1000)^2)+(0.15*(N/1000))+0.97;
BMEP=IMEP-FMEP;            % in Bar
IP=IMEP*Vd*(N/120)*10^2;      % in KW
ITRQ=(IP/W)*10^3;            % in J
BP=BMEP*Vd*(N/120)*10^2;
BTRQ=(BP/W)*10^3;
efficiency=(BP*120*10^5)/(mf*LHV*N);
end
```


In-cylinder Pressure Vs Crank Angle Plot
(x-axis: Crank Angle (degree), y-axis: Pressure (Pa))